12-2006

Development of a Test Methodology for Determining the Efficacy of One Atmosphere Uniform Glow Discharge Plasma Against Airborne Contaminants

Ronald Edward Domitrovic
University of Tennessee - Knoxville

To the Graduate Council:

I am submitting herewith a dissertation written by Ronald Edward Domitrovic entitled "Development of a Test Methodology for Determining the Efficacy of One Atmosphere Uniform Glow Discharge Plasma Against Airborne Contaminants." I have examined the final electronic copy of this dissertation for form and content and recommend that it be accepted in partial fulfillment of the requirements for the degree of Doctor of Philosophy, with a major in Engineering Science.

Masood Parang, Major Professor

We have read this dissertation and recommend its acceptance:

William S. Johnson, Anthony English, Kimberly Kelly-Wintenberg

Accepted for the Council:

Carolyn R. Hodges

Vice Provost and Dean of the Graduate School

(Original signatures are on file with official student records.)

To the Graduate Council:

I am submitting herewith a dissertation written by Ronald Edward Domitrovic entitled “Development of a Test Methodology for Determining the Efficacy of One Atmosphere Uniform Glow Discharge Plasma Against Airborne Contaminants.” I have examined the final electronic copy of this dissertation for form and content and recommend that it be accepted in partial fulfillment of the requirements for the degree of Doctor of Philosophy, with a major in Engineering Science.

Masood Parang

Major Professor

We have read this dissertation
and recommend its acceptance

William S. Johnson

Anthony English

Kimberly Kelly-Wintenberg

Accepted for the Council:

Linda Painter

Interim Dean of the Graduate School

(Original signatures are on file with official student records)

DEVELOPMENT OF A TEST METHODOLOGY FOR DETERMINING THE EFFICACY OF ONE ATMOSPHERE UNIFORM GLOW DISCHARGE PLASMA AGAINST AIRBORNE CONTAMINANTS

A Dissertation Presented
for the Doctor of Philosophy Degree

The University of Tennessee, Knoxville

Ronald Edward Domitrovic
December 2006

ACKNOWLEDGEMENTS

This work was only possible with the enduring support of my committee, with special gratitude to my advisor Dr. Masood Parang for guiding an idea into a coherent end result and to Dr. Stan Johnson for helping me to stay the course over a lengthy process. Thanks also go to Dr. Anthony English and Dr. Kimberly Kelly-Wintenberg for offering an expert perspective on biological topics. My thanks also go to Dr. Vince Mei and my ORNL colleagues who offered continuous support and encouragement, as well as to Anh Ly for computer help and critical discussions. Thanks also to AGT for enabling the experimentation and to my former colleagues at AGT for their support. Lastly, thank you to Janeen, who made this pursuit worthwhile.

R.D.

ABSTRACT

A method of analysis is developed for an atmospheric plasma reactor in a ducted air stream with the intent of enabling parametric analysis for the multi-variable problem. Industrial uses for atmospheric plasma are numerous and in this case, a particular type of plasma known as “One Atmosphere Uniform Glow Discharge Plasma” (OAUGDP™) was studied for its chemistry generation abilities and its microorganism efficacy properties. The system of an OAUGDP reactor positioned in an air duct of fully-developed turbulent flow is constructed of nineteen pertinent variables and dimensional analysis is applied according to the Buckingham Pi method, yielding fourteen dimensionless variable groups. Important Pi groups are identified, namely those relating electrical power input to chemical generation and microorganism efficacy and experimental data is gathered and presented. Ozone is measured as a representative chemical and generation rates are presented in terms of airflow Reynolds number, geometry of the reactor electrodes and power input to the reactor.

A universal generation curve is developed for a parallel electrode reactor in which ozone generation rates can be determined from the known Reynolds number, electrode diameter to electrode gap ratio and plasma power to air flow power ratio. It is shown that ozone generation follows a bell shaped curve with increasing rates of production at a low ratio of plasma power to flow power, reaching a maximum and then decreasing to nearly zero at sufficiently high values of plasma power to flow power ratio. A principal area of development for OAUGDP and other atmospheric plasmas is for their use in destroying microorganisms, both on surfaces and in air streams. The ducted OAUGDP system was experimentally tested for efficacy against *Bacillus atrophaeus* endospores and results are presented in terms of the Reynolds number, the dimensionless plasma exposure time and the plasma power to airflow power ratio. Higher Reynolds numbers require higher treatment times for a given plasma power to flow power ratio.

TABLE OF CONTENTS

LIST OF TABLES

LIST OF FIGURES

ABBREVIATIONS

Abs	Absolute value function
AC	Alternating Current
AGT	Atmospheric Glow Technologies
A.n	*Aspergillus niger*
ASHRAE	American Society of Heating, Refrigerating and Air Conditioning Engineers
B.a	*Bacillus atrophaeus*
Btu	British Thermal Unit
BWA	Biological Warfare Agents
C	Coulomb
CDC	Centers for Disease Control
CFU	Colony Forming Units
cm	Centimeter
CWA	Chemical Warfare Agents
DAS	Data Acquisition System
DBD	Dielectric Barrier Discharge
DC	Direct Current
DNA	Deoxyribonucleic Acid
EPRI	Electric Power Research Institute
eV	Electron Volt
FEP	Fluorinated Ethylene Propylene
fpm	Feet per minute

FS	Full Scale
GPIB	General Purpose Interface Bus
gr	grains (absolute humidity)
HEPA	High Efficiency Particulate Arrestance
HP	Horse Power or Hewlett Packard
HVAC	Heating Ventilating and Air Conditioning
Hz	Hertz
in	inches
IAQ	Indoor Air Quality
ID	Inner Diameter
inwc	Inches of Water Column
J	Joule
kg	kilogram
kHz	kilohertz
kV	kilovolts
kVA	kilovolt Amp
kW	kilowatts
lbm	Pound--mass
LPS	lipopolysaccharide
m	Meter
mm	millimeter
NAFA	National Air Filtration Association

NEMA	National Electrical Manufacturers Association
OAUGDP	One Atmosphere Uniform Glow Discharge Plasma
OD	Outer Diameter
PC	Personal Computer
PCO	Photocatalytic Oxidation
PID	Proportional, Integral, Derivative
PP	Polypropylene
PPM	Parts-per-million
PPMv	Parts-per-million (volume)
PTS	Plasma Test Stand
psig	Pounds per Square Inch (gauge)
PVC	Polyvinylchloride
RBD	Resistive Barrier Discharge
RER	Remote Exposure Reactor
RF	Radio Frequency
RH	Relative Humidity
RNA	Ribonucleic Acid
RTI	Research Triangle Institute
RTV	Room Temperature Vulcanizing (silicone)
scfm	Standard Cubic Feet per Minute
SCR	Silicon Controlled Rectifier
SEM	Scanning Electron Microscope
SS	Stainless Steel

STP	Standard Temperature & Pressure
TB	Tuberculosis
USB	Universal Serial Bus
UV	Ultra Violet
UVGI	Ultra Violet Germicidal Irradiation
VDC	Volts Direct Current
VOC	Volatile Organic Compound
W	Watt
WHO	World Health Organization
μm	Micro-meter

NOMENCLATURE

a_i	Fractional exponent to N_i
c_p	Specific heat
d	Duct diameter
e	Electron charge = 1.602 x 10^{-19}
f	Applied frequency to plasma reactor
g	Plasma gap
h	Flow meter static pressure
k	Bottzman's constant= 1.38 x 10^{-23}
k_i	Reaction rate for creation of species X_i
l	Duct diameter
m	# of fundamental dimensions
$\dot{m}$	mass flow (lbm•min^{-1})
n	# of independent variables
p	# of dimensionless Pi groups
s	Dielectric thickness
t	Air temperature downstream of plasma reactor
t_i	Inlet air temperature
v	Air velocity through flow meter (ft•s^{-1})
w	Plasma width

A	Cross-sectional area
C	Charge (fundamental dimension)
°C	Degrees celcius
E	Electric field strength ($V \bullet m^{-1}$)
°F	Degrees Fahrenheit
K	Kelvins
L	Length (fundamental dimension)
M	Mass (fundamental dimension)
$\dot{N}_{species(i)}$	Molar rate of chemical production
N_i	Fundamental dimensions of a variable
P	Power input to plasma
Q	Air volume flow rate through flowmeter
$\dot{Q}$	Rate of heat transfer
Re	Reynold's number
Re_d	Reynolds number wrt. duct diameter
T	Time (fundamental dimension)
T	Temperature
T'	Kinetic energy in electron volts
U	Free stream velocity
V	Applied voltage to plasma reactor
$\dot{V}$	Volume flow ($ft^3 \bullet s^{-1}$)
X	Species

Greek symbols

η	Biological efficacy
μ	Kinematic viscosity
ν	Dynamic viscosity
ϕ	Phase
ρ	Air density
ω	Specific humidity (%)
Δp	Pressure differential
Δt	$t-t_i$
ΔT	Temperature differential
Θ	Charge (fundamental dimension)
K	Dielectric permittivity
Π	Dimensionless Pi group
T	Exposure time

Other symbols

Err	Error
$Err_{\max}$	Maximum error
Err_{mean}	Mean error
$Err_{std.dev.}$	Standard deviation of error
$(\,)_{cr}$	Critical value

$( )_{data}$	Value obtained from measured data
$( )_{norm}$	Normalized value
$( )_{poly}$	Value obtained from polynomial curve fit

Chemical Symbols

HNO_3	Nitric acid
He	Helium
MnO_2	Manganese dioxide
N_xO_x	Nitrogen oxide
N_2	Nitrogen
O_2	Oxygen
O_3	Ozone
O_3*	Excited state ozone
O_2*	Vibrationally excited, ground state oxygen
$O_2(b^1\Sigma_g)$	Singlet Oxygen
$O_2(a^1\Delta_g)$	Singlet delta oxygen
$O(^3P)$	Ground-state atomic oxygen
$O(^1D)$	Excited atomic oxygen
TiO_2	Titanium dioxide

CHAPTER 1—INTRODUCTION AND PROBLEM DESCRIPTION

The heating, ventilation and air conditioning (HVAC) industry is faced with two substantial and growing challenges related to controlling and maintaining indoor air quality (IAQ). First there is the need for continuous healthy air in all types of buildings, including government facilities and offices, hospitals and residences. Air quality has been degraded in many buildings because of the conflict between maintaining strict indoor climate control and satisfying energy efficiency needs. A variety of studies exist documenting the relationship between poor indoor air quality and adverse health effects. [Meklyn 2002, Streifel 2003] Unhealthy indoor air leads to increased disease transmission, which in mild cases leads to absenteeism and lower productivity, and in severe cases leads to substantial and prolonged illnesses [Menzies 2003]. The second, less prevalent, yet more ominous challenge is to provide inherent protection of a building from a purposeful biological weapon (BWA) or chemical weapon (CWA) attack.

Filtration of unwanted particulate or gaseous contaminants is the current method typically employed for cleaning air streams. The science of air filtration is relatively mature and methods and models exist for predicting both the capture abilities of filter media, and the resultant distribution of contaminants through a conditioned space. The National Air Filtration Association Guide to Air Filtration [NAFA 2001] gives a comprehensive look at the variety of mechanisms, materials and rating standards related to air filtration. Methods associated with

commercially available particulate air filters and analysis relating filter cost, power cost and particulate capture efficiency is available in literature [Fisk 2003]. Kowalski, in several papers [Kowalski 1999 & 2002], studies the filtration of microorganism particulate and models capture and subsequent air distribution.

Ultraviolet light has been employed for many years in a variety of configurations for its germicidal effect on exposed surfaces. UV systems currently occupy a niche market in the HVAC industry for the prevention of mold growth on cooling coil surfaces. Some deployment of UV for airborne organism destruction exists, but required exposure is rather high and energy requirements for efficacy approaching sterility are prohibitive. [Kowalski 2000, Levetin 2001, Miller 2000, VanOsdell 2002]

Over the past several years, an emerging technology known as atmospheric plasma has received substantial attention from funding organizations and research institutions, principally for its use as an agent for sterilization and chemical decontamination of surfaces and air streams. Atmospheric plasma is a gas chemical process whereby an air stream is partially turned into plasma through electrical discharge, creating a short-lived soup of highly energetic and reactive atomic and molecular species that react with and kill microorganism material and decompose many chemicals. Testing has shown high degrees of killing against various types of microorganisms, including vegetative bacteria such as *Staphlococcus aureus*, mold spores, such as *Aspergillus niger* and

bacterial endospores, such as *Bacillus atrophaeus* (a testing surrogate for Anthrax). High efficacy with relatively short exposure has given atmospheric plasma systems the attention of the IAQ industry and the collective protection industry for mitigation of biological and chemical attack. To date, most research related to atmospheric plasma as a sterilizing agent has been surrounding the core technology of generating a stable glow discharge and on the efficacy against particular species of microorganisms. A comprehensive review of non-thermal plasma, its history and applications can be found in references [Roth 1995]. To date there has not been a comprehensive study quantifying the efficacy and relating it to the full range of measured atmospheric plasma parameters, like input energy and time, across the range of airborne microorganisms.

The problem of accurately and responsibly characterizing the efficacious nature of atmospheric plasma generating systems is tied to a proper understanding of the relationships between the large number of input and output variables that describe a system. Like many engineering problems, there are output variables which require optimization; in this case they include efficacy of microorganisms and rate of chemistry generation. Those outputs have complex functional relationships with numerous input variables. In simpler systems with limited inputs, a common practice is to empirically measure output values while sweeping through the parameter space defined by the inputs. With two or three inputs the task is reasonable, but as the problem is considered in a wider context

it becomes exponentially more complex. Changes in the nature of the functional dependence—e.g. from linear to non-linear—complicate any attempt to understand the output relationship through simple parameter sweeps. Using atmospheric plasma as an example, the rate of generation of a certain chemical species may be linearly related to power input at low humidity, but become non-linear at higher humidity. Such interplay among all the variables makes proper analysis critically important if any meaningful conclusions can be drawn from experimental data.

Studying the intricacies of parametric relationships is not new and methods have been long established for doing so. When attempting to characterize a relatively new subject or new application of an existing technology, particularly one that has an unusually large set of input parameters, it is imperative to approach with a systematic method that provides guidance for variable navigation and helps to prevent the easy misinterpretation of data. This work attempts to identify the most physically relevant parameters at play in a particular reactor and flow setup using atmospheric plasma as a chemistry source for killing microorganisms. Further it employs an established method in Buckingham Pi analysis to pare down the variable set to its fundamental dimensionless set. The analysis is specific to one particular airflow and reactor geometry, but the method is not limited and can be applied in a similar manner to other configurations. Lastly it applies the analytical findings to experimental procedure and draws some conclusions about the nature of atmospheric plasma chemistry generation and

microbiological efficacy. This work studies the efficacy of one particular type of atmospheric plasma, known as One Atmosphere Uniform Glow Discharge Plasma (OAUGDP™). The details of this particular plasma type and its relation to atmospheric plasma, and plasma in general, is described in the next chapter.

For any particular problem, it is up to the analyst to select those input variables that have the most significant relationship to the desired output. For this atmospheric plasma problem, the list of input variables includes those for geometry, material properties, electrical characteristics, flow dynamics, microorganism characteristics and chemical reaction kinetics. The total list of input variables would cover the entirety of the processes, including the details of plasma generation and the details of microorganism surface reactions. Such a complete study is beyond the scope of this work. Therefore, in this study the plasma generator is treated as a pseudo black box that generates chemistry which is subsequently convected onto substrates containing microorganism challenges. Theoretically this reduces the variable set to the macroscopic or continuum processes. The microscopic processes are left to future efforts.

CHAPTER 2—BACKGROUND AND LITERATURE REVIEW

2.1 Plasma—Fourth State of Matter

The fourth state of matter, plasma, is a broad category for any gaseous state where a sufficient number of the gas molecules are in an excited or ionized state, and the bulk behavior of the gas is changed. The term “Plasma” was given by Irving Langmuir, the American chemist and engineer who, among many scientific endeavors, pioneered the field of vacuum discharge. Plasma can be obtained in a variety of ways, but in general it is produced by the addition of energy to a neutral gas, just as a gas is produced by adding energy to a liquid. A gas or gas mixture such as air is neutral and non-excited at room temperature and atmospheric pressure. The motion of molecules, and the energies with which they are colliding, are not sufficient to cause statistically significant disruption of the molecules and their electron structures. As heat is added to the gas and the collision energies increase, disruption of the gas molecules begins to occur causing the onset of plasma. Excited states comprising plasma consist of molecules and atoms with electrons in higher energy orbitals and any variety of partially or fully ionized molecules and atoms. Ionized states require greater energy than non-ionized, excited states, and higher levels of ionization require higher energy.

The energy content of plasma spans a wide range from relatively cool non-thermal discharges to very hot fully ionized thermal discharges. Standard air has an average kinetic energy of approximately 0.035 eV or ~298K. Kinetic energy in electron volts and temperature in Kelvins are related by:

$$kT(K) = eT'(eV) \qquad [2.1]$$

where:

k = Boltzman's constant = 1.38×10^{-23}
e = electron charge = 1.602×10^{-19}

The kinetic energy required for electron transition and ionization reactions is on the order of 3-10 eV, and is approximately two orders of magnitude greater than the average kinetic energy of ambient air. A fully ionized gas therefore may have an equivalent temperature of tens or hundreds of thousands Kelvin. The average kinetic energy of a plasma depends on the ionization fraction which may be as small as $1/10^7$, or as high as 1 (complete ionization).

A non-thermal plasma is a plasma in which the energy is carried in free electrons and a relatively small fraction of ionized and excited species, leaving the bulk of the background gas cool. Thus, the kinetic energy of a small fraction of chemical species is very high, but the average for the entire gas volume remains relatively low, and only slightly above that of the neutral gas. By contrast, the kinetic energy in a thermal plasma is distributed evenly throughout the species and the plasma volume, yielding a large fraction of high energy species, and a relatively high average kinetic energy.

One method for creating non-thermal plasma is by the acceleration of free electrons which in turn cause cascade reactions with gas molecules. In atmospheric air—or any carrier gas, there is an average concentration of free electrons that depends on temperature; for air at STP free electron density is approximately 10,000 per cm^2. Under the application of an electric field, these electrons can be accelerated to several eV, to where they are energetic enough to cause excitation or ionization of surrounding gas molecules upon collision (**Figure 2.1**). Further reactions continue involving the new excited and ionized species as they collide with other electrons and neutral molecules. The result is a small fraction dynamic mix of excited and ionized species. These species are for the most part unstable and prone to react with other molecules or decay back down to a stable state.

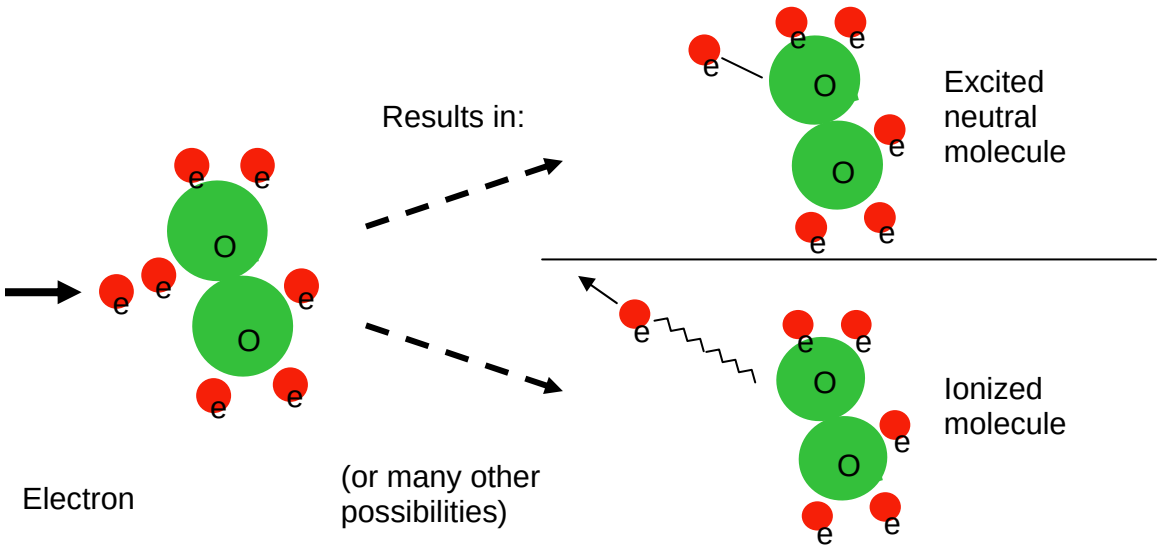

Figure 2.1—Example electron collision with a neutral oxygen molecule

Non-thermal plasmas can be classified into two regimes: filamentary discharges and glow discharges. Filamentary discharges are distinguished from glow discharges on the basis of observable points of high intensity discharge surrounded by an area of low or no discharge. Examples of filamentary discharges include coronas and dielectric barrier discharges. Though the physics is still evolving, it is postulated that the glow regime is a point of optimal energy transfer that provides for the highest collision energies for a given volumetric input power.

2.1.1 One Atmosphere Uniform Glow Discharge Plasma (OAUGDP)

One Atmosphere Uniform Glow Discharge Plasma (OAUGDP) is a particular type of non-thermal glow plasma where the carrier gas is atmospheric air [Roth 1992, 1995-1, 1995-2]. It is characterized by a diffuse barrier discharge lacking observable filamentary structure [Rahel 2004]. Non-air glow plasmas at one atmosphere had been generated with specialized gas mixtures in the 1980s and air was ultimately demonstrated as an appropriate carrier gas in 1994 at the University of Tennessee, Knoxville [Spence 1997]. Prior to the demonstration of glow plasmas at one atmosphere pressure, glow plasmas were typically generated with specialized gases or gas mixtures under vacuum, making any industrial plasma process a batch operation. OAUGDP is sustainable within a band of RF frequencies of an applied electric field of several kilovolts per centimeter. Outside the frequency band (~1-100kHz), the glow regime breaks

down to filamentary discharges, or the plasma simply does not initiate. Within the 1-100 kHz frequency band, it is suggested that a phenomenon called ion trapping occurs whereby electrons are free to impact and interact with the electrodes generating the applied field, but molecular and atomic ions are not. The electric field switches direction before the ions travel far enough in one direction to impact an electrode, and are in effect trapped in the region between electrodes. Further discussion of the theory of OAUGDP and ion trapping are found in a text by Roth [Roth 2001]. The ability to generate glow plasma with air at atmospheric conditions has enabled pursuit of continuous processes, one of which is the treatment of air streams. Because air naturally contains oxygen (~16 percent by mole) an OAUGDP process can augment oxidation of anything in contact with plasma products, at a reasonably low temperature. Evidence of rapid oxidation with OAUGDP on iron and copper surfaces has been demonstrated [Depaoli 2003].

OAUGDP exposure can be either direct or indirect. In direct exposure, the entity to be treated (surface, microorganism, fiber, etc.) is within the region of active plasma generation, or within the region of high strength oscillating electric field. The direct plasma generation region is generally identifiable by the signature purple glow of nitrogen electron transitions. By contrast, indirect exposure implies that the treated entity is outside the region of plasma generation, but within the region where convected species created by the plasma are still in sufficient concentration to produce an effect. The species created by the plasma

reactor are highly dynamic and many are short lived, making the indirect region dependant on many parameters including the required chemical species and the respective decay rate as it depends on temperature and other factors.

OAUGDP can be generated in a variety of geometries provided certain criteria are met, including a sufficient electric field present in the air gap, AC in the proper frequency range of ~several kHz - ~100 kHz, a dielectric coating on at least one electrode of sufficient thickness and dielectric constant to enable plasma formation and prevent thermal arcing and air flow across the plasma gap. **Figure 2.2** shows OAUGDP being generated between parallel cylinders and **Figure 2.3** shows it generated between concentric cylinders with a transparent outer electrode.

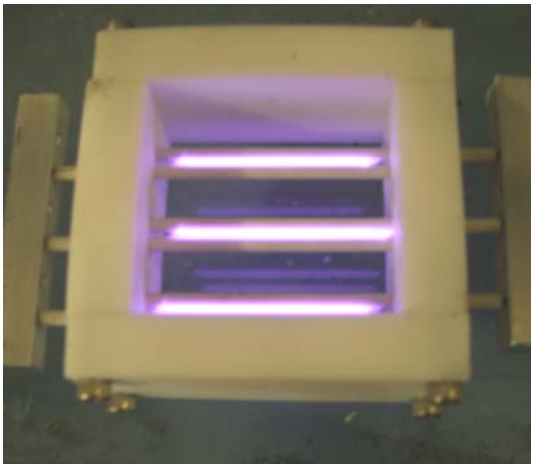

Atmospheric Glow Technologies

Figure 2.2—OAUGDP generated between three sets of parallel electrodes

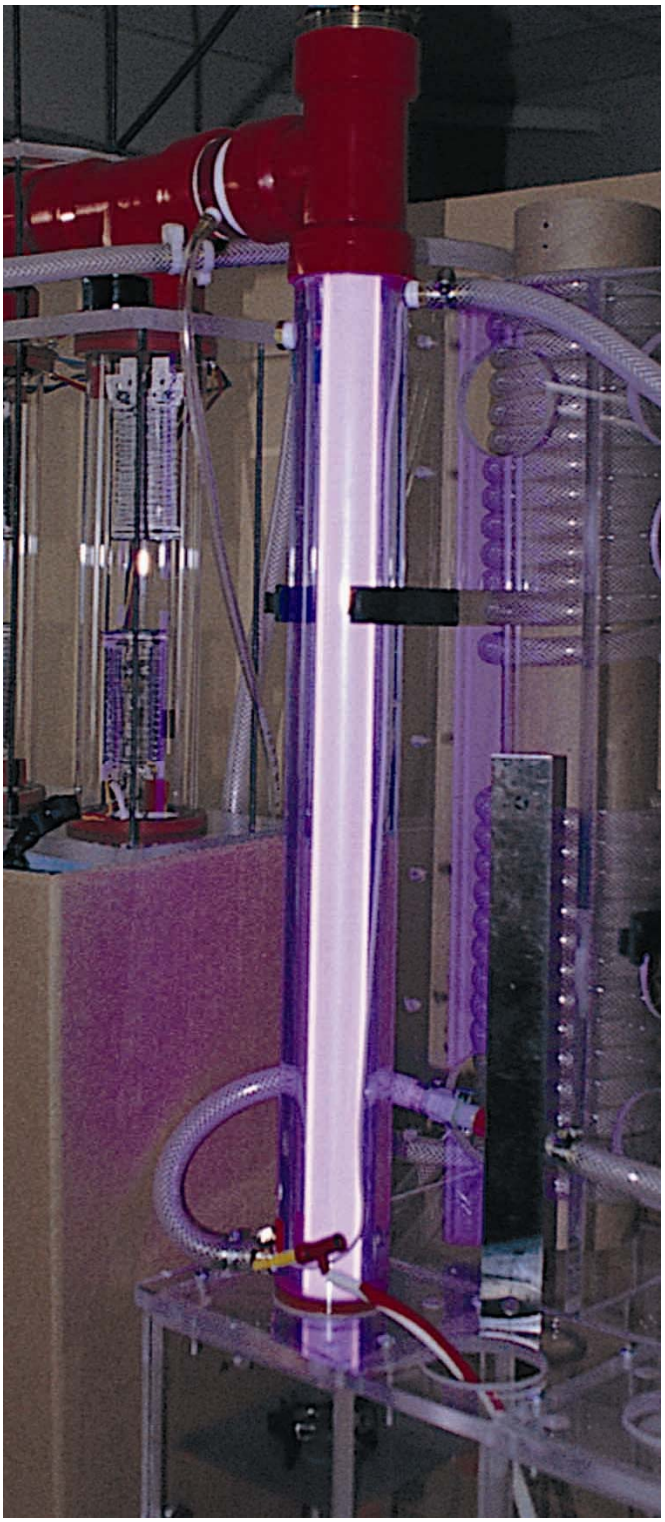

Atmospheric Glow Technologies

Figure 2.3—OAUGDP Generated between concentric cylinders

OAUGDP Chemistry

The task of identification and characterization of reactive species in OAUGDP generated by atmospheric plasma is complicated because of the variety of species present and their correspondingly short lifetimes due to high collision frequency. Vacuum plasmas by their nature have reduced collision frequencies, and are often formed with single carrier gasses, reducing the number of possible excited species. OAUGDP operating at one atmosphere and with all the constituents of air produces a large mix of continuously changing and short lived species. Experimental work to date has focused on identifying the presence of particular species, but not necessarily on quantifying them, or understanding their creation or decay dynamics.

Of particular interest in terms of plasma and its ability to sterilize biological media are the excited and ionized oxygen species because of their reactivity and oxidative properties. These species include vibrationally excited, ground state oxygen (O_2*), excited molecular oxygen species – singlet oxygen $O_2(b^1\Sigma_g)$ and singlet delta oxygen $O_2(a^1\Delta_g)$ – ground state, atomic oxygen O(^{3}P) and excited atomic oxygen O(^{1}D), and ozone (O_3) and excited state ozone (O_3*) [Kelly-Wintenberg, 2004].

Most of the species generated in the plasma are extremely short-lived (on the order of microseconds) and recombine within a short distance outside the plasma volume. However, some oxygen species, particularly the excited molecular

oxygen species, singlet oxygen and singlet delta oxygen, are of interest in the plasma exhaust due to their relatively longer lifetimes of seconds.

2.2 Microorganism Air Contaminants

The existence of microorganisms was long suspected and was finally shown by the Dutchman Anton Van Leeuwenhoek in the 1670s. He was a part time lens grinder who first used a microscope to observe living cells. Louis Pasteur in the 1870s, disproved the theory of spontaneous generation—living matter being spontaneously generated out of non-living matter—and showed that microorganisms were present in air. Pasteur's work along with others, including Francesco Redi's earlier discovery that maggots on meat were the result of depositions of fly eggs and not a spontaneous generation of the meat, was critical in advancing the germ theory of diseases. Upon acceptance of the germ theory of diseases, many simple yet highly effective advances were made to reduce the spread of diseases, the most ubiquitous of which is washing hands.

Today the spread of disease and other human affliction through airborne bioaerosols is relatively well understood, but remains difficult to prevent in many circumstances. Bioaerosols are airborne particulates derived from living organisms and include living microorganisms, viruses, spores and toxins resultant from remnants or fragments of living tissue. The spread of tuberculosis

(*Mycobacterium tuberculosis*) through airborne transmission has been responsible for much of the study for methods of capturing, killing and preventing the transport of airborne bioaerosols. Many diseases, however, including the common cold and influenza and numerous allergic afflictions causing respiratory problems, asthma and rhinitis are the result of airborne bioaerosols.

Tuberculosis (TB) has been an infectious agent to humans for all of recorded history and it is today a curable disease through a somewhat lengthy treatment process. World Health Organization (WHO) statistics show that approximately 3.8 million people are infected with TB yearly throughout the globe, 1.7 million of which die of the disease. Ninety-five percent of the infections are in developing countries [WHO, 2005]. TB is communicated from person to person through prolonged breathing of air containing *Micobacterium tuberculosis* bacteria. It is not generally transmitted by casual or limited interaction with an infected person, such as passing on a street, or riding on a bus, but rather by prolonged exposure over many hours or days. The U.S. Centers for Disease Control (CDC) offers guidelines for preventing the spread of TB in health care facilities [CDC, 1994] and many new technologies such as UVGI are employed to prevent its spread.

A multitude of other ailments, both acute and nuisance are carried by airborne microorganisms. [ASHRAE, 2005] gives an overview of classes, types and the nature of bioaerosol air contaminants. Bioaerosols are a class of airborne particulates that are derived from living organisms and include microorganisms,

spores, viruses, and allergins. A broad range of diseases and other human ailments are transmitted via bioaerosols including TB (bacterial) rhinitis and sinusitis (mold) common colds and influenza (viral) and allergies (mold, dander etc.). Control of airborne bioaerosols and in general airborne contaminants, both particulate and gaseous, has become an area of focus for building designers and facility managers. The 2004 North American air purification market for stand-alone and ducted equipment was nearly $700 million and growing at ~17% annually [Frost & Sullivan, 2004]. This is a figure for equipment only and does not include the general air filter replacement market. An apparent increase in allergies and general respiratory ailments in the United States has been loosely tied to the tightening of buildings over the last several decades driven in part by the desire for air conditioning and the corresponding need to minimize the exchange of outside air. An alternative stance is that the problem has always existed, but our perception and understanding of it has increased in recent years. Regardless of the root cause, there is a surge in interest in methods and technologies for cleaning indoor air of particulate and gaseous contaminants and there is a corresponding surge in companies trying to meet the requirements and demands of the HVAC and Indoor Air Quality (IAQ) markets. Overviews of current technologies for particulate and gaseous contaminant removal are found in [ASHRAE, 2004].

2.2.1 Microorganism Structure

Microorganisms found in ambient air may be prokaryotic as are the bacteria (both vegetative and endospore forming) or eukaryotic (mold and fungal spores). Though internally different, these airborne microorganisms are single celled and are built from many of the same molecular constituents. Viruses are genetic units that are able to replicate via infection of a host cell. Though not considered living, because of their inability to self-replicate, viruses can pose a serious threat to the health of humans, and viral infections such as colds and influenza are a leading source of school and workplace absenteeism.

Prokaryotes (Bacteria)

Prokaryotes, including all bacteria, both vegetative and endospore forming, are differentiated from eukaryotes by their lack of distinct organelles within the cytoplasm. An illustration is seen in **Figure 2.4**. They lack such structures as mitochondria and chloroplasts, and even a distinct membrane bound nucleus. Bacteria have a cytoplasmic membrane, which serves as a permeability barrier, surrounded by an outer cell wall that adds structural support and some resistance to lysis. The membrane holds the contents of the cell within and holds everything else out, while providing a transport mechanism for substances to cross into or out of the cell. The membrane consists of a phospholipid bilayer within which reside a variety of transport proteins, creating a flexible and fluid, yet structurally sound and impervious layer encapsulating the cell. Eukaryotic cells

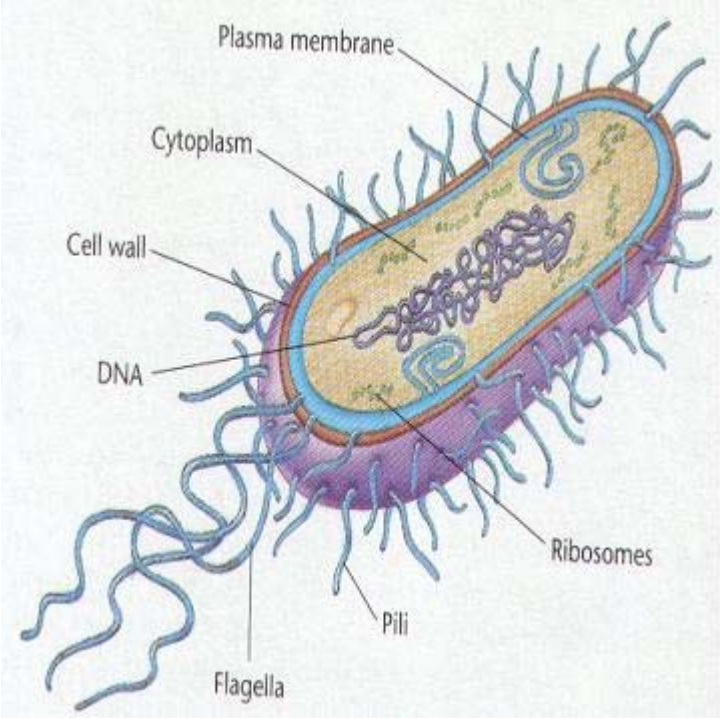

Figure 2.4—Typical prokaryote bacterial cell [Madigan 2003].

have similar membranes, but they contain additional compounds called sterols, which add rigidity and strength. It is suspected that sterols are required in eukaryotic cells because many of them lack cell walls and depend solely on the membrane for structural integrity.

Bacteria are divided into two categories called gram-negative and gram-positive as indicated by structural differences in their respective cell walls. Both gram-negative and gram-positive bacteria contain a layer of peptidoglycan as the primary rigid structure of the cell wall. Peptidoglycan is a thin sheet composed of chains of sugar derivatives, which are peptide cross-linked with amino acids. In

gram-positive bacteria the cell wall is entirely peptidoglycan in a relatively thick layer. In gram-negative bacteria, a thinner layer of peptidoglycan is further covered by a lipopolysaccharide (LPS) bilayer. The biochemical importance of this outer layer of the gram-negative cell wall continues to be investigated, but one important feature is that it is home to endotoxins. The existence of an endotoxin on the LPS is independent of the organism's pathogenic nature, and human endotoxins can be found on non-human pathogenic bacteria. Though the detailed structure is different in all the classes of microorganisms, the outer layers are generally made from lipid, protein, sugar and amino acid constituents, all of which are likely to be susceptible to damage from exposure to reactive oxygen species and high momentum ions. The resistance offered by particular organisms is likely linked to the propensity of these outer cellular layers to react with plasma species.

Some species of bacteria, most notably those in the genera *Bacillus* and *Clostridium*, are able to reform into a dormant endospore state that is highly resistant to otherwise adverse conditions such as dehydration or extreme temperature. The endospore is inactive and has no metabolic activity unless external conditions turn favorable triggering it to germinate back into a vegetative bacteria. The outer layers are more complex for endospores than for vegetative bacteria mainly because many layers constitute the shell of an endospore. A thin protein layer called the exosporium is the outermost layer of a bacterial endospore. Inside the exosporium are layers called spore coats, which are

layers of species specific proteins. Beneath the spore coat is the cortex which is a cross-linked peptidoglycan layer. Within the cortex is the core, which consists of the usual cell components: cell wall, cytoplasmic membrane, cytoplasm and nucleoid. A compound called dipicolinic acid, present in the spore core, but not in the vegetative cell, combines with calcium ions which are in abundance within the core. The dipicolinic acid and calcium may have a role in protecting DNA within the nucleoid region of the endospore core.

Eukaryotes (Fungi)

Eukaryotic cells are generally larger than prokaryotes and they are differentiated by the presence of membrane bounded organelles including an enclosed nucleus housing the cell's genetic material. Eukaryotic cells are the building blocks for all the advanced life forms including plants and animals, however, the interest of this work focuses on a simpler group of eukaryotes, the molds. Molds are filamentous fungi that reproduce by forming spores which in turn germinate into further colonies if conditions permit. Mold, and all fungi, contain cell walls that are similar in structure to plant walls, but may contain chitin rather than cellulose as the structural material. Chitin is a glucose derivative polymer, N-acetylglucosamine, that together with polysaccharides, proteins, lipids and polyphosphates make up the fungal cell wall.

Viruses

Viruses are non-living encapsulants of genetic material that replicate by invading a host cell and using its machinery for DNA / RNA replication. In the process, the host cell is often irreparably damaged, making viruses destructive to a collection of host cells. Viruses are small relative to bacteria, ranging from ~0.02 to 0.3 μm across compared to 2-10 μm for bacteria. Simple viruses, consist only of nucleic acid (DNA or RNA) and a protein capsule surrounding it which together form a nucleocapsid. Larger more complex viruses have an envelope of protein laden lipid bilayers, and may have several sections to the overall virion particle.

2.2.2 Destruction of Airborne Microorganisms

Cold plasma technologies have been under development over the past decade for use in applications to destroy airborne or surface microorganisms. This effort has seen renewed attention since the Fall of 2001 and the Anthrax incidents in the United States. Other related technologies like UV germicidal radiation (UVGI), pulsed UV radiation, photocatalytic oxidation and microorganism disruption with high strength electric fields have also seen increased interest in recent years. An overview of electro-technologies for use against bioterrorism events was produced by the Electric Power Research Institute [EPRI 2002]. It provides general descriptions of current and emerging technologies including: Microwave radiation, UV radiation, atmospheric plasmas, thermal measures, electron beam radiation, X-ray and gamma ray radiation and chemical methods.

UVGI is currently the most prevalent technology used for killing microorganisms in HVAC ducted systems. Its lethal effects against microorganisms have been known for decades and are covered extensively in literature [Rentschler, 1942, 1943], [Kowalski, 2000 & 2002]. UVGI is either positioned upstream of the cooling coil where water condensation occurs to prevent bacterial and fungal growth on the coil surface or it is positioned in the ducted air flight path to kill microorganisms as they pass. Long exposure time makes coil surface irradiation highly effective [Kowalski, 2000]. Greater UV luminosity is required for in flight destruction because residence time of an organism in the UV radiation path is relatively short. A thorough study of in flight microorganism destruction by UVGI is presented by researchers from the Research Triangle Institute (RTI) [VanOsdell, 2002 and Foarde, 2002]. The study relates UV dose requirements to microorganism species for several vegetative bacteria and fungal spores with varying humidity and organic load. In general, vegetative bacteria sustained higher kill rates than fungal spores at similar conditions. Guidelines for the application of UVGI for airborne microorganism destruction are available from a variety of sources, most notably the Centers for Disease Control (CDC) [CDC, 1999-1 & CDC, 1999-2].

Microorganism Destruction with Plasma

After its initial discovery, application pursuit for OAUGDP focused on surface treatment of materials, including changing the surface charge properties of

fibrous media [Roth 1993]. Soon after, OAUGDP effectiveness at degrading cellular material was discovered and became a research priority. Early work was centered on using OAUGDP in a parallel plate arrangement for enabling DNA extraction from cells [Madigan 2000]. The principle behind this technique is that the outer cellular surface, cell membrane or cell wall can be perforated by exposure to plasma, likely through oxidation, allowing for easy access to the nucleus or nucleoid and its DNA. This work was done with direct plasma exposure.

Direct plasma exposure was later applied to killing vegetative bacterial cells and inactivating viruses captured on a filter media. The media was embedded between electrode pairs and plasma was generated around it [Montie 2000, Kelly-Wintenberg 2002]. Killing of microorganisms by indirect exposure was later demonstrated with OAUGDP by placing *samples of Esherichia coli and Staphlococcus aureus* downstream of a “remote exposure reactor” (RER), demonstrating 4 log reduction in microorganism viability after 25 seconds of exposure [Roth, 2000]. Later work further explored different genera including bacterial endospores, fungal spores and viruses using concentric tube electrodes and parallel electrodes in a ducted air stream [Kelly-Wintenberg, 2004]. Some recent work has qualitatively demonstrated airborne killing of aerosolized microorganisms including *Staphlococcus aureus*.

Several other groups have pursued the use of various forms of atmospheric plasmas for the destruction of microorganisms and device sterilization, destruction or inactivation of chemical agents and for the modification material surface properties. The Applied Plasma Technology Laboratory, Old Dominion University, in conjunction with the Microwave & Plasma Laboratory, University of Tennessee has written extensively on plasma interaction with microorganisms. [Laroussi 2001, 2002 & 2003 & Richardson 2000] present results for efficacy of a resistive barrier discharge (RBD) plasma against Gram-negative *E.coli* and Gram-positive *Bacillus subtillus* (now *Bacillus atrophaeus v. niger*). Some insight is given into the possible mechanism of cell death based on internal cell pressure leading to membrane rupture at points of stress concentration resultant from plasma induced cellular damage. The RBD is a modified version of a traditional direct current (DC) dielectric barrier discharge (DBD) which operates at 60 Hz and several kV [Laroussi, 2002].

A group at the Stevens Institute of Technology and subsequently the PlasmSol Corporation, (both of Hoboken, NJ) have worked on what is termed “Capillary Discharge Non-Thermal Plasma”. Atmospheric pressure plasma is formed between two electrodes with one or two perforated dielectric sheaths forming micro-capillaries through which jets of atmospheric plasma are generated [Kunhardt, 1999 and 2000]. Capillary discharge non-thermal plasma has been shown to kill a variety of microorganisms. [Panikov, 2002] presents results of efficacy for a He and $He/N_2/O_2$ capillary plasma versus bacterial cultures placed

on glass or alumina substrates. The authors express kill rate 'k' in terms of an exponential decay law:

$$y(t) = y_0 \bullet e^{-(kt)} \qquad [2.1]$$

where y_0 is the initial cell concentration at t = 0. Reductions in colony forming units (CFU) depend on variations in treatment time and ranged up to 10^4 for He plasma and 10^8 for $He/N_2/O_2$ plasma.

Destruction Processes

Augmented oxidation is believed to play a key role in the ability of OAUGDP to kill microorganisms in relatively short order, for both direct and indirect exposure. Other mechanisms including ion bombardment and UV radiation exposure may also be at play. Ion bombardment is a mechanical process where high speed ions act as bullets on the surface of microorganisms. Each type of microorganism (virus, vegetative bacteria, bacterial endospore and fungal spore) has a different structural makeup, but all are made of oxidizable agents such as proteins and lipids. It is likely that structural differences in microorganism types that are responsible for the observed range of resistance to destruction by plasma gas. Though the chemical mechanisms responsible for microorganism destruction are not fully understood and only partially identified, it is of substantial importance to understand the structural makeup of the microorganism types. The similarities and differences in cellular structure are in all probability linked to

efficacy rates under controlled plasma exposure. It is believed that once the cytoplasmic membrane is perforated beyond repair, the cell is dead and the spore is incapable of germinating, and likewise, once a virus is damaged to where it cannot infect a host cell, it is considered inactivated. **Figure 2.5** is an electron micrograph of (a) a *Bascillus anthrasis* endospore, and (b) a similar *B. anthrasis* endospore after 20 minutes of direct plasma exposure showing substantial damage to the outer structure [Atmospheric Glow Technologies, 2006]. **Figure 2.6** Shows *Aspergillus niger* fungal spores in various states: a) control—no plasma exposure, b) after 1 minute of direct plasma exposure and c) after 4 minutes of direct plasma exposure [Atmospheric Glow Technologies, 2006]. Note that the scale in **2.6** (c) is 2x the scales in (a) & (b) and that the fungal spore size is of the same order in all three images.

2.2.5 Destruction of Chemicals

There is strong interest in the use of non-thermal plasmas for the destruction of airborne and surface chemicals. Industrial processes, construction materials and microorganisms are all producers of unwanted Volatile Organic Compounds (VOC) air contaminants such as formaldehyde, acetone, toluene and methanol. As well, the various military agencies have pursued non-thermal plasma as a means for neutralizing equipment contaminated with chemical warfare agents (CWA).

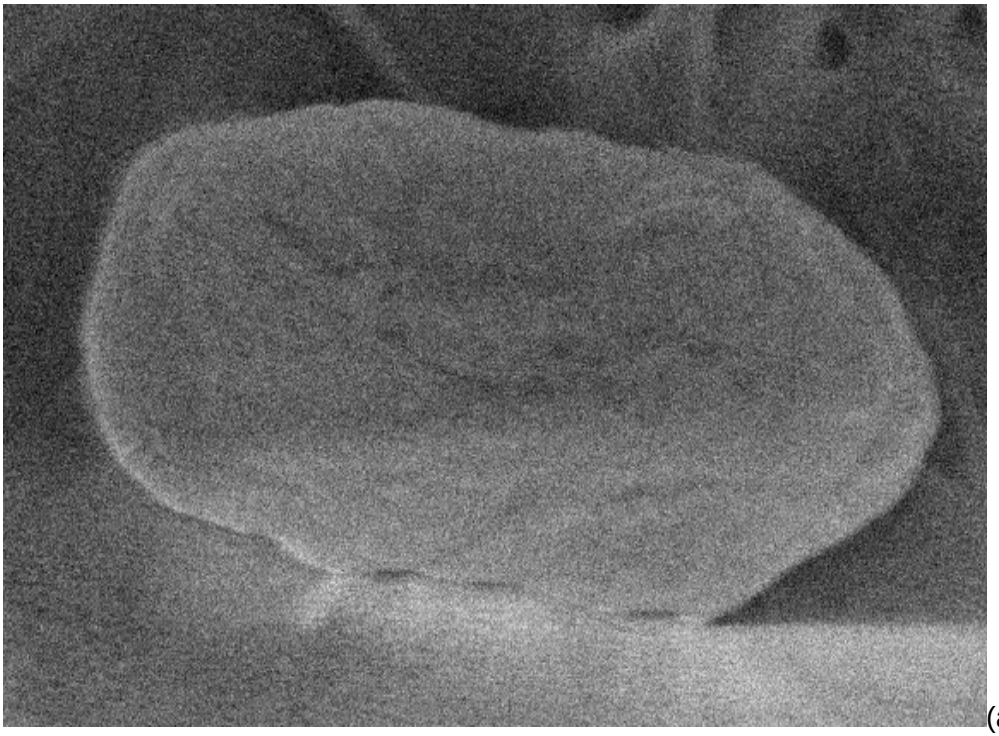

(a)

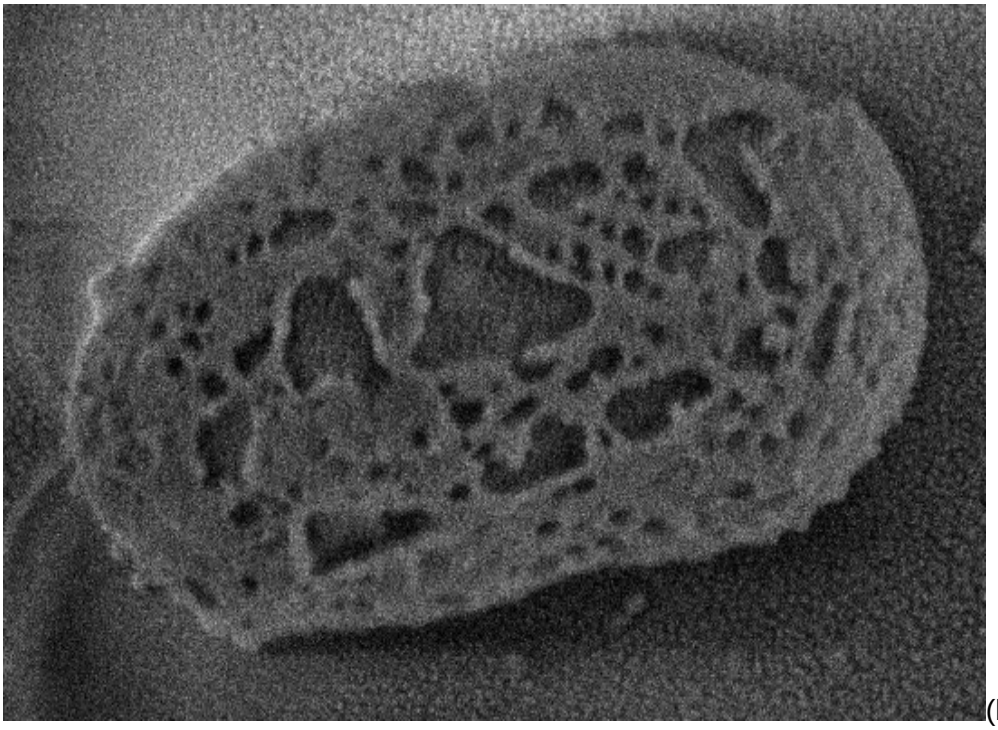

(b)

Figure 2.5—(a) *Bacillus anthrasis* endospore and (b) *Bacillus anthrasis* endospore following a lethal dose of direct plasma exposure [AGT, 2006].

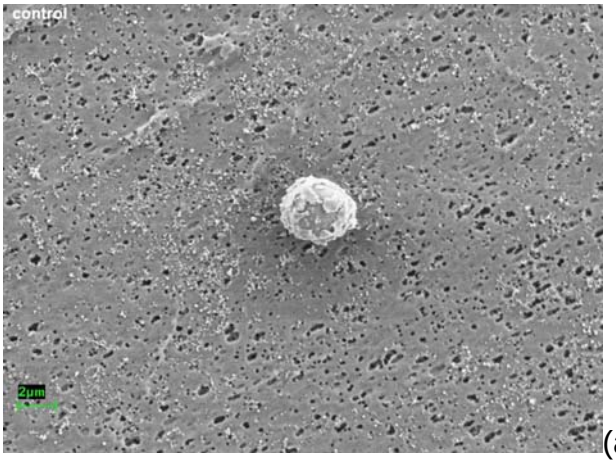

(a)

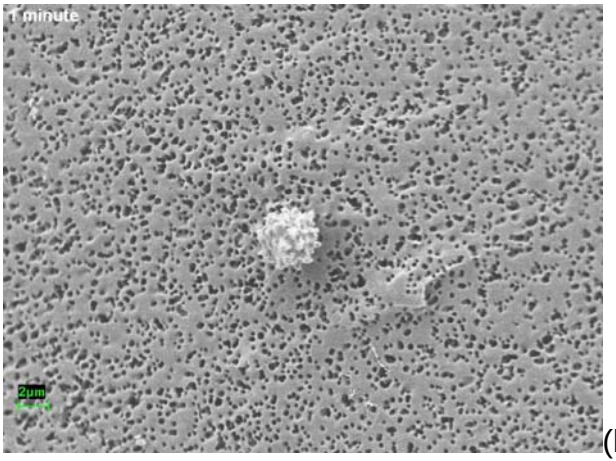

(b)

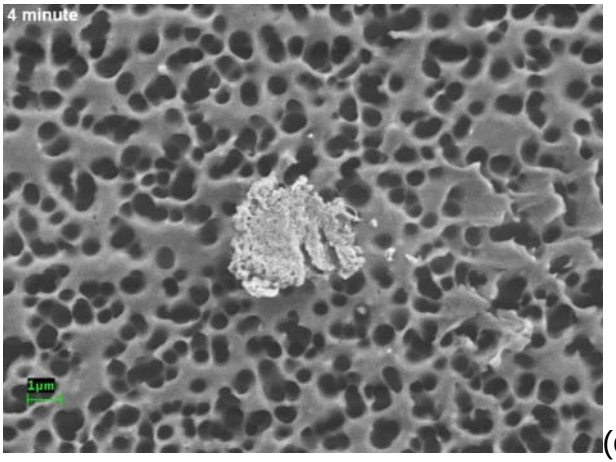

(c)

Figure 2.6—SEM images of A. niger: a) control, b) 1 minute direct OAUGDP exposure, c) 4 minutes direct OAUGDP exposure [AGT, 2006].

[Hunter, 2000] gives a review of current technologies employed for control of VOC emissions, including non-thermal plasma and various other techniques such as photocatalytic oxidation (PCO), whereby a UV activated photocatalyst such as TiO_2 creates OH radicals in the air stream which react with airborne VOC molecules. The use of non-thermal plasma as a means for controlling industrial process VOCs has substantial potential as a means for cutting manufacturing overhead costs associated with controlling unwanted byproducts that may cause regulatory compliance restrictions on manufacturing capacity or efficiency. A study by [Urashima, 2000] provides a review of recent work using non-thermal plasmas to destroy acid gasses (NOx, SOx) and VOCs. Findings indicate that the most promising area is likely the use of non-thermal plasmas in conjunction with catalytic material for low temperature oxidation [Oyama, 2004 & Seman, 2004].

CHAPTER 3—METHODOLOGY & OUTLINE OF ANALYSIS

3.1 Parameter Dependence of Plasma Generation and Efficacy

In this work, analysis is performed on the nature of a parallel cylinder plasma generator placed in a ducted air flow. The goal is to develop a reasonable system for measuring the efficacious effects of the plasma products on microorganisms (output of the system) that relates that output to relevant system inputs—fluid, thermal, electrical and geometrical. At the core of this effort is a parametric study intended to identify the important relationships between input parameters and output efficacy. The physics of the problem reveals a large number of input variables that must be accounted for if any true relationships to output are to be accurately measured or predicted.

Figure 3.1 shows a basic schematic of the problem with relevant inputs and outputs labeled. Air flows through a duct at some known velocity and passes over a set of parallel electrode plasma generators of known geometry and material properties. An electric field, sufficient to generate a glow discharge is established across paired electrodes. As air passes over these generators, reactions take place with the incoming air molecules and new chemistry is produced, including some very short lived species that do not survive outside the visible plasma region as well as longer lived species that convect well down

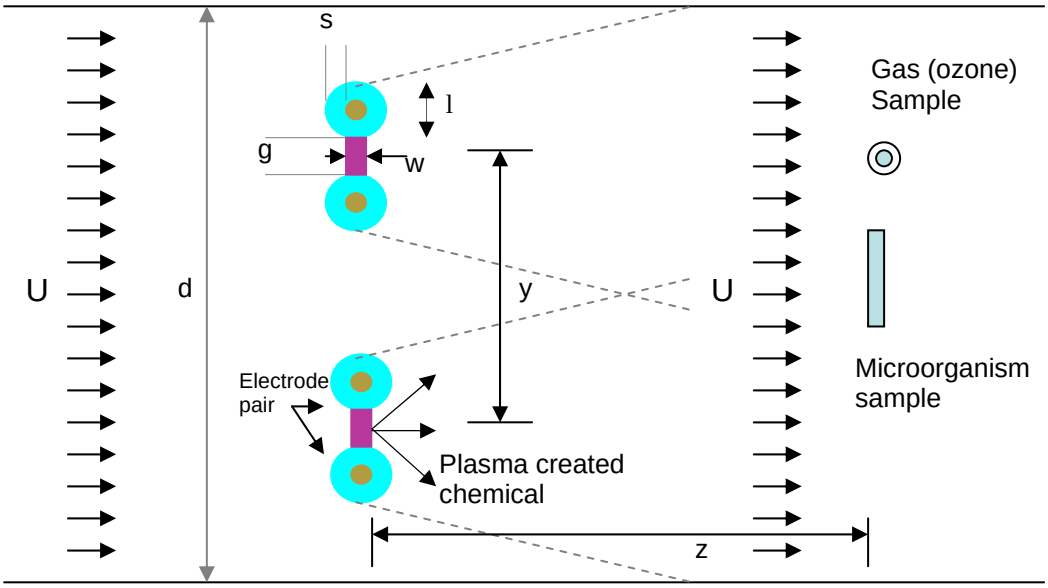

Figure 3.1—Schematic of plasma generation region.

stream. Most of the new chemical compounds are created endothermically and are prone to react further in pursuit of a lower energy state. These secondary reactions are of interest because they are useful downstream in the duct outside the active plasma region: e.g. to kill microorganisms, treat a material surface or react with airborne contaminant gases. As such, the plasma generator acts as a line source of chemicals and has a similar effect as a line source injector used in some continuous reactors. In the greater industry, there is interest in the chemistry generated directly in the active plasma region (the visible region immediately surrounding the electrodes) since it has many potential applications, particularly for surface treatment, but that topic is beyond the scope of this work. The focus of this study is to determine the relative importance of input

parameters on measured outputs of chemical generation or microorganism efficacy, while treating the plasma generation process as a pseudo black box.

At the plasma generator, an AC high frequency potential is established across the electrode gap. The alternating electric field across the gap locally accelerates free electrons and causes them to gain momentum over short distances. At a sufficient electric field strength, the electrons gain enough energy to cause reactions with neighboring molecules, which in turn react further with other electrons and other molecules causing a cascade electrical breakdown. The nature and rate of what is created in the reacting soup of the plasma discharge region is highly dependant on many input parameters.

Parallel cylindrical electrode plasma generators can be made in two ways: 1) with flexible wire pulled taught in a frame or 2) with straight rigid electrodes mounted in a frame. Flexible wire electrodes are limited to flexible dielectric coatings, usually hydrocarbon or silicone elastomers, whereas rigid electrodes may use the same elastomers or a variety of ceramic and glass dielectrics. The experimental portion of this work exclusively uses rigid electrode configurations with alumina dielectric. However the analysis is general to any selection of dielectric material and can be applied to rigid or flexible arrangements.

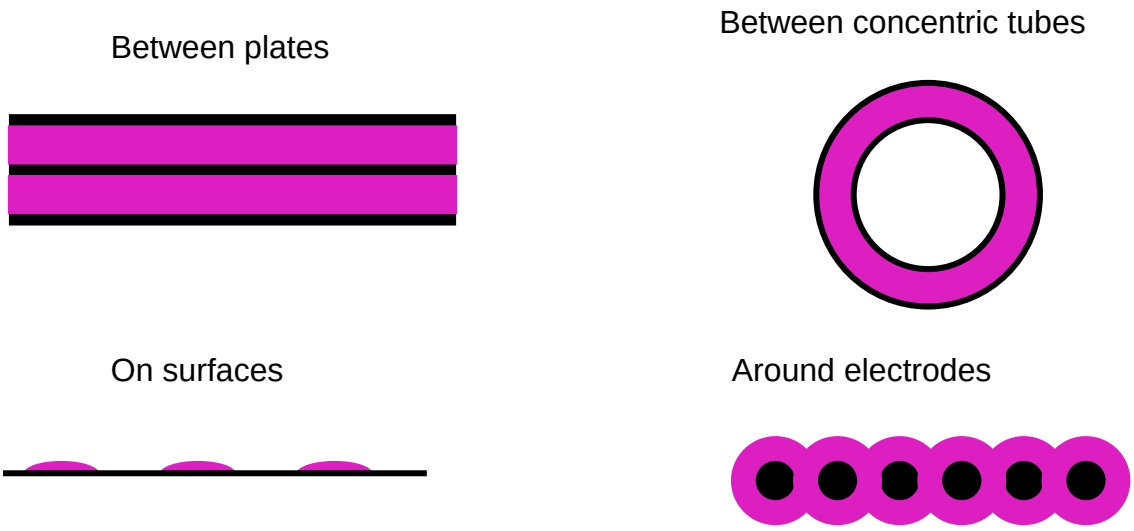

Figure 3.2—Plasma generation in various geometries.

The convention is to name plasma generators based on their structure (flexible or rigid) serially as they are constructed. Hence the generators discussed later in the document have designations such as Rigid #2, #5, #10 etc. Their geometric details are outlined.

Atmospheric plasma can be generated in a variety of geometries with the basic requirement that a sufficient electric field strength is imposed across a region of atmospheric pressure air or other gas. **Figure 3.2** show atmospheric plasma generated on a flat plate, between concentric cylinders and between parallel cylinders respectively.

In studying the efficacy of an atmospheric plasma generator against a challenge, the generator can, in a general sense, be regarded as a chemical species

generator. The generator produces some molar flux of chemical species and the magnitude of that flux and the resultant concentration of chemical species at a downstream treatment location is dependant on a lengthy list of variables including those describing the kinematics and geometry of the gas flow, the electrical input to the plasma generator and the material properties affecting electrical behavior.

$$\dot{N}_{species(i)} = f(P, U, d, g, V, f, \rho, K, \mu ...) \qquad [3.1]$$

Where:

$\dot{N}_{species(i)}$	->	molar rate of chemical production
P	->	power input to plasma
d	->	duct diameter
g	->	plasma gap
V	->	applied voltage to plasma reactor
f	->	applied frequency to plasma reactor
ρ	->	air density
K	->	dielectric constant
μ	->	air viscosity

There is a hierarchy of importance to the meaningful parameters, and some may have little or no effect on efficacy over ranges of interest. Where it is possible to shed light on the hierarchy, it will be done, but the main objective is to develop a systematic approach for exploration of variable dependencies.

The approach is to identify the variables of interest and to perform a dimensional analysis based on the Buckingham Pi Theorem to reduce the full parameter set to a set of dimensionless groups that are valuable in correlating efficacy to input variables. In **Chapters 5 & 6** experimental data is presented for ozone generation and for biological efficacy versus a challenge agent, *Bacillus atrophaeus,* and overlaid onto the dimensional analysis.

The nature of the problem—plasma generation of chemical species in a gas flow of some geometry, reacting with some challenge agent—is inherently complex because it involves different types of parameters: flow, electrical, material, chemical, biological, and others. A full analysis of all possible configurations is difficult, but analysis of distinct relationships for a particular configuration under a limited set of variables is possible and can be a basis for dimensionless analysis of other configurations. For this study, air flow at one atmosphere pressure, across a parallel cylinder plasma generator is considered. Refer back to **Figure 3.1** for a general schematic of the plasma generator and flow geometry that forms the basis for analysis.

This work is principally interested in biological efficacy as the desired result of plasma chemistry, and the chemical processes that yield this result are only beginning to be explored and understood. At this point plasma efficacy is still somewhat of a black-box model where the chemical mechanism of destruction is not known. It is reasonable to assume that some chemical (*species X*) is produced in the plasma which upon contact with the cell wall of a microorganism, reacts with it in a detrimental way, ultimately killing it. Whether there is only one *species X*, or many, and how they react with the organism is under investigation but not fully understood at this point. With the assumption that more interactions of *species X* with the microorganism will produce higher levels of efficacy, then the system of plasma generator and its surrounding airflow can be viewed as a generator in need of optimization for *species X*. If *species X* is not known, *(Species X may be different for different microorganisms, and different still for different processes)*, then the variable used to gauge effectiveness of the plasma generating system is efficacy.

Ideally, if the chemistry responsible for efficacy is known, then the chemistry could be measured in the mixed exhaust gas of the plasma discharge and input parameters could be tuned to provide the most efficient production of the desired chemical species. Even without knowing which chemicals are desired, the exhaust chemistry can be examined with a number of experimental tools. Specific gas concentration analyzers are available for some gasses such as ozone (O_3) and various N_xO_x compounds. Results are presented in **Chapter 5**

for a study of the nature of ozone generation as it depends on input parameters. Infrared and Raman spectroscopy offer the best methods for identifying and quantifying individual species that are created by a plasma reactor. Gaining a complete profile of the chemistry produced by the plasma is a tedious process for several reasons. The full extent and the nature of species being created are not usually known; for an air plasma there may be more than 100 newly created chemical species. Many of these species have extremely short lives (nano-microseconds) and never make it outside the direct region of plasma creation. Others may live for fractions of a second and decay quickly into neutral molecules or into other reactive and potentially useful species. There are numerous studies on the interactions of non-thermal plasma with contaminant gasses such as methane and halocarbons, but surprisingly few on the species creation in non-thermal air plasma under atmospheric pressure.

A generic model for the relationship of efficacy to input variables states that efficacy is a function of chemistry which is in turn a function of fluid kinematics, geometry and electrical variables:

$$\eta = f\left(chemistry\left(fluid, electrical, geometry\right)\right) \qquad [3.2]$$

Table 3.1 is a partial list of variables by category that may affect plasma generated chemical species in air.

Table 3.1—Variables affecting plasma chemical species generation.

Fluid			**Geometry**			**Electrical**		
variable	description	units	variable	description	units	variable	description	units
ν	viscosity		d	electrode diameter	L	V	voltage	
ρ	density	ML^{-3}	g	plasma gap	L	f	frequency	
U	velocity	LT^{-1}	S	duct diameter	L	P	power	
ω	humidity ratio		t	dielectric thickness	L	K	dielectric permittivity	
T	free-stream temperature	Θ				E	field strength	
ΔT	temperature rise	Θ						

This list assumes a fixed geometrical configuration, namely paired cylindrical electrodes in a cross-flow of air. Some features of the problem change for a different fundamental geometry like flow through an annular region between two concentric cylindrical electrodes, though the basic analytical approach remains the same.

3.2 Geometry and Flow Dependencies

Pressure driven room air flows through a duct to a fully developed laminar or turbulent state where it encounters a pair of cylindrical electrodes running perpendicular to the direction of flow. The pair of cylindrical electrodes is defined by the diameter of the individual electrodes (*l*) and by the gap spacing separating them (*g*). Air passing between the electrodes flows through a region of radio

frequency (RF) oscillating high electric field and undergoes electrical breakdown forming a visible plasma with a purple glow. Air convecting through the plasma region is chemically altered and exits the distil end of the plasma generator as a different mixture of chemicals comprised of a variety of Oxygen and Nitrogen species in various levels of excitation and other compounds that can be formed by the incoming components of moist air. The electrode pair acts as a one dimensional line reactor producing a two dimensional sheet or jet of products that mixes in the wake behind the electrodes with the bulk air flow that is bypassing the electrodes. The resulting chemical mixture that is convected downstream of the plasma reactor is the useful process stream that can produce some desired effect; for example killing microorganisms on a surface, reacting unwanted chemicals to more benign products or treating the surface of a material to alter a property such as wetability.

Bulk flow through the duct encounters the parallel cylinder electrodes. A fraction of the air stream flows through the plasma gap and the remainder flows through the un-energized space between electrode sets. A duct Reynolds number based on the characteristic duct diameter describes the bulk flow. For flow near electrodes, local Reynolds numbers can also be based on the characteristic lengths of the electrode geometry, namely, the electrode diameter (*l*) or the electrode gap (*g*). The details of flow kinematics through the plasma gap (g) are not explored in this work, as that is considered within the black box. Because of the high level of ionization and high electric field strength present in the gap,

description of the flow through the energized plasma region requires inclusion of magneto-hydrodynamic forces. However, earlier work by [Depaoli 2003] showed that killing across the duct cross-section was uniform at a downstream distance of approximately ten times the electrode pair spacing. This indicates that relevant chemical species created in the plasma line sources, diffuse and mix sufficiently in the downstream wake to have uniform efficacy over the entire cross-section. Tests were performed with challenge organisms placed at various distances downstream of a parallel electrode plasma generator. At close distances (<10 times the electrode pair spacing) results showed killing in striped regions over the cross-section, affected by the separated wakes from each electrode pair. Regions not in the wake of an electrode pair remained viable. At downstream distances greater than 10 times the electrode pair spacing, full killing was observed, indicating that chemical products had mixed sufficiently to provide killing over the entire cross-section. The distance after which full killing is reached is somewhat dependant on air velocity, but it was observed that this dependence is weak over the range between 50 fpm and 200 fpm (Re_d = $1.46x10^3$ – $6.7x10^3$). All experimentation for this work was performed at distances sufficiently downstream of the plasma generator to ensure uniform killing.

As neutral air travels into the active plasma region, some fraction of the molecules are chemically altered before they are convected out of the active region and begin mixing with the bulk air flow in the electrode wake. In the limit

of zero air velocity, there is no convection of newly created species out of the plasma volume, nor is there transport of new neutral molecules into the plasma volume. In this case, some equilibrium will be reached where a mix of chemical species are created and maintained at concentrations appropriate to the power, temperature, and other relevant parameters of the reactor. There will be continuous decomposition and re-creation of some species. As velocity is increased above zero, new neutral air molecules (N_2, O_2, Ar, CO_2, H_2O, etc.) are introduced to the plasma region, diluting the plasma and altering the energy content of the gas in the plasma volume. Likewise, new plasma generated species will be displaced out of the plasma volume and carry away some of the energy. Referring to **Figure 3.3**, a control volume analysis of the region surrounding the plasma generator yields the following conservation equations:

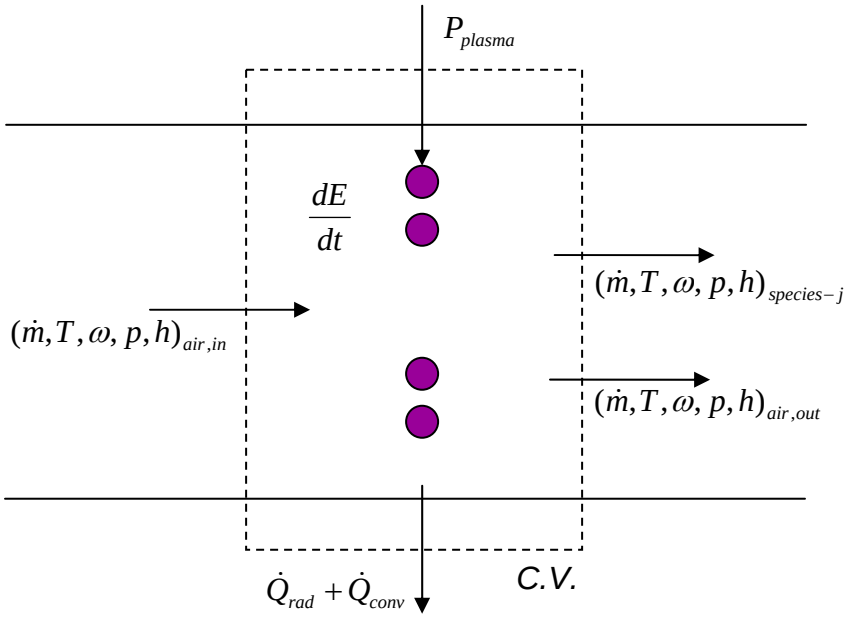

Figure 3.3—Control volume around a plasma generator in a ducted air stream.

Conservation of mass

$$\frac{dm_{cv}}{dt} + \sum \dot{m}_{out} - \sum \dot{m}_{in} = 0 \qquad [3.3]$$

The inlet and exit mass flow rates are summations of the constituent gasses; in the steady-state and with constant density, the mass balance reduces to;

$$\dot{m}_{in,cv} = \sum_m \dot{m}_{i,in} = \dot{m}_{out,cv} = \sum_n \dot{m}_{i,out} \qquad [3.4]$$

The second term represents the summation of the mass flow rates of each individual chemical species of the entering neutral air (N_2, O_2, Ar, etc.). 'i' is the index of species and 'm' is the number of individual species. Likewise, the fourth term represents the summation of the mass flow rates of each exiting chemical species where 'j' is the index and 'n' is the number of individual species. The exit stream is comprised of a greater number of species than the inlet stream because it includes any new species created in the plasma region. This is similar to a standard combustion reaction except that the exit stream may contain anywhere from a dozen to as many as one hundred additional species of varying decay rates.

Conservation of energy

$$\dot{m}_{in,cv} h_{in} + P_{plasma} - Q_{radiation} = \dot{m}_{out,cv} h_{out} \qquad [3.5]$$

where:

$$\dot{m}_{in,cv} h_{in} = \sum_m \dot{m}_i h_i \qquad [3.6]$$

and

$$\dot{m}_{out,cv} h_{out} = \sum_n \dot{m}_j h_j \qquad [3.7]$$

The first term in equation [3.5] is the energy flowing into the control volume carried by incoming air; equation [3.6] represents that term as a summation of energy content of each incoming chemical species. Likewise, the fourth term of equation [3.5] is the energy flowing out of the control volume and equation [3.7] represents the same as a summation of energy content of each exiting species.

In a non-reacting, steady-state fluid stream the energy transferred to or from the control volume is simply the mass flow times the change in enthalpy:

$$\dot{Q} = \dot{m} \Delta h \qquad [3.8]$$

For ideal gasses this reduces to simply the mass flow times the specific heat, times the temperature difference between the entrance and exit of the control volume.

In reacting fluid streams where the reactants and the products are known, the conservation of energy is derived on a molar basis as:

$$Q_{cv} + \sum_r n_i \bar{h}_i = \sum_p n_j \bar{h}_j \qquad [3.9]$$

Where subscript ‘r’ represents reactants and subscript ‘p’ represents products. The enthalpy terms are composites of the enthalpy of formation, $\bar{h}_f^\circ$ and the change in enthalpy from a reference state for the reactant state and the products.

In the plasma reactor system, many of the products are not known. For the small fraction of the products that are identified, measuring molar fractions for short lived species is difficult because the measurement technique is limited to the time order of the species lifetime. The first-law energy balance equation for reacting systems can be formulated as:

$$\dot{m}_{in,cv} h_{in} + P_{plasma} - Q_{radiation} = \sum_p n_{out} \left(\bar{h}_f^\circ + \Delta \bar{h} \right)_{out} \qquad [3.10]$$

The previous analysis is presented to give some insight into the process taking place within the plasma generator. This study looks at the effects and products of the plasma generation process, treating the generator as a black box, but it is important to keep in mind that all the processes follow the fundamental conservation laws. Measures of efficiency can be applied to the overall system, for instance, chemical production as a function of power input, without complete knowledge of the generation process. The control volume approach allows for checks to be made regarding the conservation of mass, energy and species, even with only a limited understanding of the plasma generation process.

3.3 Electrical and Material Dependencies

Electric field in the gap between electrodes is a function of applied voltage, dielectric thickness, dielectric permittivity and gap distance between the two closest tangent surfaces of opposite polarity electrodes. This is a simplified model and there are other factors at play including the frequency of oscillation and the curved nature of the electrode surfaces. In **Chapter 4**, dimensional analysis is applied to four variables, (voltage, V; dielectric thickness, s; permittivity, K; gap, g) but others can be considered in a similar manner.

Electric potential is applied between the conductors of two neighboring electrodes which creates a potential field between them, passing through both dielectrics and the air gap. Prior to initiation of plasma discharge, the electric

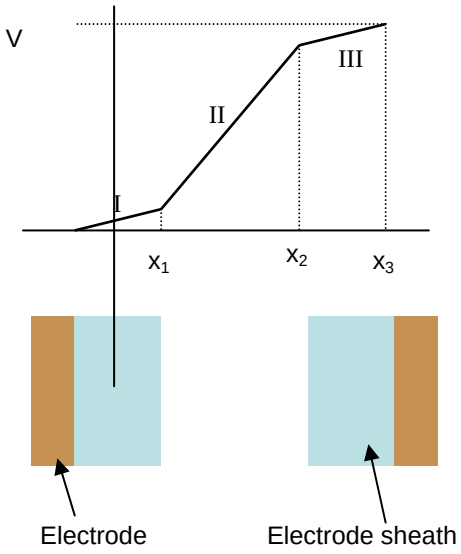

Figure 3.4—Instantaneous pre-ignition electric potential across three regions of dielectric.

field is present through three dielectric layers: electrode sheath, air, and electrode sheath. Calculation of instantaneous DC field strength in the air gap is reasonably straight forward and depends on the applied potential, the respective distances '*s*' and 'g' and on their respective permitivities. The higher the permittivity of the electrode sheath, the higher the field strength within the air gap. **Figure 3.4** shows a typical description of potential across an electrode pair where sheath permittivity is greater than that of air (> 1.0).

Regions I & III are electrode sheath dielectric and Region II is the air gap. The relative shallow slopes of the lines in regions I & III shows that the charge build-up on the conductor imparts buildup of the opposite charge relatively easily

through the sheath dielectric and concentrates the field in the air gap. Higher sheath permittivity for a constant geometry will produce higher field within the air gap and in turn lower voltage is necessary to form plasma.

In a sense, the effect of the dielectric sheath is to extend the charge concentration from the conductor further out into the gap, reducing the gap over which the charge imposes a field. Unlike the conductor, the charge on the dielectric is bound tightly and reduces the propensity for arcing. Materials with higher dielectric constant materials are better able to transmit charge and approximate the behavior of a conductor, while maintaining bound charge. An electric field generated between two conducting plates separated by an air gap with a charge distribution imposed on them by some voltage, V has field lines normal to the electrode surfaces. If a second conductor is placed between the plates but is not touching them, the charges on the new conductor will redistribute such that equal and opposite charges face the original conductors. If the applied voltage is maintained, then more charge will build up on all the conductor surfaces creating higher field strength in the remaining gaps. The voltage/charge relationship is:

$$V = \frac{\sigma}{\varepsilon_0}(d - b) \qquad [3.11]$$

Where σ is the charge distribution on the original conductors, and the electric field (*E*) in the air gap is σ/ε_0. With a conductor in the gap, the charge redistribution is nearly perfect meaning that all of the charge on the original conductors creates an opposite charge on the new conductor, without any resistance to the imposition—the charges simply flow around and assume a new distribution. In a dielectric, there is resistance to the redistribution of charge which is characterized by the electric susceptibility χ and represented by the polarization vector $\vec{P}$, where:

$$\vec{P} = \chi \varepsilon_0 \vec{E} \qquad [3.12]$$

and $\vec{E}$ is the field within the dielectric, resultant from any external field plus the field created by polarization within the dielectric. The dielectric constant K is defined as:

$$K = (1 + \chi) = \frac{\varepsilon}{\varepsilon_0} \qquad [3.13]$$

It is simply the ratio of the permittivity of the dielectric material to the permittivity of free space. The higher the dielectric constant of a material, the more able, or "susceptible" it is to allow internal charge to redistribute and, in effect, transfer the charge of the conductor to the opposite face of the dielectric where it helps to

establish field in the gap. This general model leads to the conclusion that a higher K material on a plasma generator electrode will allow plasma initiation at a lower total applied voltage than a low K material—of the same thickness. Or, stated slightly differently, the higher K material will enable the same field strength in the gap with a lower applied voltage to the electrodes. Dielectric properties do not necessarily change the power consumption of a plasma device for a given amount of chemistry produced, but they affect the amount of power that can be put into a device given a limitation on available voltage. Thorough explanations of the electrostatics and electrodynamics of dielectric materials are available in a variety of texts [Griffiths, 1989 and Feynman, 1964].

Plasma formation by an AC potential is dynamic and the simple model above is far from describing the entirety of the problem. Once plasma is initiated, the air changes from dielectric to conductor and the electric field structure changes. Also, a cycle of charge build up, plasma ignition, full plasma and quenching happens twice per cycle of the applied voltage; for instance at 8kHz, there are 16,000 plasma initiations per second.

A deeper understanding of the electrical and material physics of OAUGDP plasma generation will be of great benefit in optimizing plasma generators to produce desired chemistry. That coupled with further understanding of the chemical and biochemical reactions occurring at the reaction site (airborne

contaminants, material surface, etc.) will enable optimization of plasma systems to achieve desired results.

3.4 Experimental Design

In order to test and optimize the parallel electrode plasma generator and its resultant chemistry generation and biological efficacy, an experimental approach and in turn an experimental test stand were developed. The experimental approach is to identify key system input variables and determine important output variables that quantify system performance. These variables are cast in dimensionless form and discussed in **Chapter 4**.

Two sets of experiments were conducted to test (a) ozone generation and (b) efficacy against *Bacillus atrophaeus* placed downstream of the plasma reactor. For both cases, controlled experiments were performed based on developed Pi groups. Inlet air flow conditions in both cases were allowed to reach equilibrium (defined as constant duct air temperature (±1.0°C) and constant inlet air humidity, defined as 45 grains of water [±2 grains]) before plasma was energized.

3.4.1 Test Stand Design and Fabrication

Two ducted air test stands were designed and constructed over the course of approximately twelve months to enable multiple input parameter sweeps for

testing plasma chemical production and resultant efficacy on exposed microorganisms and/or airborne chemicals. The system design provides maximum flexibility for control and measurement of input and output variables. The stands are capable of controlling the inlet air state and velocity, the concentration of contaminant (gas or bioaerosol) and plasma input power conditions. The systems are designed to be easily adapted for a variety of ducted air testing requirements, including filtration efficiency, catalyst efficiency and other needs that are not covered in this document, but that are in the interest of furthering the study of airborne contaminant removal or destruction. The two test stands, Plasma Test Stand-1 (PTS-1) and PTS-2 are similarly constructed as small ducted air systems with wide range control over the process air state, velocity and contaminant concentration level. The stands are highly modular and can be adapted for a variety of testing needs including gas analysis, biological efficacy measurement, chemical destruction efficacy measurement and air flow analysis. The stands were generally designed to be used with parallel electrode plasma generators, but can be adapted to use any generator suitable for ducted air environments. A detailed description of the design, components and operation of the two PTS test stands is given in **Appendix I** The following is a summary description.

The PTS stands are scaled versions of HVAC style ducted air systems with fine control of the process air state and with substantial provisions for measurement of air and plasma conditions. The main test sections are 4” x 4” (interior

dimensions) acrylic duct with flanged ends for easy change out and matching with additional duct sections. A schematic of PTS-I is shown in **Figure 3.5**. Air is forced through the duct sections by a combination compressed air at the inlet and vacuum at the outlet, enabling the test section to be maintained at positive pressure, negative pressure or near zero psi Δp, with respect to ambient. Entering compressed air passes through a desiccant air dryer, a High Efficiency Particulate Arrestance (HEPA) particulate filter and a granulated activated carbon bed for VOC filtration, providing clean, dry air to the conditioning section. In the conditioning section, a Proportional, Integral, Derivative (PID) controlled humidifier and air heater bring the process air to a desired steady-flow state. Process air can be maintained in the ranges of 60°F – 180°F and ~5 - 150 gr. For colder testing conditions a pre-cooler can be added to the inlet compressed air line, or to the inlet duct section. Testing has concentrated with air at room temperature hotter ranges with no pre-cooler used.

Process air temperature is controlled by an electric resistance heater in the inlet duct section powered via a PID controlled Silicon Controlled Rectifier (SCR) heater relay with temperature feedback from a type-K thermocouple in the process duct.

Injection ports for contaminant gasses for chemical destruction testing, and an aerosolization port for bioaerosol injection are positioned downstream of the

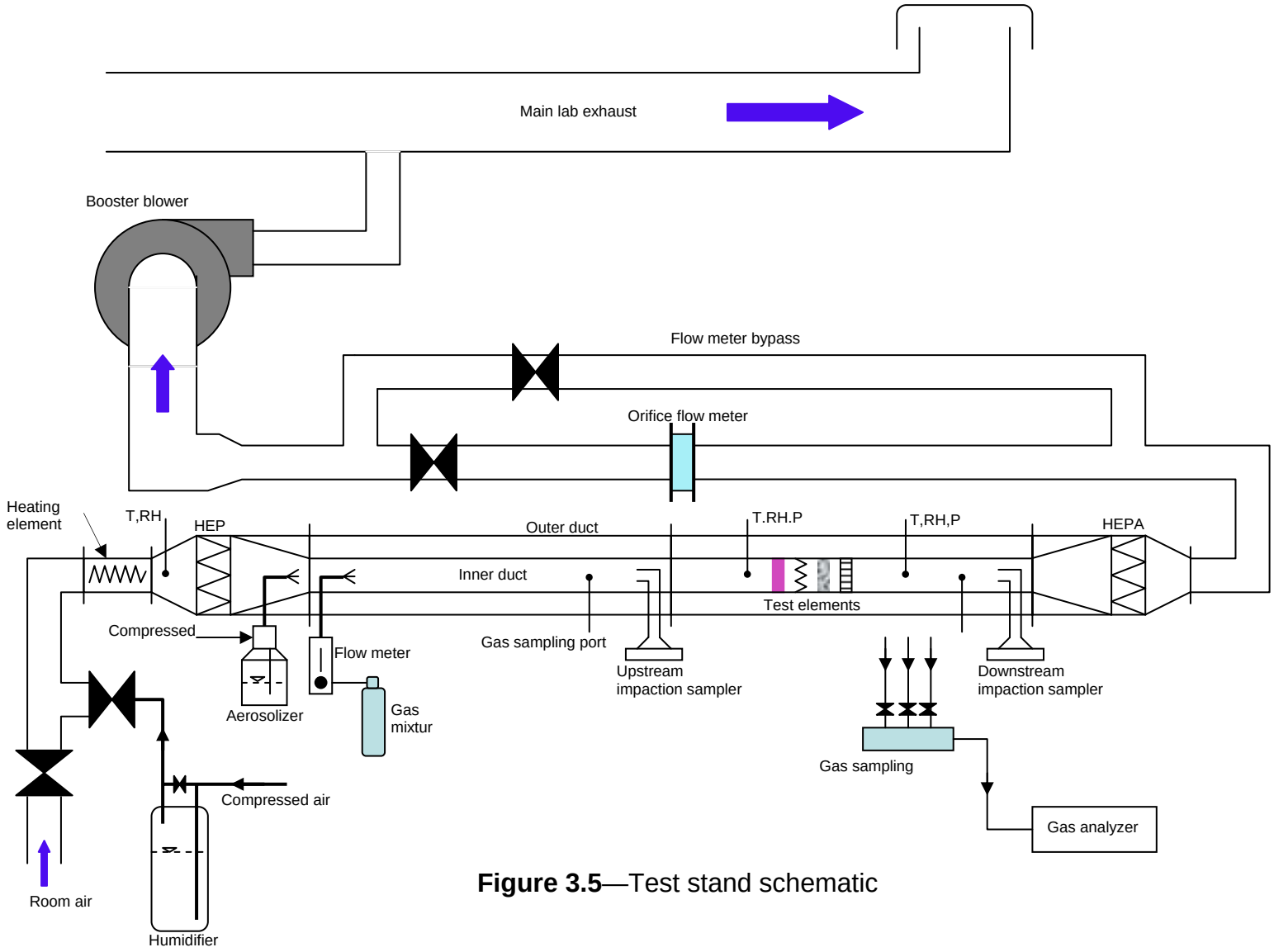

Figure 3.5—Test stand schematic

conditioning section. Contaminant gases (such as VOCs) can be metered through the four port manifold into the process stream approximately six feet upstream of the plasma test section. A contaminant source can be either bottled gas, such as acetone-doped compressed nitrogen, or an air stream bubbled through a contaminant liquid. Bioaerosols can be introduced to the air stream with a nebulizer or a atomizer connected to a ½" diameter stainless-steel inlet port located along the center axis of the duct, also approximately six feet upstream of the plasma test section. A static mixer and a small DC fan are located approximately 6 inches downstream of the chemical and bioaerosol inlet ports to provide thorough mixing of the air stream.

A four foot straight duct section follows the contaminant injection section and allows for mixing of the air stream and development of the flow cross section. This section of duct has ports for temperature, humidity and air velocity measurement and for upstream air sampling. Chemical sampling is done through ¼" ports with polytetrafluoroethylene (PTFE) sampling tubes and biological sampling is done with a single stage Anderson impaction sampler. A similar sampler is positioned downstream of the plasma test section.

The plasma test section consists of selectable modular units that are sandwiched together into a desired test configuration. Components include:

1) plasma generator

2) particulate filtration module

3) gas adsorption module

4) ozone catalyst

5) gas sampling module

6) air heater

7) biological exposure module

8) temperature/instrumentation module

Any desired combination and order of these component modules can be built up and placed in the test section of the stand per the needs of a particular test. **Figure 3.6** shows a schematic and **Figure 3.7** shows a picture of the test section for ozone generation and catalytic removal testing.

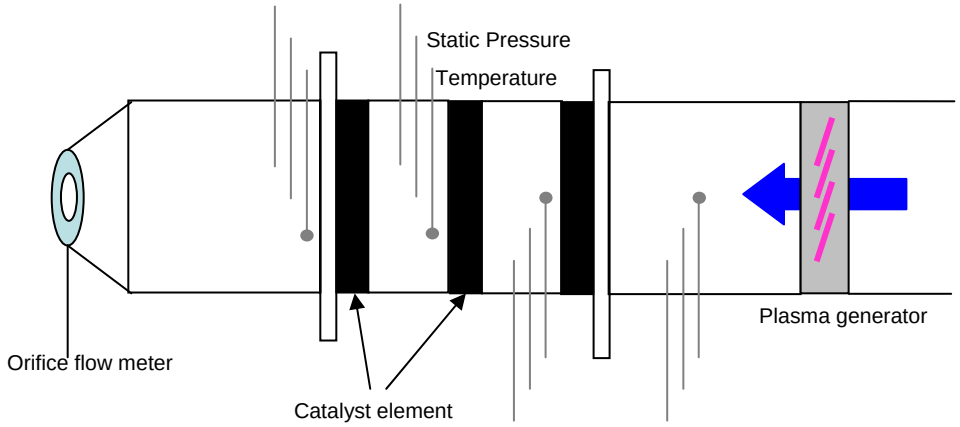

Figure 3.6—Schematic of ozone generation and catalytic destruction test setup.

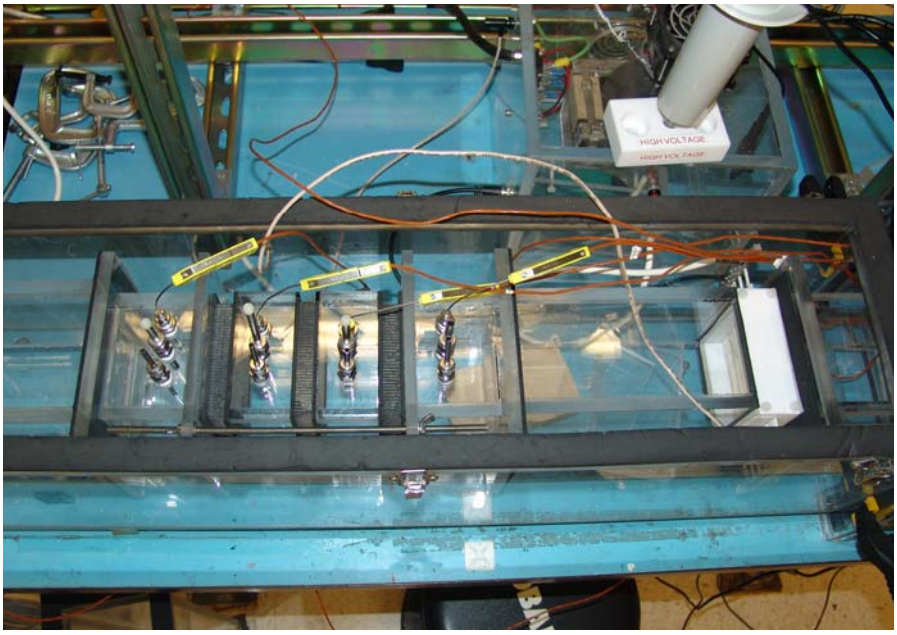

Figure 3.7—Picture of ozone generation and catalytic destruction test setup.

CHAPTER 4—DIMENSIONAL ANALYSIS

4.1 Definition of Parameters

Dimensional analysis was performed on a parallel cylindrical plasma arrangement in a ducted airflow according to the Buckingham Pi Theorem. This method produces solutions which are non-unique, but rather guided by intuition and knowledge of the physics of the problem which is in turn reflected by the Pi groups. Nineteen variables were identified as having distinct relevance to the behavior of the system of interest, as detailed in **Chapter 3**. These nineteen variables are listed in **Table 4.1**, and are categorized in **Table4.2** as either material/fluid properties, geometric variables, input variables or measured variables. Repeating variables for this analysis were chosen to be: inlet air temperature (t_i), air density (ρ), fully developed duct velocity (U), duct diameter (d) and dielectric constant (K). This set represents all five fundamental dimensions (mass, time, length, charge and temperature), but does not produce a Pi group without the inclusion of a sixth variable. Repeating variables for Buckingham Pi analysis are highlighted in **Table 4.2**. The measured output variables include power, which may also be considered an input (externally imposed) depending on how experiments are operated. If power is set as an input value, then voltage, frequency or gap may become a dependant output variable. For the sake of this analysis, power is considered an output variable. The two principal output variables that define system performance are the

Table 4.1—Variable set considered for dimensional analysis.

	Variable	Description	Units	
1	U	velocity	LT^{-1}	
2	P	power	ML^2T^{-3}	
3	l	electrode diameter	L	
4	g	electrode gap	L	Dimensions:
5	s	dielectric thickness	L	**M**: mass
6	w	plasma width	L	**L**: length
7	d	Duct diameter	L	**T**: time
8	ρ	air density	ML^{-3}	**C**: charge
9	N	generation rate	MT^{-1}	**Θ**: temperature
10	μ	viscosity	$MT^{-1}L^{-1}$	
11	K	dielectric permitivity	$C^2M^{-1}L^{-2}T^2$	
12	E	electric field	$MLT^{-2}C^{-1}$	
13	ω	specific humidity		
14	V	voltage	$ML^2T^{-2}C^{-1}$	
15	t_i	inlet air temperature	Θ	
16	T	exposure time	T	
17	Δt	t-ti	Θ	
18	c_p	specific heat	$M^{0}T^{0}\Theta^{-1}$	
19	η	efficacy		

Table 4.2—Variable groupings.

Externally imposed	Property	Geometric	Output (measured)
E	ρ	l	P
ω	μ	g	N
V	K	d	Δt
t_i	c_p	s	η
T		w	
U			

Indicates repeating variable for Buckingham Pi analysis

chemical generation rate (N) and the biological efficacy (η); temperature rise (Δt) is a consequence of power addition to the fluid.

There are five fundamental dimensions shared by the 19 independent variables: mass (M), length (L), time (T), electric charge (C) and temperature (Θ). The independent variables were chosen based on their relevance to the physics of the ducted plasma/air system as derived in **Chapter 3**. The variable list is sufficient for the specific intent of this analysis, namely the study of chemical generation and microorganism efficacy in ducted air stream, but does not include all possible variables. More focused parts of the problem could be further derived into constituent variable sets that capture more fundamental physics, for instance related to chemical reactions either within the plasma volume or at the reaction substrate (on the surface of a microorganism). The current approach treats plasma generation as a control volume, or a pseudo black box where such macroscopic parameters as plasma power, plasma gap and dielectric thickness are considered, but the resulting analysis does not describe the intermediate physics within the plasma volume. This is also true at the reaction substrate, where no insight is implied, for instance, about the mechanisms of destruction of a microorganism. Both the mechanisms for plasma / chemical species creation in the plasma volume, and the substrate reactions warrant independent analysis by similar techniques with appropriately derived variable sets based on the physics of the process. Other variables which are not considered in this work may be appropriate for additional study including variables which further define

the manner in which power is applied to the plasma generator and those which affect conversion of input power to electric field in the plasma gap.

4.2 Application of the Buckingham Pi Theorem

According to the Buckingham Pi Theorem, and proved later by Langhaar (1951), a set of homogeneous variables defining a system and sharing a fundamental set of dimensions may be recast into a finite set of dimensionless groups. The number of dimensionless groups is equal to the number of independent variables minus the number of dimensions:

$$p = n - m \qquad [4.1]$$

Where n is the number of independent variables, m is the number of fundamental dimensions and p is the number of possible independent dimensionless groups. The dimensionless groups (p), or Pi groups, are designated as $\Pi_1, \Pi_2, \Pi_3 \ldots \Pi_p$. The dependence of n independent variables is related by:

$$(N_1^{a_1})(N_2^{a_2})(N_3^{a_3})\ldots(N_m^{a_m})\ldots(N_n^{a_n}) = \prod_i \qquad i = 1,2,3\ldots p \qquad [4.2]$$

where N_i represents the fundamental dimensions of a variable and a_i is a corresponding fractional exponent. The problem at hand has 19 independent

variables and with five available dimensions, a total of 14 dimensionless Π groups are expected.

Five repeating variables were selected from the 19 independent variables: air velocity (U), duct diameter (d), air density (ρ), dielectric permittivity (K) and temperature rise (Δt). The repeating variables are selected such that they collectively represent all five dimensions, but that they do not together form any dimensionless groups and the addition of any sixth variable will result in a dimensionless group. Two of the 19 variables are already dimensionless—efficacy (η) and humidity ratio (ω)—and are therefore defined as Π_1 & Π_2 respectively. The remaining groups, Π_3 – Π_{14} are determined through a formal scheme where the five repeating variables and one non-repeating variable are substituted into eqn. [4.2] and the respective exponents are solved. This is repeated 12 times to find all of the fundamental dimensionless groups. Certain groups are relatively obvious and can be determined by visual inspection, these include:

$$\Pi_3 = \frac{\Delta t}{t_i} \qquad [4.3]$$

and the four length ratios:

$$\Pi_4 = \frac{l}{d} \qquad [4.4]$$

$$\Pi_5 = \frac{g}{d} \qquad [4.5]$$

$$\Pi_6 = \frac{s}{d} \qquad [4.6]$$

$$\Pi_7 = \frac{w}{d} \qquad [4.7]$$

The remaining groups are found according to the following example method using electric field (E) as the non-repeating variable to find Π_{11}. The general form of the equation to solve for Π_i is:

$$(R_1^{a_1})(R_2^{a_2})(R_3^{a_3})(R_4^{a_4})(R_5^{a_5})(N_i) = \Pi_i \qquad [4.8]$$

Or substituting U, d, ρ, K, Δt for the repeating variables and E for the non-repeating variable:

$$(U^{a_1})(d^{a_2})(\rho^{a_3})(K^{a_4})(\Delta t^{a_5}) \times (E\ ) = \Pi_{11} \qquad [4.9]$$

The exponents are found by solving simultaneous equations for each dimension. Substituting dimensions into eqn. [5.8] and setting the product equal to zero gives:

$$(LT^{-1})^{a_1}(L)^{a_2}(ML^{-3})^{a_3}(C^2M^{-1}L^{-2}T^2)^{a_4}(\Theta)^{a_5} \times (MLT^{-2}C^{-1}) = 0 \qquad [4.10]$$

Separating dimensions yields five equations:

$$L: \ a_1 + a_2 - 3a_3 - 2a_4 + 1 = 0 \qquad [4.11]$$

$$M: \ a_3 - a_4 + 1 = 0 \qquad [4.12]$$

$$T: \ -a_1 + 2a_4 - 2 = 0 \qquad [4.13]$$

$$C: \ 2a_4 - 1 = 0 \qquad [4.14]$$

$$\Theta: \ a_5 = 0 \qquad [4.15]$$

Equations [4.15] and [4.14] give $a_5 = 0$ and $a_4 = ½$. Using these results in [4.12], [4.13] and [4.11] give $a_3 = -1/2$ and $a_2 = -1/2$. Substituting the exponents into equation [4.9] gives the dimensionless Π_{11} group.

$$(U^{-1})(d^{-1/2})(\rho^{-1/2})(K^{1/2}) \times (E\ ) = \Pi_{11} \qquad [4.16]$$ or

$$\Pi_{11} = \frac{K^{1/2} E}{U^1 d^{1/2} \rho^{1/2}} \qquad [4.16a]$$

This dimensionless group is the relative strength of the imposed electric field to air mass transport.

Repeating the process for the remaining six non-repeating variables (P, N, μ, V, T, c_p) yields the following Π groups:

$$\Pi_8 = \frac{\rho U d}{\mu}$$ -> Duct Reynolds Number [4.17]

$$\Pi_9 = \frac{P}{U^3 \rho d^2}$$ -> Dimensionless input power [4.18]

$$\Pi_{10} = \frac{N}{U d^2 \rho}$$ -> Dimensionless rate of species generation [4.19]

$$\Pi_{12} = \frac{V K^{1/2}}{U d^{3/2} \rho}$$ ->Dimensionless gap voltage [4.20]

$$\Pi_{13} = \frac{UT}{d}$$ ->Dimensionless exposure time [4.21]

$$\Pi_{14} = \frac{c_p \Delta t}{U^2}$$ ->Dimensionless heat gain [4.22]

The calculation of Π groups is summarized in **Table 4.3**. Π_8 is immediately recognizable as the Reynolds number based on the duct diameter (Re_d). Reynolds number for flow around an electrode is found by multiplying Re_d (Π_7) by the electrode-to-duct diameter ratio l/d (Π_4).

$$\Pi_8 \times \Pi_4 = \left(\frac{\rho U d}{\mu}\right)\left(\frac{l}{d}\right) = \left(\frac{\rho U l}{\mu}\right) = \mathrm{Re}_l$$ [4.23]

Table 4.3—Dimensionless Π groups.

Repeating		Non-repeating			Dimensionless	
Variable	Dimension	Variable	Dimension	Π groups	Variable	Description
$U_o^{a_1}$ d ρ^c K^a Δt^e	(LT^{-1}) (L) (ML^{-3}) $(C^2M^{-1}L^{-2}T^2)$ (Θ)					
				Π_1	ω	specific humidity
				Π_2	η	efficacy
		t_i	Θ	Π_3	$\Delta t/t_i$	temperature rise
		l	L	Π_4	l/d	dimentionless electrode diameter
		g	L	Π_5	g/d	dimentionless electrode gap
		s	L	Π_6	s/d	dimentinless dielectric thickness
		w	L	Π_7	w/d	dimentionless plasma width
		μ	$MT^{-1}L^{-1}$	Π_8	$\rho Ud/\mu$ (Re)	duct Reynolds Number
		P	ML^2T^{-3}	Π_9	$P/U^3\rho d^2$	dimentionless input power
		N	MT^{-1}	Π_{10}	$N/Ud^2\rho$	dimentionless rate of species generation
		E	$MLT^{-2}C^{-1}$	Π_{11}	$EK^{1/2}/Ud^{1/2}\rho^{1/2}$	dimentionless field strength
		V	$ML^2T^{-2}C^{-1}$	Π_{12}	$VK^{1/2}/Ud^{3/2}\rho^{1/2}$	dimentionless gap voltage
		T	T	Π_{13}	UT/d	dimentionless exposure time
		C_p	$M^2T^{-2}\Theta^{-1}$	Π_{14}	$C_p\Delta t/U^2$	dimentionless heat gain

Reynolds number for flow through the electrode gap is found in a similar way:

$$\mathrm{Re}_g = \left(\frac{\rho U g}{\mu} \right) \qquad [4.24]$$

Reynolds numbers can be established based on various length scales. However, the most relevant Reynolds numbers related to the physics of the flow are based on *g* and *d*. Ten total length ratios are possible, Π_4, Π_5, Π_6 Π_7, plus six additional formed by their respective combinations:

$$\frac{\Pi_4}{\Pi_5} = \frac{\left(l/d \right)}{\left(g/d \right)} = \frac{l}{g} \qquad [4.25]$$

$$\frac{\Pi_6}{\Pi_4} = \frac{\left(s/d \right)}{\left(l/d \right)} = \frac{s}{l} \qquad [4.26]$$

$$\frac{\Pi_6}{\Pi_5} = \frac{\left(s/d \right)}{\left(g/d \right)} = \frac{s}{g} \qquad [4.27]$$

$$\frac{\Pi_4}{\Pi_7} = \frac{\left(l/d \right)}{\left(w/d \right)} = \frac{l}{w} \qquad [4.28]$$

$$\frac{\Pi_5}{\Pi_7} = \frac{\left(g/d \right)}{\left(w/d \right)} = \frac{g}{w} \qquad [4.29]$$

$$\frac{\Pi_6}{\Pi_7} = \frac{\left(s/d\right)}{\left(w/d\right)} = \frac{s}{w} \qquad [4.30]$$

Equations [4.25] and [4.26] relate to the geometry of the electrode arrangement. [4.25] is the ratio of electrode electrode gap to electrode diameter and is influential in both determining the flow field in the vicinity of the electrodes and in the dynamics of plasma formation. For l/g >> 1, electrode diameter is large relative to the plasma gap and the region of plasma generation approaches that formed by parallel planar electrodes. As seen in **Figure 4.1**, the plasma region thickens in the direction of the tangent, and for a constant gap length plasma volume increases as l/g grows. For l/g <<1, the problem approaches point source electrodes with a long thin plasma region as shown in **Figure 4.2**.

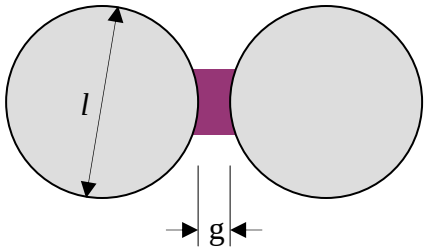

Figure 4.1-- g/l **<<1**

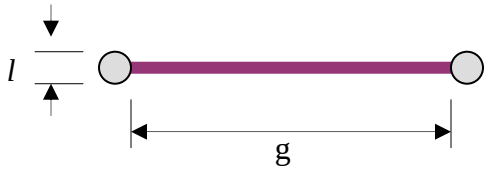

Figure 4.2-- g/l **>>1**

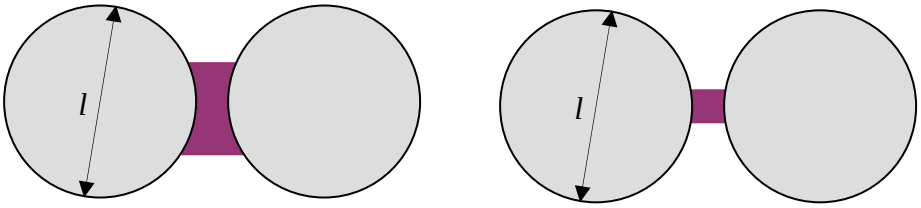

(a) (b)

FIgure 4.3—Characteristic of plasma volume ratio (c_1): $c_1(a) > c_1(b)$

Energized plasma volume follows a relationship:

$$c_1(l \cdot g) = Vol \qquad [4.31]$$

where c_1, valued between zero and one, characterizes the width of the plasma region (in the flow direction) relative to l, as shown in **Figure 4.3**. For small gap lengths, where the plasma width is on the order of g, the curvature of the electrode surface distorts the volume relationship.

Π_9 ($P/U^3\rho d^2$) is the ratio of power input to the plasma generator versus the rate of kinetic energy, or the power, of the gas flowing through the duct and past the plasma generator. The length '*d*' is the duct diameter and is independent of the presence of a plasma generator, such that the denominator of Π_9 is strictly a function of flow through the duct. In a limiting case where the duct diameter (*d*) is equal to the plasma gap (*g*), then the denominator ($U_3\rho d^2$) reflects the kinetic energy rate of gas flow through the plasma generator. This specific case is not addressed in this study but is of interest because it further confines variables about the plasma generation air flow system. In the cases tested experimentally, the actual portion of air flowing through a given electrode set is unknown; this is one of several reasons for treating the plasma generator as a pseudo black box, and making measurements sufficiently far upstream or downstream of the generator to ensure that the air stream is well mixed.

Π_{10} ($N/Ud^2\rho$) is the ratio of chemical generation versus mass flow of gas through the duct. N can represent any chemical species of interest and has units of mass generated per unit time. It may be convenient to consider chemical generation in terms of moles per unit time by dividing by the molecular weight of a particular species—for instance ozone at 48 kg/km—but for consistency of analysis, mass units were used. Since there are many new chemical species generated by the plasma reactor, N represents many and possibly hundreds of species generation

rates. N, and in turn, Π_{10} should be referenced to the particular chemical species of interest—e.g. N_{O_3} or Π_{10,O_3}.

Π_{11} ($EK^{1/2}/Ud^{1/2}\rho^{1/2}$) and Π_{12} ($VK^{1/2}/Ud^{3/2}\rho^{1/2}$) relate the electric properties of the plasma generator to the kinematics of flow through the duct. The scaling distance was chosen to be '*d*' for the sake of computation, but dividing by *(l/d)*, *(s/d)*, or *(g/d)* (raised to ½ for Π_{11} or 3/2 for Π_{12}) will reference them to '*l*', '*s*', or '*g*' respectively. Together Π_9, Π_{11} & Π_{12} form three ratios of plasma electrical input to flow kinematics:

$$\Pi_{11} = \frac{K^{1/2}E}{U^1 d^{1/2}\rho^{1/2}} \qquad [4.32]$$

$$\Pi_{12} = \frac{K^{1/2}V}{U^1 d^{3/2}\rho^{1/2}} \qquad [4.33]$$

$$\Pi_9 = \frac{P}{U^3 d^2 \rho} \qquad [4.34]$$

4.3 Summary of Dimensional Analysis

Nineteen variables were determined to be physically relevant to the problem of measuring chemical generation and microorganism efficacy by atmospheric plasma in a ducted air flow. Those 19 variables were recast into dimensionless

form by applying the Buckingham Pi Theorem and resulted in 14 dimensionless groups. Of the 14 Pi groups, several are fixed due to the apparatus design specifications and effects of several Pi groups (Π_4, Π_5, Π_6, Π_7) can be expressed by one ratio: Π_5/Π_4 = g/l. Other Π groups will have to be assumed invariable due o either fixed ambient conditions (Π_1) or are excluded from specific measurement (Π_3, Π_{11}, Π_{12}, Π_{14}). The design of experiments and experimental results proved that the key remaining groups are:

Chemical Generation

Π_8	$\frac{\rho U d}{\mu}$	Duct Reynolds Number
Π_9	$\frac{P}{U^3 \rho d^2}$	Power Flow Number
Π_{10}	$\frac{N}{U \rho d^2}$	Generation Flow Number
$\frac{\Pi_5}{\Pi_4}$	$\frac{g}{l}$	Gap to Diameter Ratio

Microorganism Efficacy

Π_2		Efficacy
Π_{13}	$\frac{UT}{d}$	Dimensionless Exposure Time

CHAPTER 5—EXPERIMENTAL RESULTS FOR CHEMICAL GENERATION

A variety of experiments were performed to measure rates of ozone generation under various input conditions, changing velocity (Reynolds number), voltage, frequency, power and relative humidity. Results are generally presented in dimensionless form with the exception of presenting some dimensional results only to illustrate a detail. In the previous chapter dimensionless group Π_{10} was derived as a measure of chemical species generation and given the name Generation Flow Number:

$$\Pi_{10,i} = \frac{N_i}{Ud^2\rho} \qquad [5.1]$$

Where *i* represents a particular species, which in this chapter is selected to be ozone. $\Pi_{10,ozone}$ is the rate of mass generation of ozone divided by the rate of mass flow of air across the plasma generator and. Experiments were performed according to the procedures and with the instrumentation discussed in **Chapter 3**.

5.1 Ozone Generation

Power input to the plasma generator is dependant on the applied voltage and frequency, but in terms of the electrical input variables, ozone generation appears to be solely dependant on power input. **Figure 5.1** shows Generation Flow Number (Π_{10}) as a function of Power Flow Number (Π_9) parametrically with applied frequency at a Duct Reynolds Number of 1.46×10^3 for various values of frequency. The results show that there is no apparent dependence on frequency. The same is true for applied voltage. Increases or decreases in ozone generation due to a change in applied voltage or frequency relates directly to the associated power change, and effects of voltage and frequency have no independent effect over the ranges tested. The dependence of power on applied frequency and voltage were determined by independent tests. Dimensional plasma power input depends nearly linearly on applied frequency (**Figure 5.2**) and to approximately the third power of voltage (**Figure 5.3**). On both graphs, power is in units of Watts per centimeter of energized electrode pair. **Figure 5.4** is a graph of Generation Flow Number (Π_{10}) versus Power Flow Number (Π_9) at $Re_d = 1.46 \times 10^3$, with voltage and frequency recast in terms of dimensionless power. On the left half of the curve, ozone generation increases approximately linearly with increasing power input through $\Pi_9 \sim 4 \times 10^5$, and reaches maximum generation at $\Pi_9 = 7.6 \times 10^5$. Further increases in marginal power input produce diminishing returns of ozone

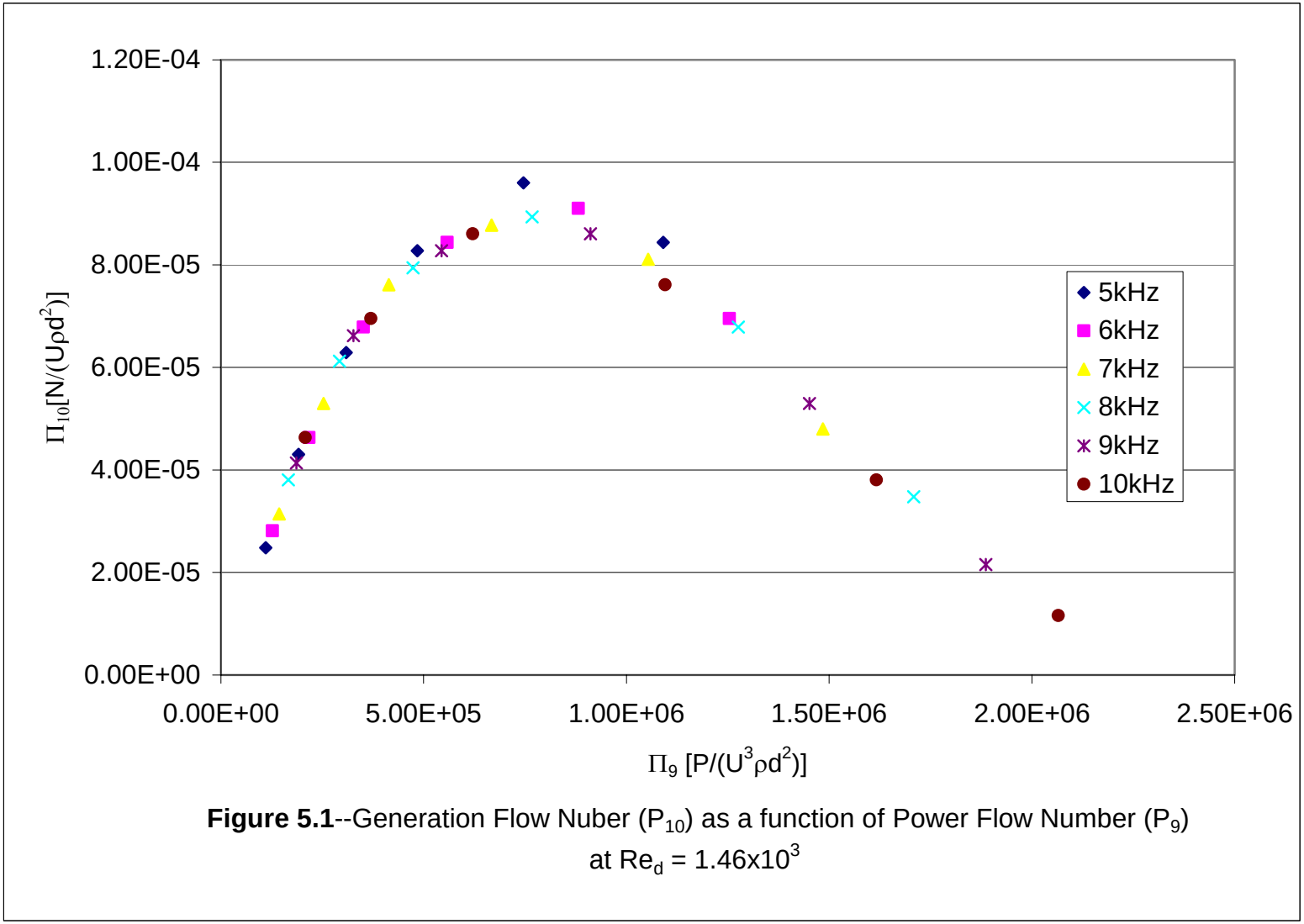

Figure 5.1--Generation Flow Nuber (P_{10}) as a function of Power Flow Number (P_9) at $Re_d = 1.46x10^3$

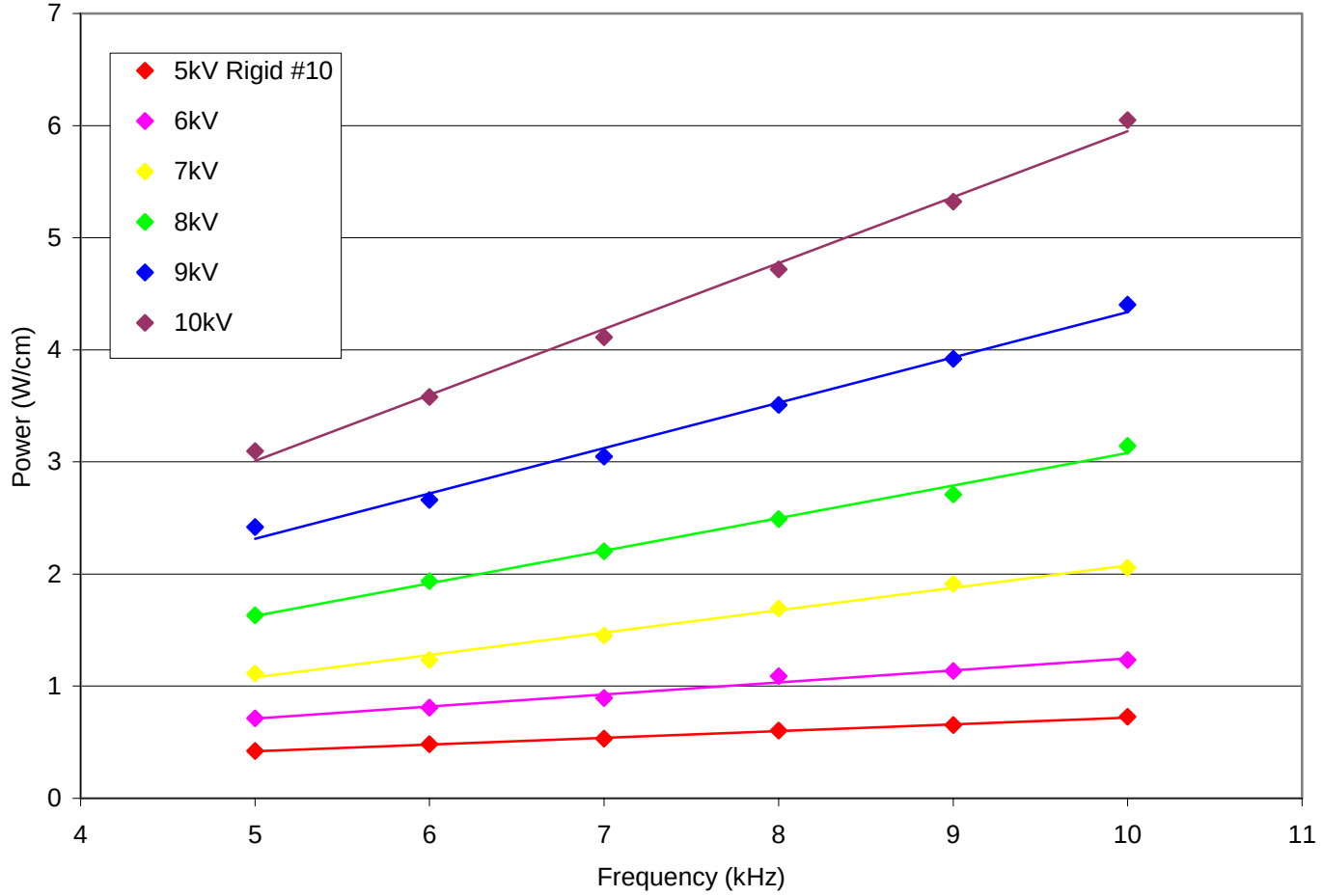

Figure 5.2--Plasma power vs. applied frequency
d = 0.5mm; Re_d =1.46x10^3 ; T ~25°C; RH = 50%

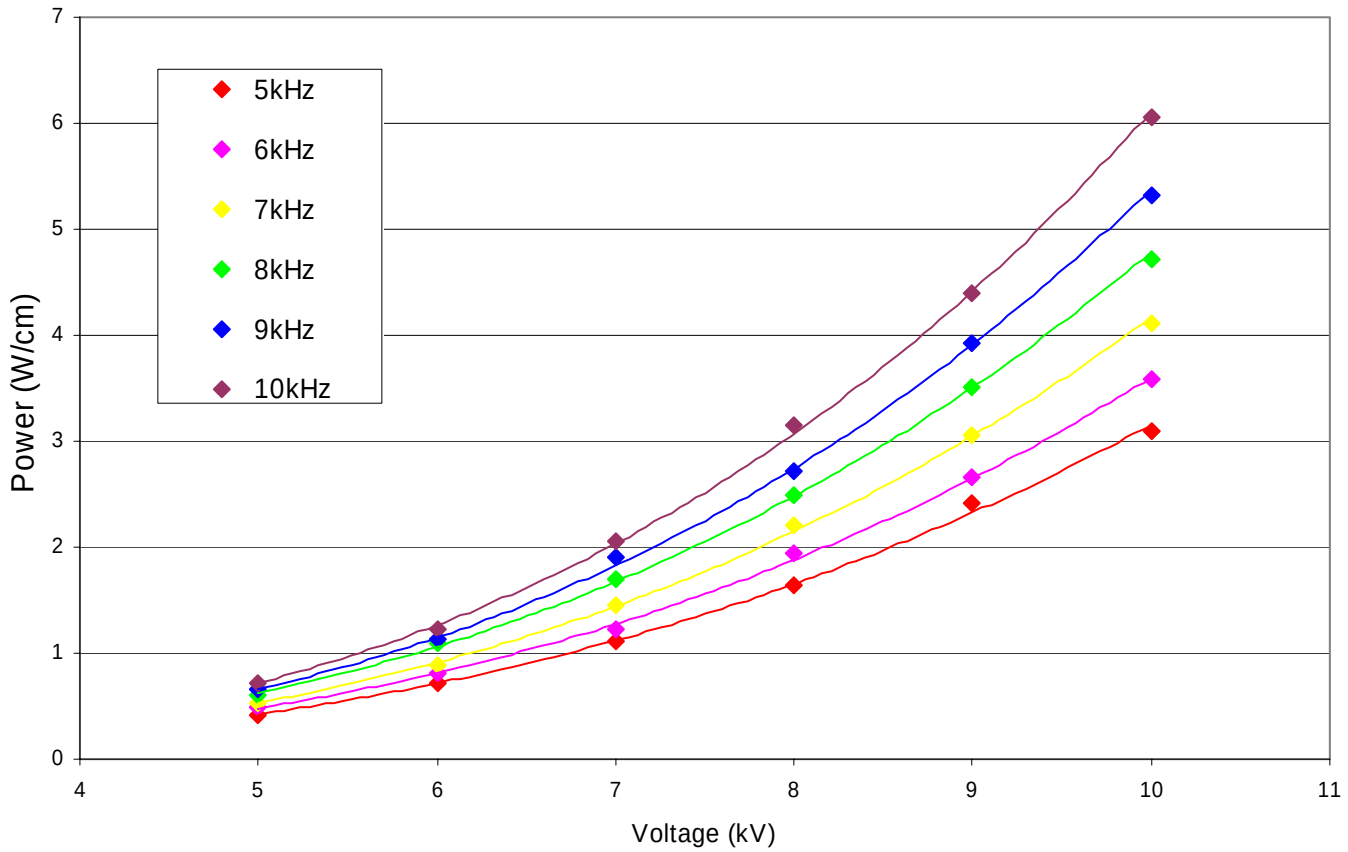

Figure 5.3--Plasma power vs. applied voltage

d = 0.5mm; Red =1.46x103 ; T ~25°C; RH = 50%

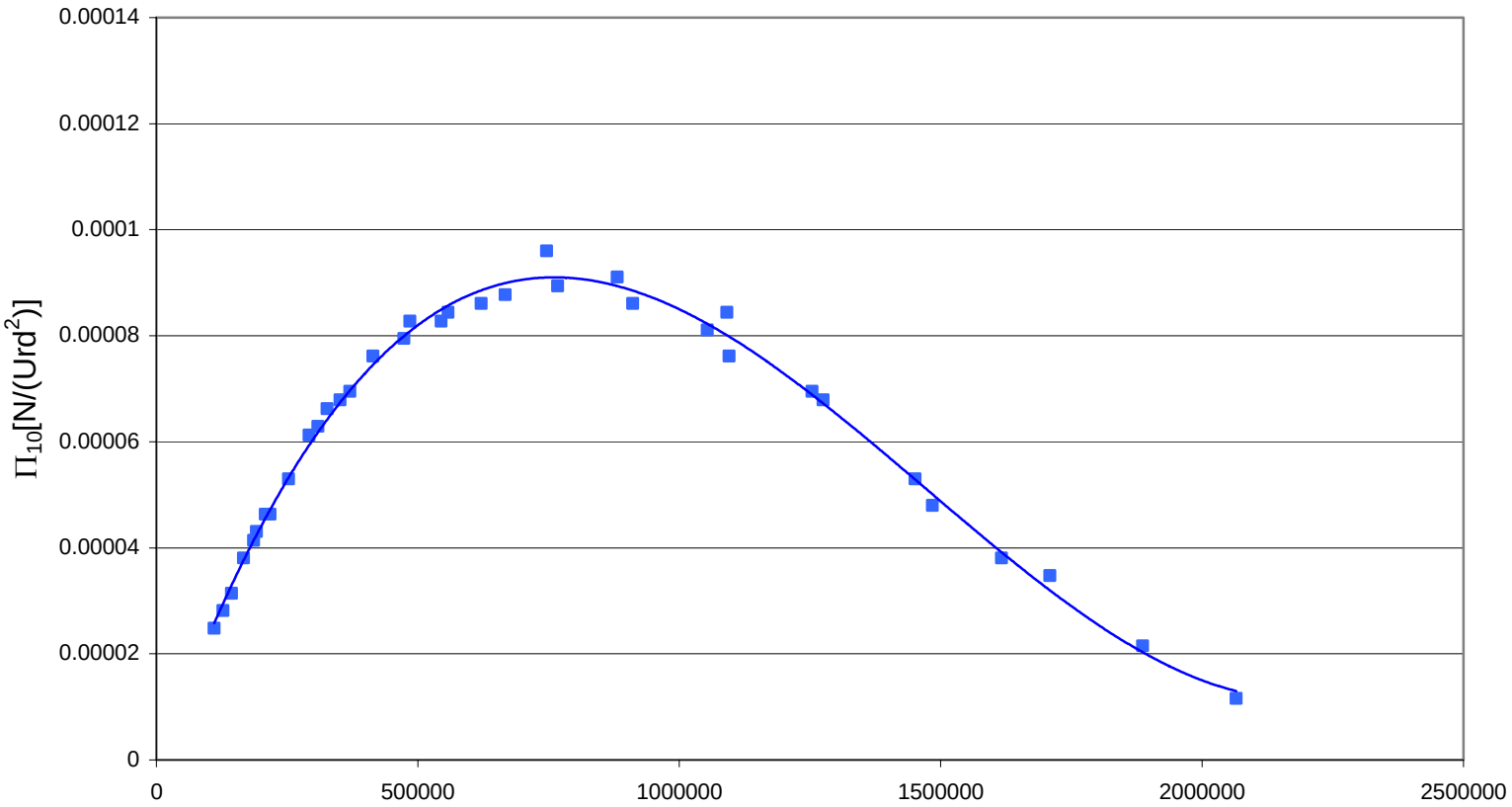

Figure 5.4--Generation Flow Number (Π_{10}) vs Power Flow Number (Π_9) at $Re_d = 1.46x10^3$

production. The results show that there is a clear maximum ozone generation point at a specific Plasma Flow Number at a fixed Re. Reactions for both the production and ensuing decomposition of ozone are temperature dependant. This may explain the upward slope of the generation curve as power density increases causing a continuing local temperature increase of the immediate electrode vicinity. Air in the region near the electrodes may be reaching temperatures at which ozone decomposition rapidly increases. At this point, the results seem to suggest that a balance between ozone generation and decomposition is achieved giving rise to the particular shape of the curve observed.

As Reynolds number is increased, the generation curve maintains the same general shape, but shifts to lower values of Plasma Flow Number (Π_9) and Generation Flow Number (Π_{10}) as seen in **Figure 5.5** for $Re_d = 1.46x10^3$, $2.2x10^3$ and $2.93x10^3$. The same characteristic maximum is apparent, but at correspondingly lower values of Π_9 and Π_{10}. The left sides of the curves for each Reynolds number follow the same path until tailing off toward their respective maxima. At $Re_d = 6.7x10^3$ the maximum generation was not reached, because a sufficiently high input power, as captured by Power Flow Number (Π_9) could not be applied (See **Figure 5.6**) There are physical limitations, including dielectric breakdown that prevents high input power at this Reynolds number. At larger Reynolds numbers, the required real power necessary to reach

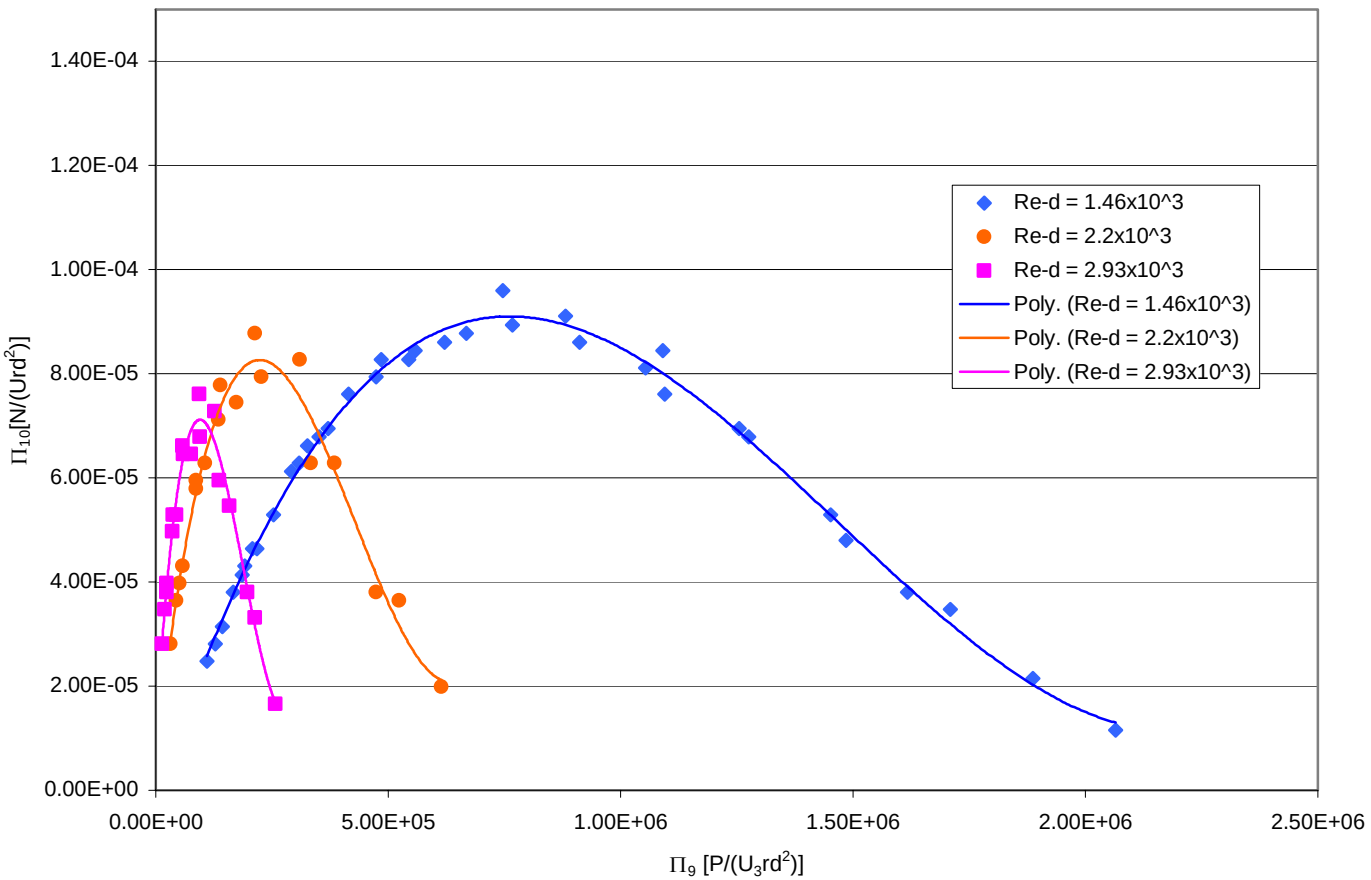

Figure 5.5--Generation Flow Number (Π_{10}) vs Power Flow Number (Π_9) at $Re_d = 1.46x10^3$

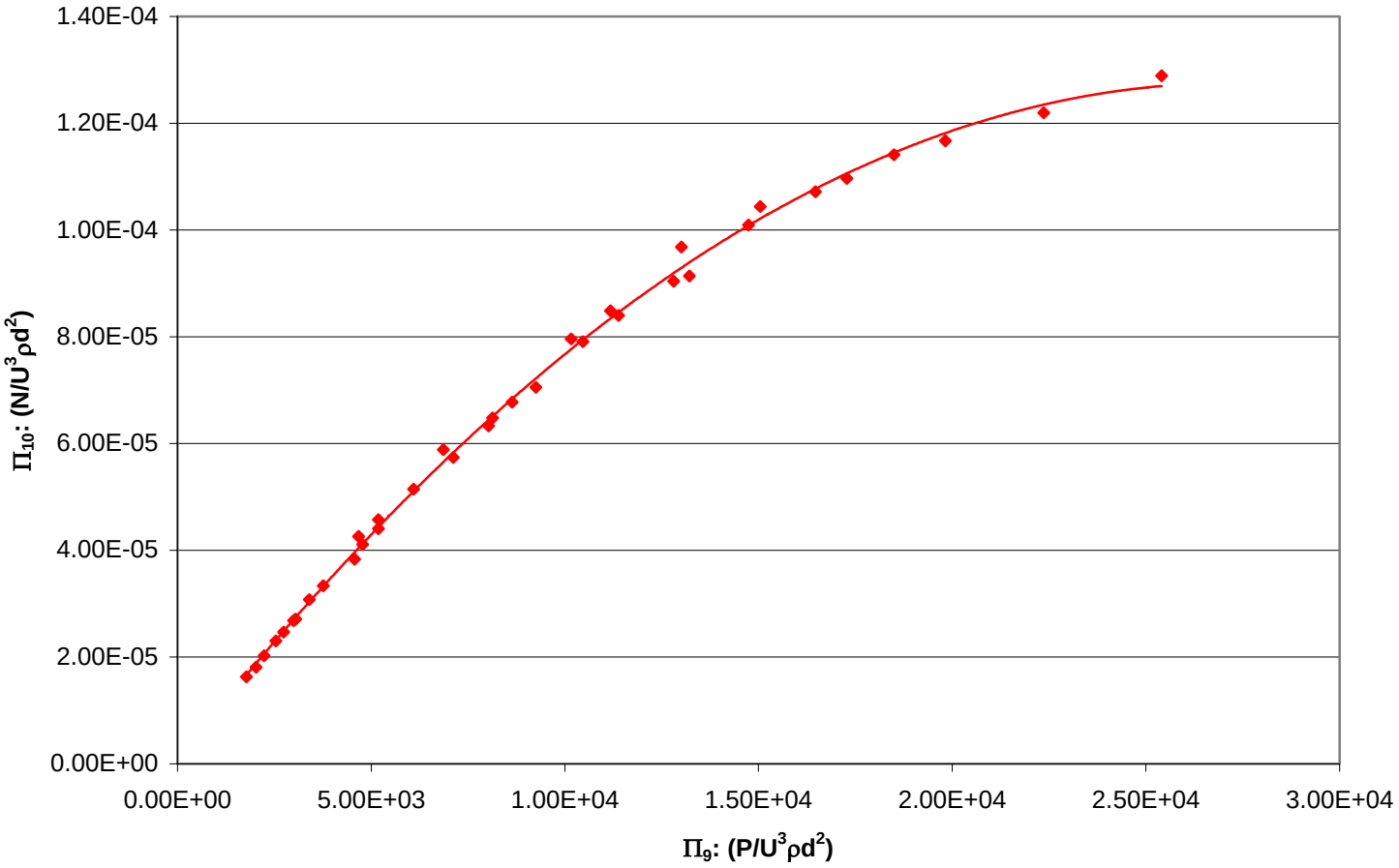

Figure 5.6--Generation Flow Number (Π_{10}) as a function of Power Flow Number (Π_9) at $Re_d = 6.7x10^3$

increasing levels of Power Flow Number (Π_9) rise and at a point surpass the material capabilities of the plasma generator. The highest power input for tests performed at all Reynolds numbers was approximately 8.2 Watts/cm of energized electrode pair, which corresponds nominally to 10kV and 10kHz. Beyond these levels dielectric breakdown is likely to occur.

By normalizing the three generation curves for Re_d = 1.46x10^3, 2.2x10^3 and 2.93x10^3, a universal curve can be obtained which, along with critical values for corresponding Reynolds numbers, can be used to capture a wider range of dimensionless ozone generation as a function of dimensionless power and Reynolds number. These curves are developed for several reasons:

a) They are universal in nature and can be applied to different data ranges.
b) They follow a methological approach to similar presentations of data in other engineering disciplines.
c) They offer convenience as a tool for design engineers.

The normalized variables are developed as:

Normalized Power Flow Number: $$\Pi_{9,norm}(\mathrm{Re}) = \Pi_9(\mathrm{Re}) \Big/ \Pi_{9,crit}(\mathrm{Re}) \qquad [5.2]$$

Normalized Generation Flow Number: $$\Pi_{10,norm}(\mathrm{Re}) = \Pi_{10}(\mathrm{Re}) \Big/ \Pi_{10,crit}(\mathrm{Re}) \qquad [5.3]$$

Table 5.1—Critical Power Flow Number (Π_9) & Generation Flow Number (Π_{10}) values for normalized ozone generation curves as a function of Re_d			
Re_d	$1.46x10^3$	$2.20x10^3$	$2.93x10^3$
$\Pi_9(x)$	$7.55x10^5$	$2.22x10^5$	$9.75x10^4$
$\Pi_{10}(y)$	$1.41x10^3$	$5.69x10^4$	$2.75x10^4$

The critical values used are the maximum values observed for the respective dimensionless groups from **Figure 5.5**. The maximum is found by using differentiation of a third-order polynomial curve fit for results presented in **Figure 5.5**. These critical values are tabulated in **Table 5.1** with the normalized curves shown in **Figure 5.7**.

A universal curve is constructed by combining the normalized data sets and applying a third order polynomial curve fit to the data. The universal curve is shown in **Figure 5.8**; the third order curve fit to the universal curve data is shown as:

$$y = 0.2516x^3 - 1.4554x^2 + 2.1536x + 0.0502 \qquad [5.4]$$

Where x is the value of Normalized Power Flow Number ($\frac{\Pi_9}{\Pi_{9,crit}}$) and y is the value of Normalized Generation Flow Number ($\frac{\Pi_{10}}{\Pi_{10,crit}}$). The data points at the bottom of the graph show the absolute error, or deviation, of the polynomial curve from the actual data points (left side scale):

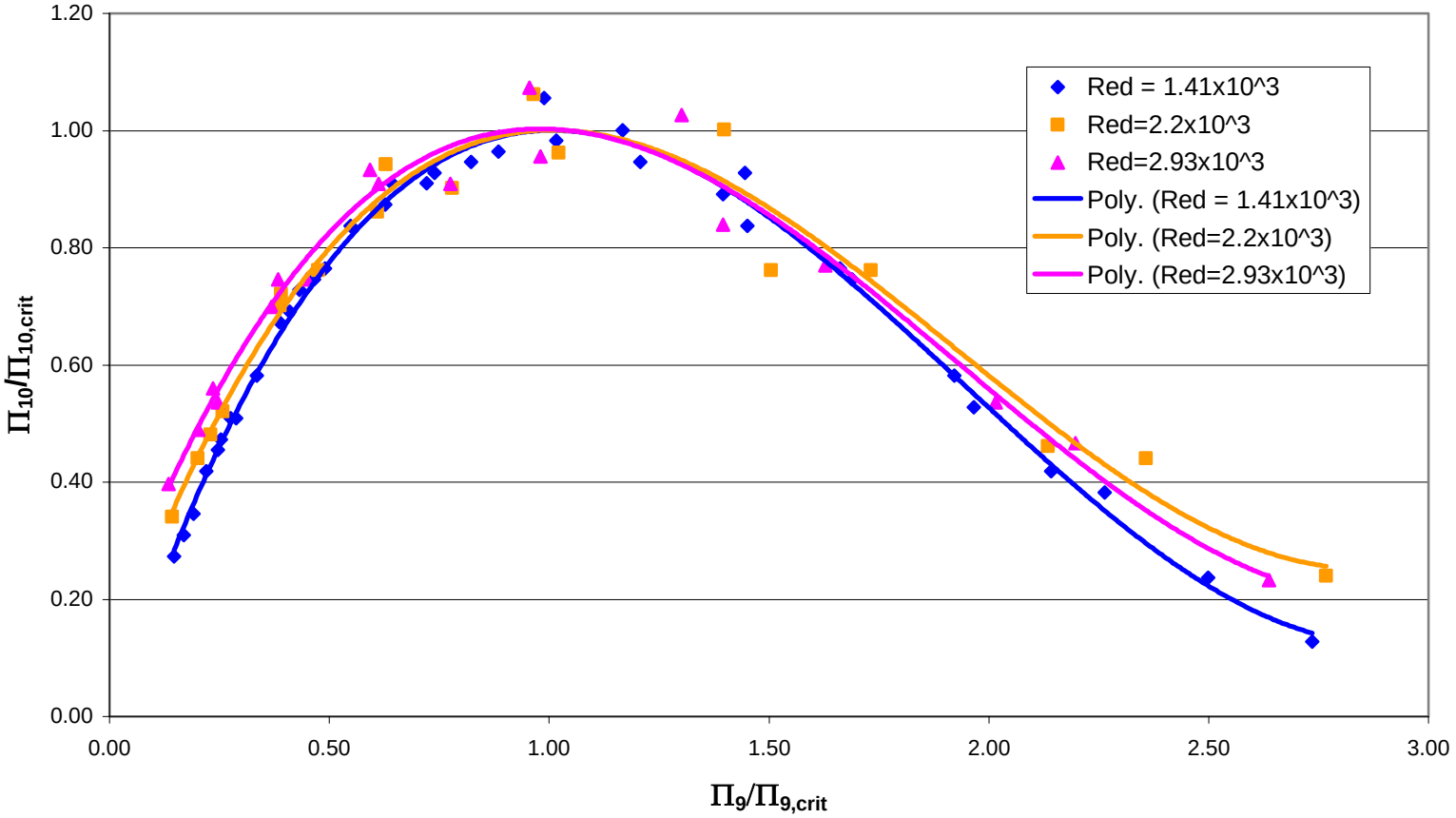

Figure 5.7--Normalized Generation Flow Number as a function of Normalized Power Flow Number at various Re_d

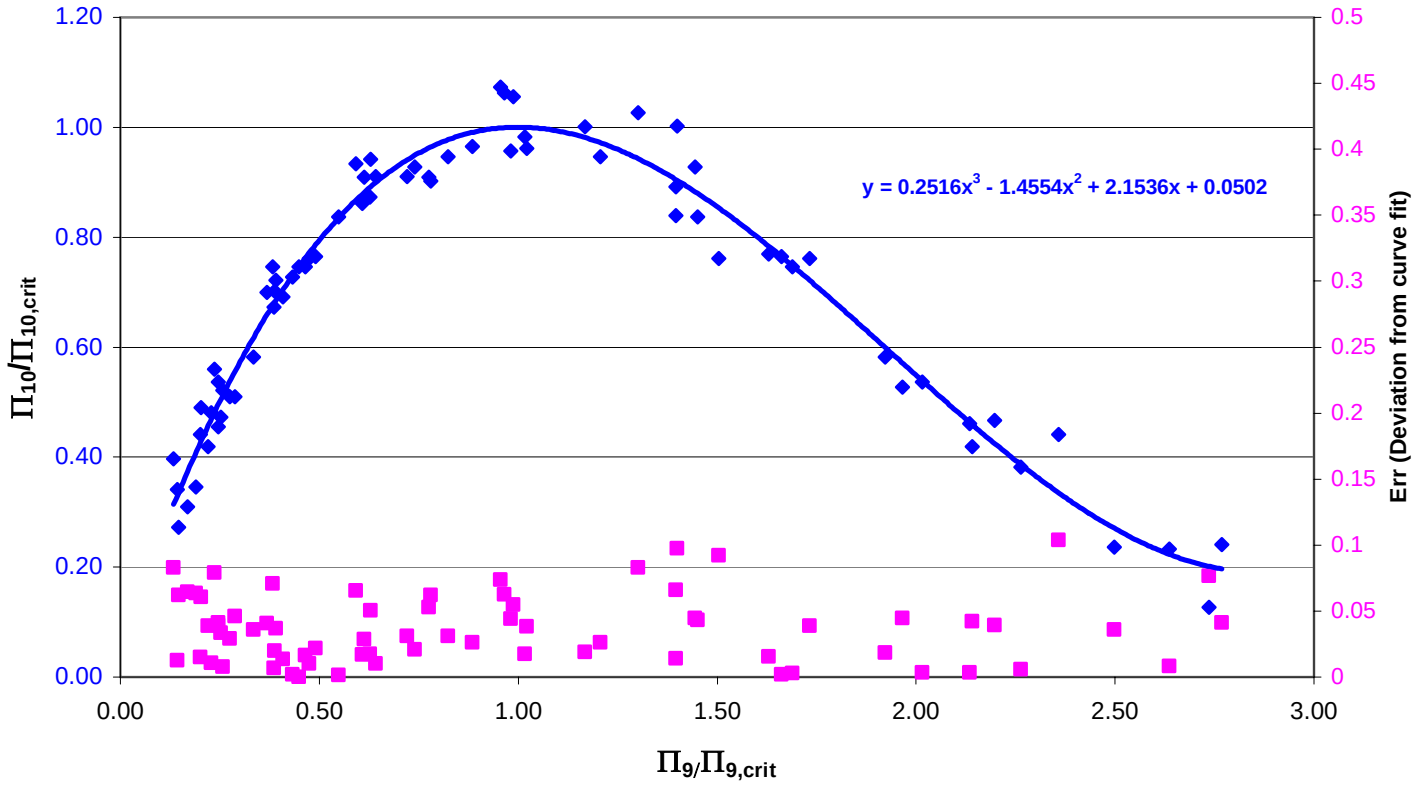

Figure 5.8--Normalized Generation Flow Number as a function of Normalized Power Flow Number; universal generation curve wrt. Re_d

$$Err = abs\left[\left(\Pi_{10}/\Pi_{10,crit}\right)_{poly} - \left(\Pi_{10}/\Pi_{10,crit}\right)_{data}\right] \qquad [5.5]$$

The mean error, (Err_{mean}) is 0.037, with a maximum ($Err_{\max}$) of 0.103 and a standard deviation ($Err_{std.dev.}$) of 0.026. Average spread of data about the curve is on the order of four percent with a maximum spread of just greater than ten percent.

5.2 Ozone Generation versus Plasma Gap (*g/l*)

Experimental runs at three different Gap to Diameter Ratio (g/l) values, obtained by varying plasma gap (g) showed only a week relationship between Power Flow Number and Generation Flow Number (Π_{10} vs Π_9). Runs were performed at constant Re = 1.46×10^3, at three g/l ratios: 0.157, 0.315 & 0.787. Electrodes were constructed of the same electrodes with constant dielectric thickness (0.031 in; 0.79mm) and diameter (0.125 in, 3.175mm). Varying input powers, the relationship between Power Flow Number ($\Pi_9 = \frac{P}{U^3 \rho d^2}$) and Generation Flow Number ($\Pi_{10} = \frac{N}{U \rho d^2}$) was determined.

With input power and frequency held constant, the electric field strength within the plasma gap increases as applied power increases. It is likely that stronger field strength gives rise to more energetic molecular and electron collisions within the plasma volume and therefore alters the chemistry generation. In the limited data set with three Gap to Diameter Ratios (g/l) described above, there is evidence that a smaller gap (lower g/l ratio) produces increased production of ozone. **Figure 5.9** shows Generation Flow Number (Π_{10}) as a function of Power Flow Number (Π_9) for the three g/l ratios. There is an evident decrease in Generation Flow Number (Π_{10}) over the range of Power Flow Number (Π_9) for increasing values of g/l. The relatively small range of g/l limits the applicability of results. The Gap to Diameter Ratio (g/l) for 0.125 in diameter electrodes can be taken to approximately 2.5 before plasma ignition becomes irregular and ceases at larger values. The dynamics of chemistry generation are complex and are affected by local temperature, air density and the types of species present. Ozone is the only measured indicator in these experiments and it is not necessarily indicative of the generation behavior of other species. These results are valid for ozone generation only. They indicate that ozone generation appears to drop off at plasma flow number. This may be because at sufficiently high local temperature rapid breakdown to diatomic oxygen occurs. Other species such as Nitrogen dioxide (NO_2) and Nitrous oxide (N_2O) may behave differently and would require independent experimentation.

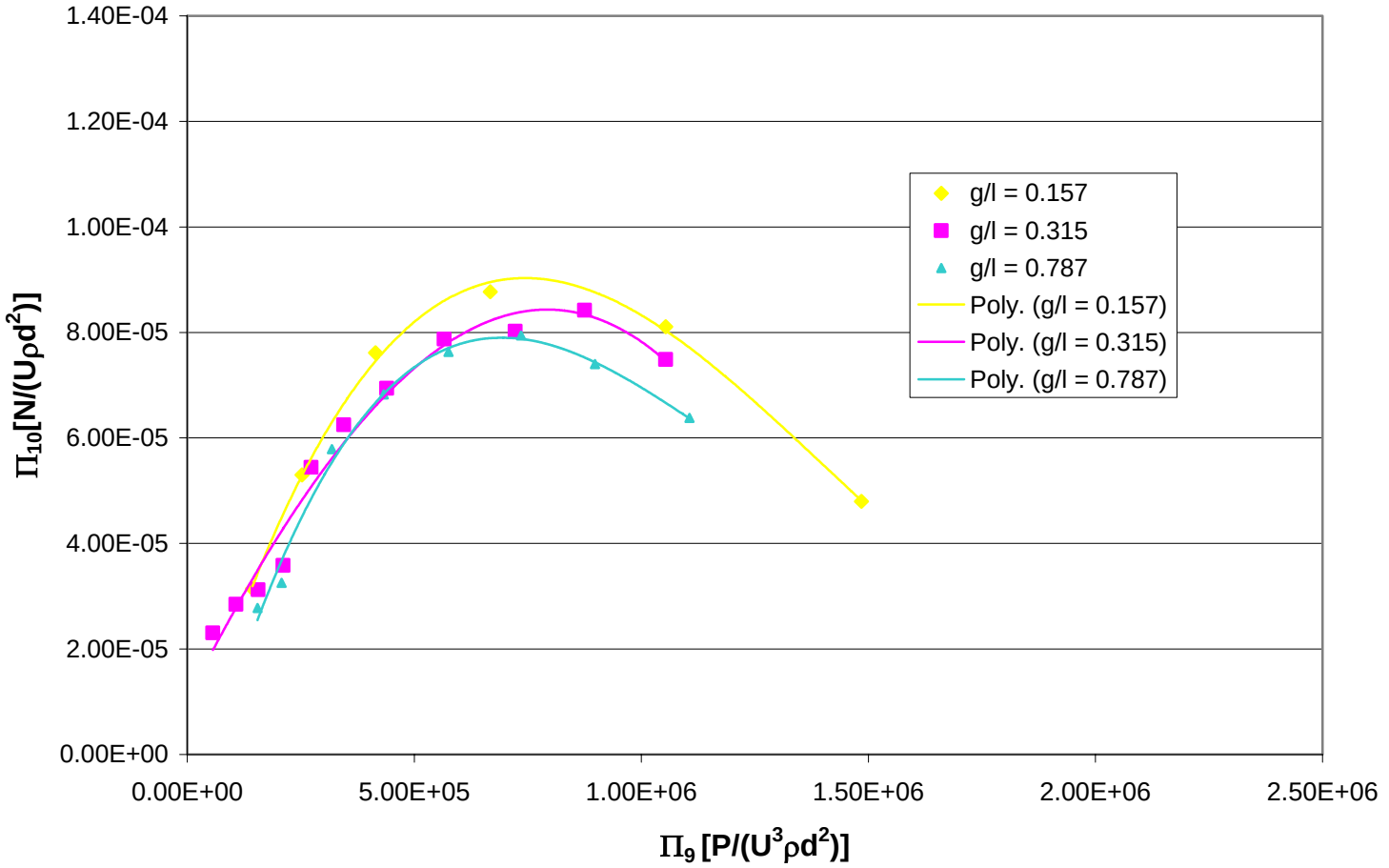

Figure 5.9--Generation Flow Number (Π_{10}) as a function of Power Flow Number (Π_9) at various g/l values

Table 5.2—Critical Power Flow Number (Π_9) & Critical Generation Flow Number (Π_{10}) values for normalized ozone generation curves vs. g/l ratio.			
Re_d	$1.46x10^3$	$2.20x10^3$	$2.93x10^3$
$\Pi_9(x)$	$7.55x10^5$	$2.22x10^5$	$9.75x10^4$
$\Pi_{10}(y)$	$1.41x10^3$	$5.69x10^4$	$2.75x10^4$

A similar procedure to that used for the Reynolds number dependant universal curve was followed to construct a g/l dependant universal curve for Generation Flow Number (Π_{10}) as a function of (Π_9). **Table 5.2** shows critical values used in developing normalized values. Normalized curves for Π_{10} versus Π_9 at the same three g/l ratios is shown in **Figure 5.10** and the combined universal curve is given in **Figure 5.11**.

For convenience, and as a design tool, **Figures 5.8** and **5.11** can be combined to provide a compact and general graph illustrating normalized variables at all Reynolds Numbers and Gap to Diameter Ratios within the limitations of the performed experiments. The results are shown in **Figure 5.12**.

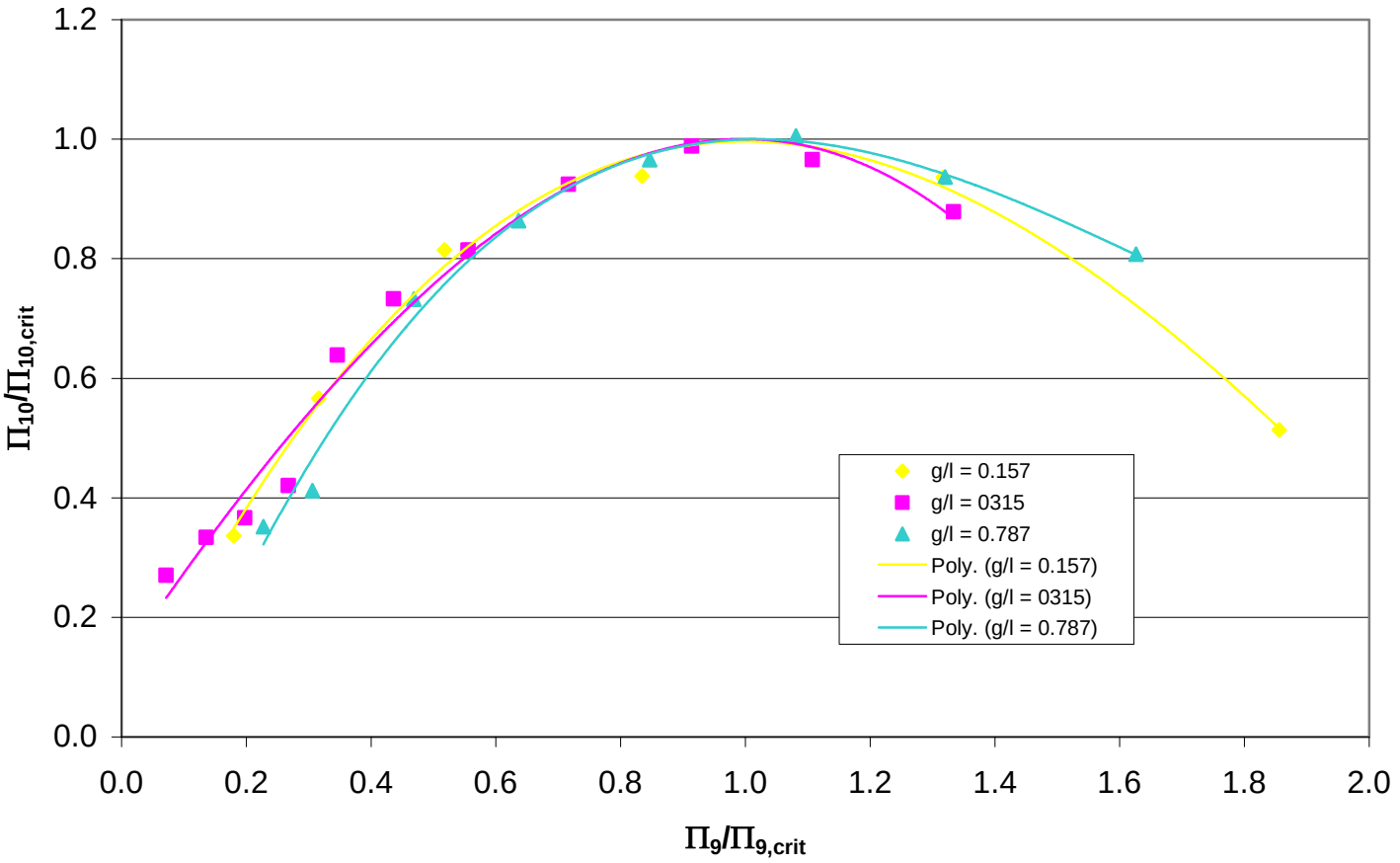

Figure 5.10--Normalized Generation Flow Number as a Function of Power Flow Number at various g/l ratios; $Re_d = 1.46x10^3$

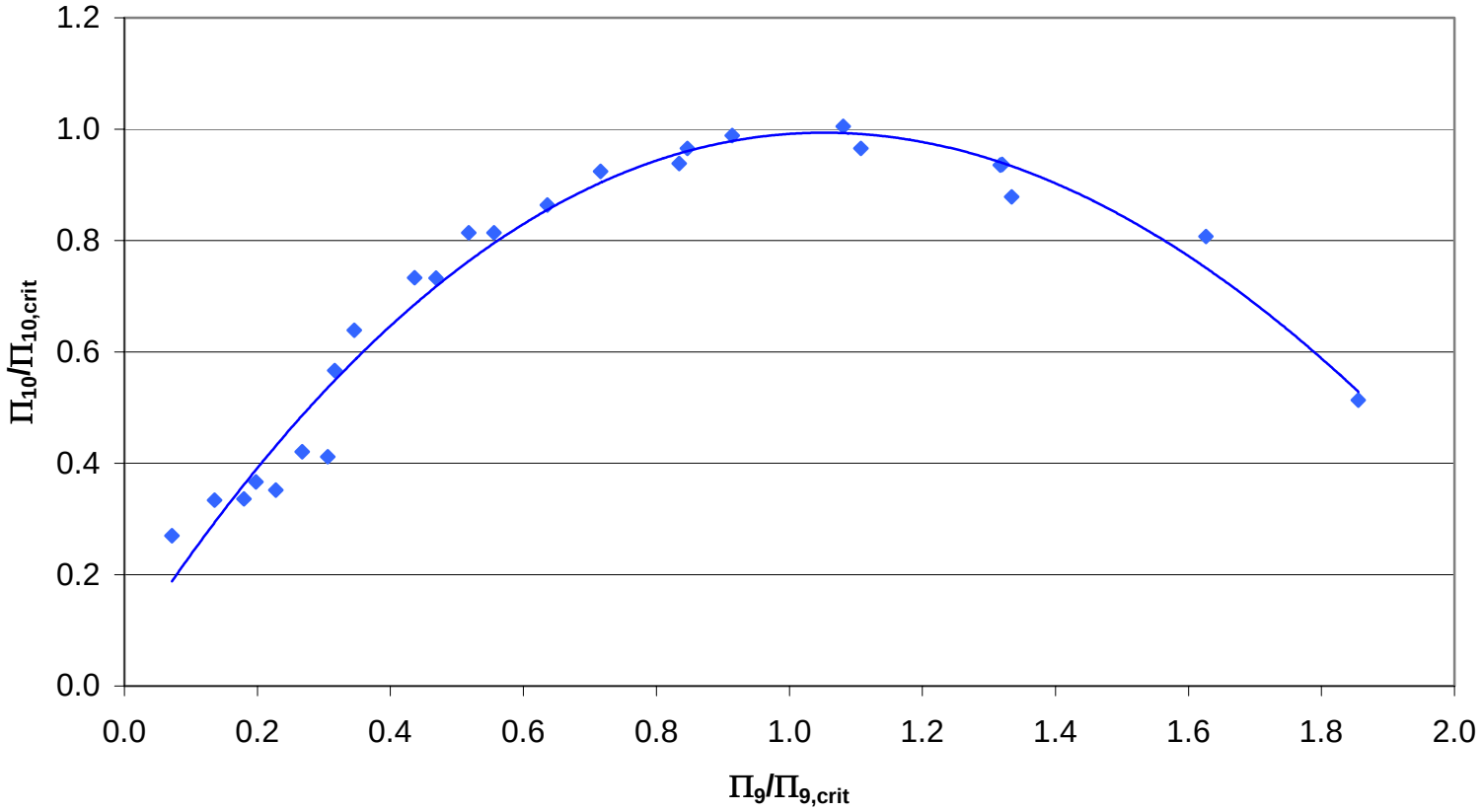

Figure 5.11--Normalized Generation Flow Number as a Function of Normalized Power Flow Number: universal generation curve wrt. g/l ratio; $Re_d = 1.46x10^3$

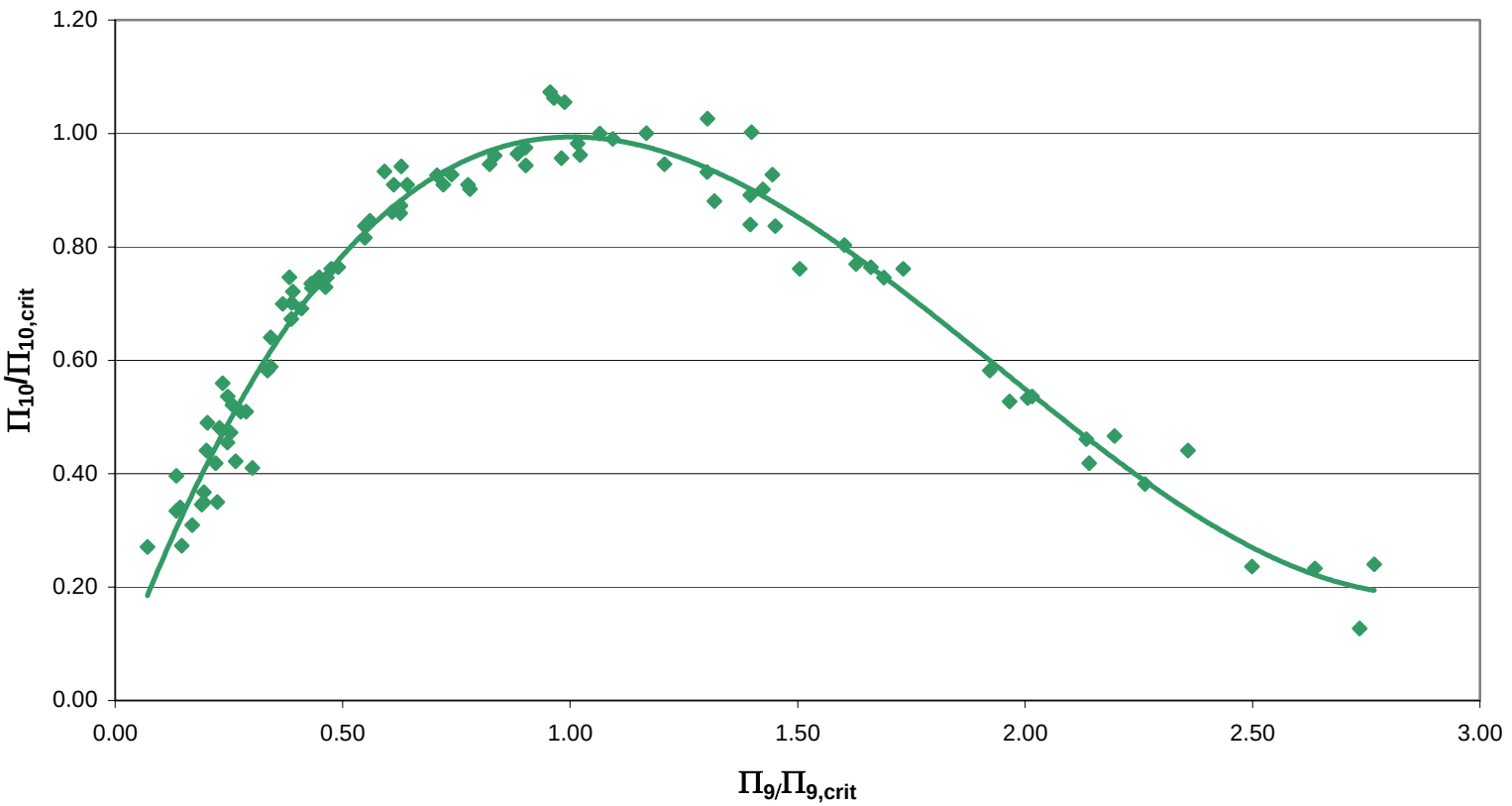

Figure 5.12--Normalized Generation Flow Number as a Function of Normalized Power Flow Number; Universal Generation Curve
-combined data from Re dependance & g/l dependance

CHAPTER 6—EXPERIMENTAL RESULTS FOR BIOLOGICAL EFFICACY

Experiments were conducted to measure the efficacy of plasma exhaust on a select species of microorganism: *Bacillus atrophaeus (B.A.)* endospores. *Bacillus atrophaeus* was selected because it is a commonly used surrogate of *Bacillus anthraces*, the bacteria which causes anthrax. B.A. is commonly used as an indicator of sterility in autoclaves. Other organisms may be used as indicators as well, depending on the desired challenge. Vegitative bacteria such as *Staphlococcus. Aureus* may be used to test for real-time aerosolized airborne destruction, and *Aspergillys niger* is a typical choice for testing mold spore destruction. The organisms were placed in the plasma test duct and subjected to parameter sweeps for plasma power, air duct velocity and exposure time. These parameter sweeps are captured and presented in the text by their respective non-dimensional counterparts:

Π_9	$\mathbf{P/(U^3\rho d^2)}$	-Power Flow Number
Π_8	$\mathbf{\rho Ud/\mu}$	-Reynolds Number
Π_{13}	**UT/d**	-Dimensionless Exposure Time

The condition for air entering the plasma generator and duct geometry were held constant for all test runs. The internal duct dimensions used was 4” x 4” and the flow was observed to be fully developed entering the plasma generator. Temperature at the challenge sample does change according to the power input to the plasma and the Reynolds number of the airflow and is captured by Flow

energy number (Π_{14}). Bacillus atrophaeus endospore samples were commercially available spore strips with nominally 10^6 viable spores per strip. Actual viable numbers for control and post-plasma exposure samples are quantified by performing serial dilutions and plate counts. The processing method is a standard microbiological process for endospore quantification.

6.1 Efficacy Dependence at Ambient Temperature Conditions

Efficacy of B.A. is strongly dependant on the temperature of the microorganism reaction site, resulting in two distinct killing regimes: ambient temperature (<~50°C) regime and high temperature (>~50°C) regime. This section details results of ambient temperature efficacy. Ambient temperature efficacy is characterized by relatively longer treatment times and hence larger values of Dimensionless Exposure Time (Π_{13}) for given values of Re_d and Power Flow Number (Π_9).

Figure 6.1 shows the log destruction rate against B.A. endospores subjected to varying time exposures of plasma and to varying Reynolds number. Gap to Diameter Ratio (g/l) is held constant at 0.157 and duct diameter is constant, the power input to the plasma is held at 71 Watts or 1.9 Watts/cm_{plasma} and inlet air state is held constant at 70°F and 50%.

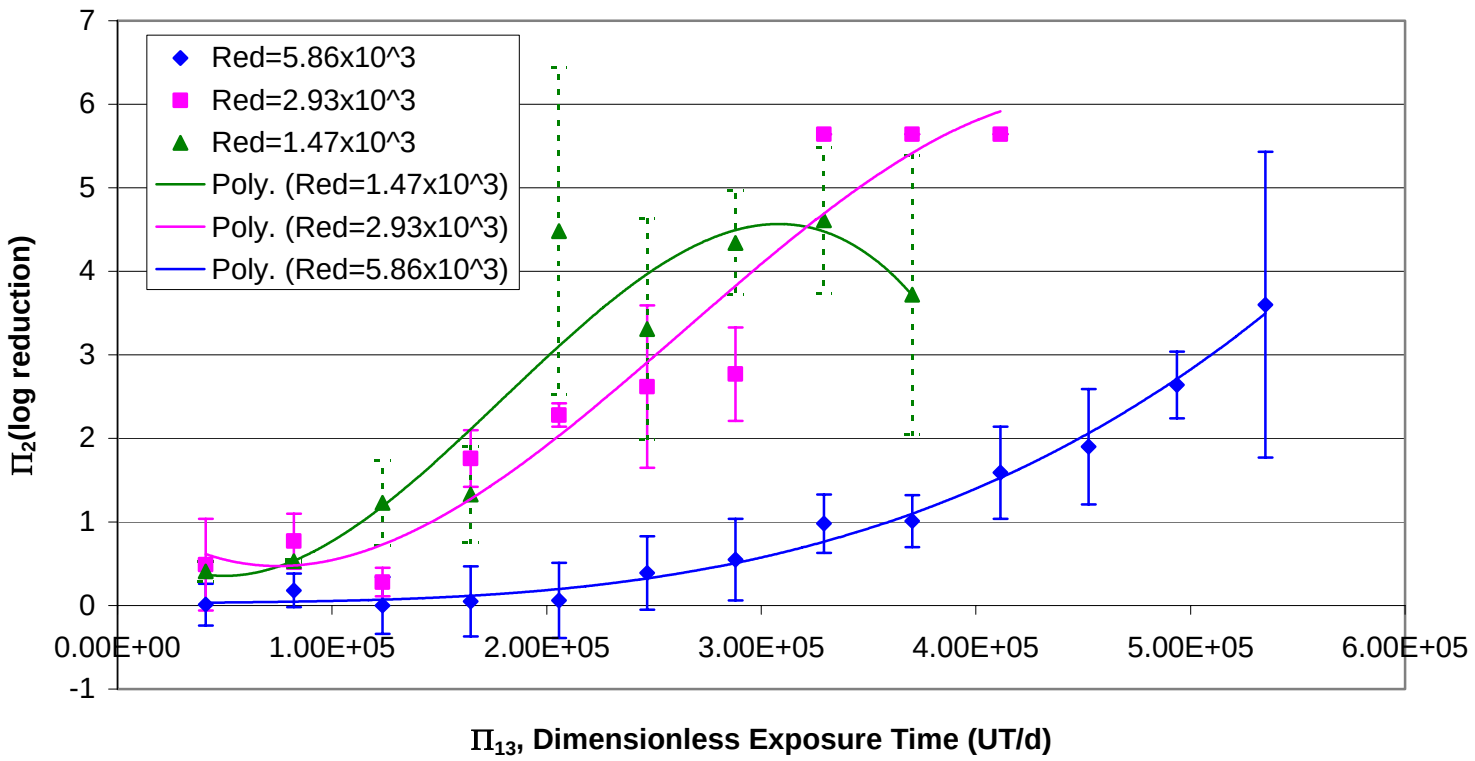

Figure 6.1--Π_2(efficacy against Bacillus atrophaeus endospores) as a function of Dimensionless Exposure Time (Π_{13}) at various Reynolds numbers; $\Pi_9 = 7.22 \times 10^3$

The Power Flow Number (Π_9), is held constant at 7.22×10^3. Each data point represents an average of three to six test results at identical conditions. Error bars represent ± one standard deviation of the data generating each graph point. Trend lines are 3rd order polynomial curve fits, intended to indicate the general trends of data. Outlier analysis was performed using the modified three sigma method; raw data is found in **Appendix III**. Data sets were plotted and identified to have a Gaussian distribution, and mean value ($\bar{x}$) and variance (S'_x) were calculated for each data set. Outlying data points from each set were identified by the *modified-three-sigma* method and removed [Figliola 1995]. By this method, a modified z is calculated as:

$$z_0 = \left| \frac{x_i - \bar{x}}{S_x} \right| \qquad [6.1]$$

which is used to calculate probability values for each data point n_i, from the Normal Error Function:

$$P(z_0) = \frac{1}{(2\pi)^{1/2}} \int_0^{z_0} e^{-\beta^2/2} d\beta \qquad [6.2]$$

Data points were considered outliers if the value [$0.5\text{-}P(z_0(n_i)$] was less than or equal to 0.1 (outside 99.8% probability of occurrence). With the outliers removed, a

Table 6.1—Mean control CFU counts for tests at various Re_d.

Reynolds Number	$1.47x10^3$	$2.93x10^3$	$5.86x10^3$
Mean CFU (control)	$5.61x10^5$	$5.64x10^5$	$5.43x10^5$

new mean value (x_m), variance (S_x^2) and standard deviation (S_x) were calculated on which data comparisons were based.

The general trend for destruction of B.A. endospores at the three Reynolds numbers tested shows a period of relatively low destruction rate with a gradual slope upward, followed by a rapid increase in destruction rate and lastly a period with sustained high destruction rate. At Re = 1.47x103 and 2.93x103, all three periods are evident; at Re = 5.86x103, the third period of sustained efficacy level is not reached. The results of tests for control samples of endospores exposed to airflow (but not exposed to plasma) at corresponding Re are given in **Table 6.1**. The control sample count is representative of the number of CFU present on an untreated endospore sample and thus represents the maximum number of CFU that can be destroyed by the plasma and provides an upper limit on the log reduction level.

It can generally be seen in **Figure 6.1** that higher efficacy levels are reached sooner (i.e. at lower Dimensionless exposure Time [UT/d] values) for lower Reynolds number flow. Changes in Reynolds number in these experiments are

entirely due to varying air velocity. This indicates that B.A. challenges are killed more quickly with lower velocity or more residence time with and all other parameters held constant. As Reynolds number is increased, the onset of high log destruction is delayed and may ultimately not be achievable at sufficiently high Re.

Figure 6.2 shows data from experiments aimed at measuring the effect of changing power input to the plasma, with a constant Reynolds number with all other parameters held constant. The curve for Power Flow Number (Π_9) = 7.22×10^3 is taken from **Figure 6.1** at Re = 5.86×10^3. At higher values of Power Flow Number (Π_9), B.A. destruction reaches higher levels at correspondingly lower values of Dimensionless Exposure Time (Π_{13}). A similar graph for Re_d = 8.79x103 in **Figure 6.3** illustrates the same general trend, namely, that higher efficacy is attainable with higher Power Flow Number (Π_9) at a given Dimensionless Exposure Time (Π_{13}). These results are unique to the setup considered and to the microorganism tested: *Bacillus atrophaeus* (B.A.) endospores. B.A. is a relatively hearty challenge organism, particularly compared to vegetative bacteria. It is expected that these results for B.A. define a limit for efficacy in that efficacy for less resistant bacterial strains would occur at correspondingly lower Dimensionless Exposure Time (Π_{13}).

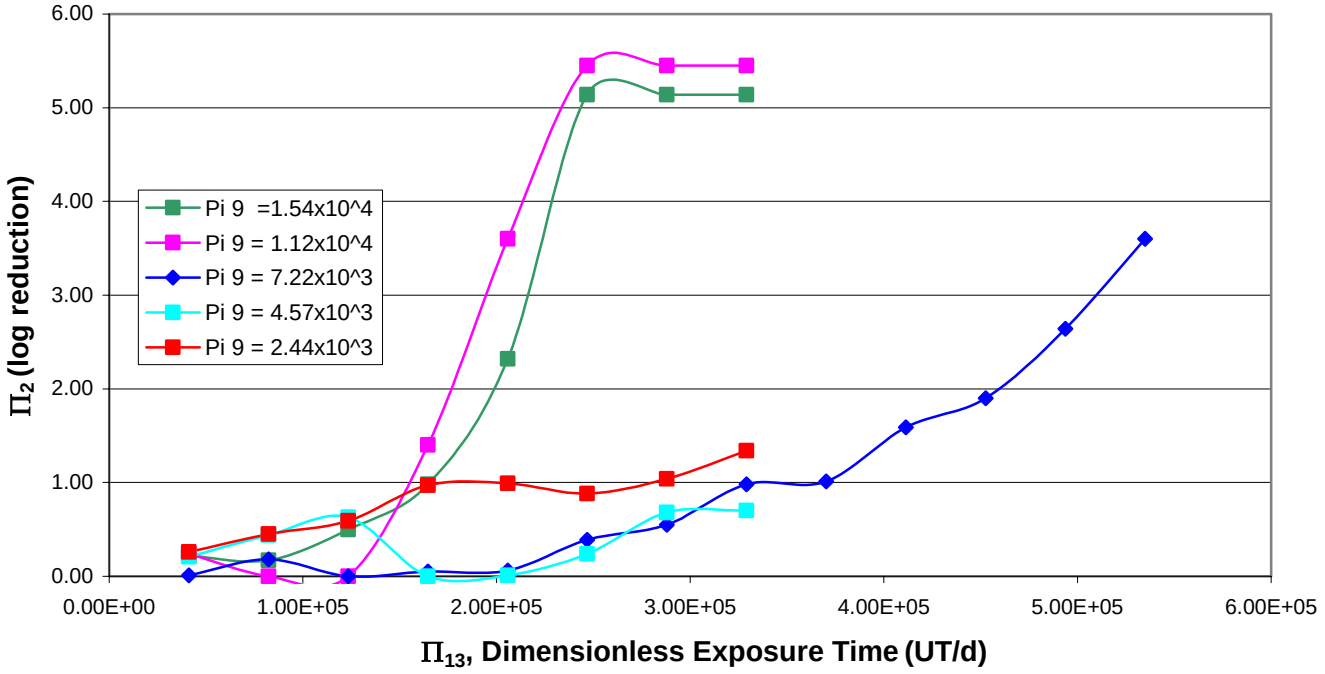

Figure 6.2--Π_2 (η–Bacillus atrophaeus) as a function of Dimensionless Exposure Time (Π_{13}); $Re_d = 5.86x10^3$

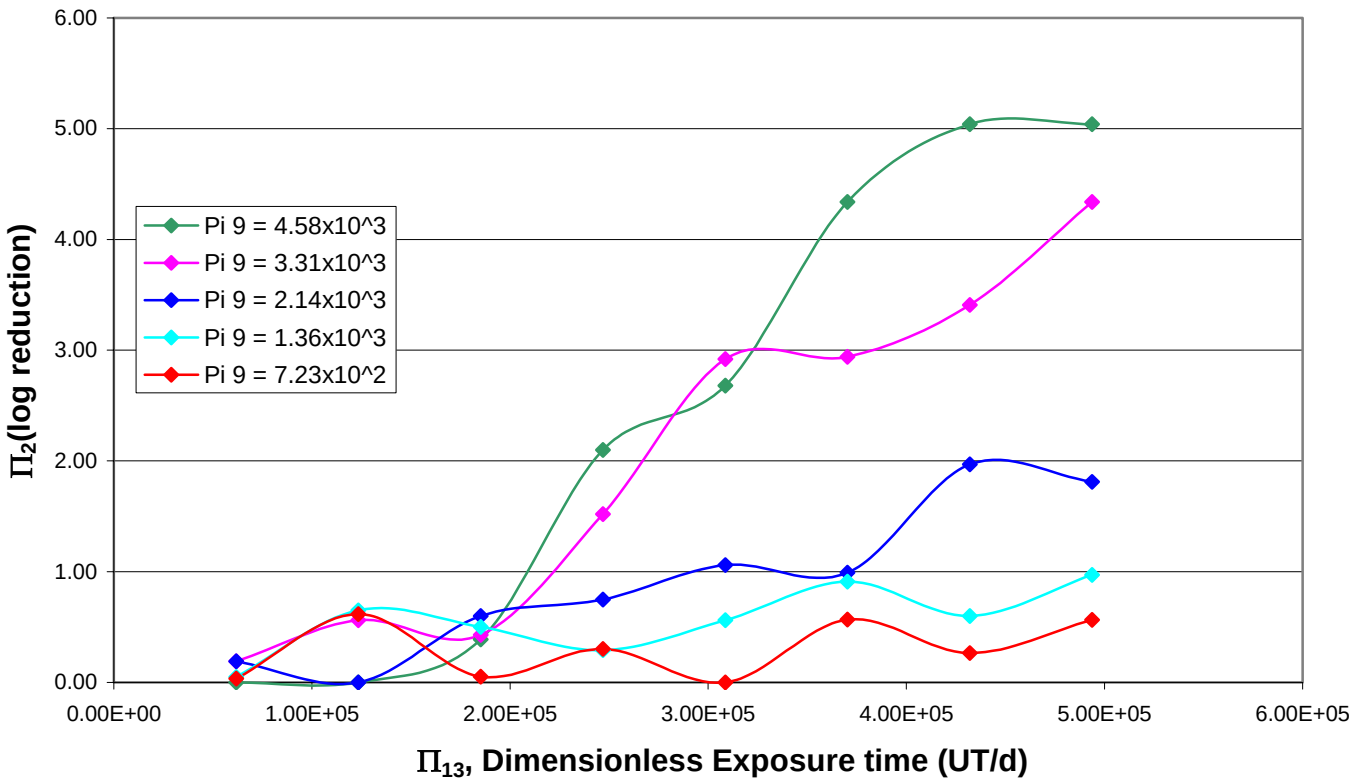

Figure 6.3--Π_2 (η-Bacillus atrophaeus) as a function of Dimensionless exposure Time (Π_{13}); $Re_d = 8.79x10^3$

CHAPTER 7—CONCLUSIONS & RECOMMENDATIONS FOR FUTURE WORK

7.1 Conclusions

A test facility was designed and fabricated and experiments were conducted to analyze the many parameter problem of One Atmosphere Uniform glow Discharge Plasma (OAUGDP) chemical generation and corresponding biological organism destruction. The problem of plasma generated chemical species reacting with and destroying microorganisms is approached by establishing a set of relevant variables consisting of input parameters, material properties and measured outputs, and developing a set of non-dimensional and normalized variables using the Buckingham Pi theorem.

A subset of the 19 most physically relevant variables was chosen and used as the basis of non-dimensionalization and experiments; the variable set is given in **Table 4.1**. The 19 variables were reduced to 14 dimensionless Π groups, and are displayed in **Table 4.2**. A key objective of this study was to provide a framework for analysis of atmospheric plasma that is appropriate for any geometry of plasma reactor but that is tailored to the specifics of the parallel cylinder plasma reactor system used in this study. The nineteen variables identified for nondimentionalizing are not wholly complete for reactor geometries,

but additional variables can easily be integrated into the analysis to build an appropriate set of Π groups. Another important objective was to provide universal results, convenient for use by design engineers in this field.

Data presented shows the relationship between chemical species generation (ozone in this case) and Reynolds number, relative plasma gap and dimensionless power input. A family of generation curves are developed at various Reynolds numbers which are then normalized and merged to form a universal generation curve. Generation curves for other species can be developed in the same manner.

The mechanism of destruction of microorganisms is still under investigation, but it likely involves perforation of the outer cell structure via oxidation, ion bombardment or a combination of the two. A general theory is that the cell structure is immersed in a concentration of chemical species (X_i) that react with the cellular material according to some reaction rate k. Cell death likely occurs after sufficient reactions occur on the outer structure, disabling normal cellular operation. As is the case with any stress to a microorganism colony, some cells are more resistant to destruction than others and the population likely declines exponentially. Individual cells that are more resistant to dying may either be less prone to react with surrounding species because of subtle structural differences, or because of heartier construction. Such details were not investigated and

remain to be explored in future studies. However, the ideas behind microorganism death remain the context and informs present investigation. Given the general idea that a microorganism structure reacts with species X_i with reaction rate k_i, then it follows that any of the following should increase the destruction rate of organisms: 1) an increase in concentration of species X_i, 2) an increase in the reaction rate k_i, and 3) an increase in time of exposure of the organism to species X_i. More than one species may participate in cell destruction, in which case there are multiple reactant concentrations and reaction rates, but the reaction kinetics follow the same trends to increase with temperature and concentration and for total reaction to increase with exposure time.

Changes in plasma input power, changes in the g/l ratio and changes in flow Reynolds number are believed to have the effect of changing the species concentration. This was demonstrated with ozone as an indicator species in this study. Additionally, changes in Reynolds number and power also change the microorganism site temperature, which in turn will affect the reaction rates with the organism structure for a given species. As is shown in this study, changes in power, geometry and Reynolds number have multifaceted effects on species generation. Expected gains in species production rates with increased power may be offset by local temperature effects that speeds reactions in the opposite direction. Thus one can not simply double the input power and necessarily expect to double the species production or in turn double the microorganism

destruction rate. The same is true for changes in Reynolds number because it plays a key role in the convection of heat away from the plasma region.

7.2 Recommendations for Future Work

This work was conducted treating the plasma generator and the microorganism reaction site as “black boxes” in that the internal mechanisms that create specific chemical species in turn cause reaction with an organism are not explored in any detail. Those two areas are in need of more fundamental exploration. At the plasma generator, an understanding of how species are created and how parameters influence generation is essential for developing applications from first principles, biological or otherwise. Such work may be done analytically, through modeling or experimentally and likely will include all three.

At the reaction site, again, biological or otherwise, it is important to explore the specific reactions that produce desirable effects and to understand how relevant parameters affect reactions. Such work is interdisciplinary and will also require analytical, modeling and experimental approaches.

REFERENCES

ASHRAE Handbook, Fundamentals Volume., 2005, Chapter 9.

ASHRAE Handbook, Systems and Equipment Volume., 2004, Chapters 24 & 25.

CDC. 1994. Guidelines for Preventing the Transmission of Mycobacterium Tuberculosis in Health-Care Facilities. Centers for Disease Control and Prevention, Atlanta, GA.

CDC. 1999-1. Guidelines for the Application of Upper-Room Ultraviolet Germicidal Irradiation for Preventing Transmission of Airborne Contagion—Part I: Basic Principles. Centers for Disease Control and Prevention, Atlanta, GA.

CDC. 1999-2. Guidelines for the Application of Upper-Room Ultraviolet Germicidal Irradiation for Preventing Transmission of Airborne Contagion—Part II: Design. Centers for Disease Control and Prevention, Atlanta, GA.

DePaoli, S., Domitrovic, R., Kelly-Wintenberg, K., Ly, A., South, S., Whelchel, B., *Technical Report on EPS Experimental Progress,* Atmospheric Glow Technologies, September, 2003.

EPRI, Electrotechnologies for Countering Bioterrorism, Palo Alto, CA: 2002. 1006903.

Feynman, R.P., Leighton, R.B., Sands, M., *The Feynman Lectures on Physics, Volume II*, Addison-Wesley, Menlo-Park, CA, 1964.

Figliola, R. S. and Beasley, D. E., Theory and Design for Mechanical Measurements, Second Edition. John Wiley & Sons, New York, 1995.

Fisk, W.J., et.al., Particle Air Filtration in HVAC Supply Air Streams., *Heating Piping and Air Conditioning*, July 2003.

Foard, K. & VanOsdell, D. 2002. Inactivation of Airborne Environmental Bacteria and Fungi by In-Duct UVC Lamps.Proceedings of the Indoor Air Quality-Filtration Conference, Cincinnati, OH. 2002.

Frost & Sullivan, Analysis of the North American Air Purification Markets., September 2004.

Griffiths, D.J., *Introduction to Electrodynamics*, Second Edition., Prentice Hall, Englewood Cliffs, NJ, 1989.

Hunter, P., and Oyama, S.T., Control of Volatile Organic Compound Emissions., John Wiley and Sons, New York, 2000.

Kelly-Wintenberg, K., Sherman, D., Tsai, P., Ben Gadri, R., Karakaya, F., Chen, Z., Roth, J., Montie, T., Air Filter Sterilization Using a One Atmosphere Uniform Glow Discharge Plasma (the Volfilter). IEEE Transactions on Plasma Science, Vol. 28 No. 1, February 2000.

Kelly-Wintenberg, K. Indoor Air Biocontaminant Control by Means of Combined Electrically Enhanced Filtration and OAUGDP Plasma Sterilization. EPA Report: Contract No. 68-D-99-025-0002, 2002.

Kelly-Wintenberg, K., Final Report: Decontamination Using One Atmosphere Uniform Glow Discharge Cold Plasma. DAAD-19-02-C-0004, Atmospheric Glow Technologies, 2004.

Kowalski, W.J., Bahnfleth, W.P., Airborne Microbe Filtration in indoor Environments., *Heating Piping and Air Conditioning*, January, 2002.

Kowalski, W. J. et.al., Filtration of Airborne Microorganisms: Modeling and Prediction. *ASHRAE Transactions*., v. 105, 1999.

Kowalski, W. J. and Bahnfleth, W.P., UVGI Design Basics for air and Surface Disinfection., *Heating, Piping and Air Conditioning*, January, 2002.

Kowalski, W. J. and Bahnfleth, W.P, Effective UVGI System Design Through Improved Modeling., *ASHRAE Transactions*, 2000.

Kunhardt, E. & Becker, K., Glow Plasma Discharge Device Having Electrode Covered with Perforated Dielectric., U.S. Patent No. 5,872,426, February 16, 1999-1.

Kunhardt, E. & Becker, K., Method for Generating and Maintaining a Glow Plasma Discharge., U.S. Patent No. 6,005,349, December 21, 1999-2.

Kunhardt, E. & Becker, K., AC Glow Plasma Discharge Device Having an Electrode Covered with Apertured Dielectric., U.S. Patent No. 6,147,452, November 14, 2000.

Levetin, E. et.al., Effectiveness of Germicidal UV Radiation for Reducing Fungal Contamination within Air-Handling Units., *Applied and Environmental Microbiology*, August, 2001.

Laroussi, M., Richardson, J.P., and Dobbs, F.C., 2001 Biochemical Pathways in the Interaction of Non-equilibrium Plasmas with Bacteria, *Proc. Electromed 2001* (Portsmouth, VA, 2001) p33.

Laroussi, M., Alexeff I., Richardson, J.P., and Dyer, F.F., 2002 The Resistive Barrier Discharge, *IEEE Trans. on Plasma Science* **30** 158.

Laroussi, M., Richardson, J.P., and Dobbs, F.C., 2002 Effects of Non-equilibrium Atmospheric Pressure Plasmas on the Hererotrophic Pathways of Bacteria and on their Cell Morphology *Applied Physics Letters*. **81** 772.

Madigan, M.T., Martinko, J.M, and Parker, J., Brock Biology of Microorganisms, Ninth Edition, Prentice Hall, 2000.

Meklyn, T., et.al., Microbial Exposure and Health of Children in Schools., *Proceedings of the Indoor Air Quality-Filtration Conference of the AFS*, November, 2002.

Menzies, D., et.al., Effect of Ultraviolet Germicidal Lights Installed in Office Ventilation Systems on Workers' Health and Wellbeing: Double-Bilnd Multiple Crossover Trial. *The Lancet*, vol. 362, November, 2003.

Miller, S. L., and Macher, J. M., Evaluation of a methodology for Quantifying the Effect of Room Air Ultraviolet Germicidal Irradiation on Airborne Bacteria.

Montie, T.C., Kelly-Wintenberg, K., and Roth, J.R., (2000) An Overview of Research Using the One Atmosphere Uniform Glow Discharge Plasma (OAUGDP) for Sterilization of Surfaces and Materials. *IEEE Transactions on Plasma Science* **28** (1). 41-50.

NAFA Guide to Air Filtration, Third Edition, National Air Filtration Association., 2001.

Oyama,, S.T., K. Murata, M. Haruta, Direct Oxidation of Propylene to Propylene Oxide, *Shokubai*, 2004, 46, 13-18.

Rahel, J, and Sherman, D., M., The Transition from a Filamentary Dielectric Barrier Discharge to a Diffuse Barrier Discharge in Air at Atmospheric Pressure., *Journal of Physics D: Applied Physics*, 38 (2005) 1-8.

Rentschler, H. C., R. Nagy, et al. "Bactericidal Effect of Ultraviolet Radiation." J. Bacteriol. 42: 745-774. 1941.

Rentschler, H. C. and R. Nagy. "Bactericidal Action of Ultraviolet Radiation on Air-borne Microorganisms." J. Bacteriol. 44: 85-94. 1942.

Richardson, J.P., Dyer, F.F., Dobbs, F.C., Alexeff, I. and Laroussi, M. 2000, On the Use of the Resistive Barrier Discharge to Kill Bacteria: Recent Results *Proc. IEEE Inte. Conf. on Plasma Science* (New Orleans, LA, 2000) p 109.

Roth, J.R., Tsai, P.P., Liu, C., Steady-State Glow Plasma. U.S Patent 5,387,842, February 7, 1995.

Roth, J.R., Tsai, P.P., Liu, C., Laroussi, M., Spence, P.D., One Atmosphere Uniform Glow Discharge Plasma., U.S. Patent 5,414,324, May 9, 1995.

Roth, J. R., *Industrial Plasma Engineering*, *Volume 1, Principles*. Institute of Physics Publishing, Bristol, 1995.

Roth, J.R., Sherman, D., Ben Gadri, R., Karakaya, F., Chen, Z., Montie, T., Kelly-Wintenberg, K., and Tsai, P., A Remote Exposure Reactor (RER) for Plasma Processing and Sterilization by Plasma Active Species at One Atmosphere. IEEE Transactions on Plasma Science, vol.28, No. 1, February 2000.

Roth, J. R., *Industrial Plasma Engineering, Volume 2, Applications to Nonthermal Plasma Processing*, Institute of Physics Publishing, Bristol, 2001.

Roth, J. R. Laroussi, M, and Liu, C., Experimental Generation of a Steady-State Glow Discharge at Atmospheric Pressure, *Proc. 19th International Conference on Plasma Science*, Tampa, FL, 1992.

Roth, et.al., One Atmosphere Glow Discharge Plasma for Surface Treatment of Nonwovens, *Proc. 3rd Annual TANDEC Conference on Meltblowing and Spunbonding Technology*, Knoxville, 1993.

Spence, P.D. and Roth, J.R. Electrical and Plasma Characteristics of a One Atmosphere Glow Discharge Plasma Reactor., *Proc. 21st IEEE Int. Conference on Plasma Science*, Santa Fe, NM June, 2004.

Seman, M., J. N. Kondo, K. Domen, C. Reed , S. T. Oyama., Direct Observation of Surface Intermediates Formed by Selective Oxidation of Alcohols on Silica-Supported Molybdenum Oxide *J. Phys. Chem.* 2004, 108(10), 3231-3239.

Streifel, A.J., Airborne Infectious Disease: Best Practices for Ventilation Management., *Heating Piping and Air Conditioning*., September, 2003.

Urashima, K., and Chang., J. Removal of Volatile Organic Compounds from Air Streams and Industrial Flue Gases by Non-Thermal Plasma Technology., IEEE Transactions on Dielectrics and Electrical Insulation., Vol. 17, No. 5, Oct. 2000.

VanOsdell, D., and Foarde, K., Defining the Effectiveness of UV Lamps Installed in Circulating Air Ductwork., Final Report to ARTI, ARTI-21CR/610-40030-01, November, 2002.

VanOsdell, D. and Foarde, K. 2002. Defining the Effectiveness of UV Lamps Installed in Circulating Air Ductwork. Final Report for Air Conditioning and Refrigeration Technology Institute, Arlington, VA.

WHO, Global tuberculosis control - surveillance, planning, financing, World Health Organization Report 2006, WHO/HTM/TB/2006.362

WHO, World Health Organization, Annexes of Global TB Control, Report 2005.

APPENDIX I—EXPERIMENTAL TEST STAND DESIGN AND CONSTRUCTION

AI.1 System Overview

The ducted air Plasma Test Stands (PTS) are model HVAC ducts with extensive instrumentation and control to provide steady-state operating conditions for testing OAUGDP effects when operated in an air stream. There are two stands, PTS-1 and PTS-II, each of which can be operated independently, but which can also interchange many parts. PTS-I was originally designed to test a setup using filter media sandwiched between flexible electrodes. After downstream killing was established, the stand was modified slightly to be more amenable to downstream plasma sample treatment. PTS-II was built after PTS-I, and after downstream treatment was routine. It is modeled generally after PTS-I, but with several improvements, including a larger outer duct to allow more room for test section-setup and a larger exhaust fan providing higher static pressure (vacuum). PTS-II is also fitted with impaction samplers for aerosolized microorganism sampling and with gas introduction and sampling ports for VOC analysis. PTS-II is the preferred system for airborne efficacy testing for microorganisms or VOCs, but PTS-I has limited capabilities for aerosolized microorganism testing. Both systems are built around an inner test duct which can be arranged with components for particular test setups, microorganisms, VOCs, ozone, etc.

Test sections are modular and are built up according to the needs of a particular experiment. Both systems use modular plasma grids like the one shown in **Figure AI.1**. Other modules are used to hold particulate filter media, carbon

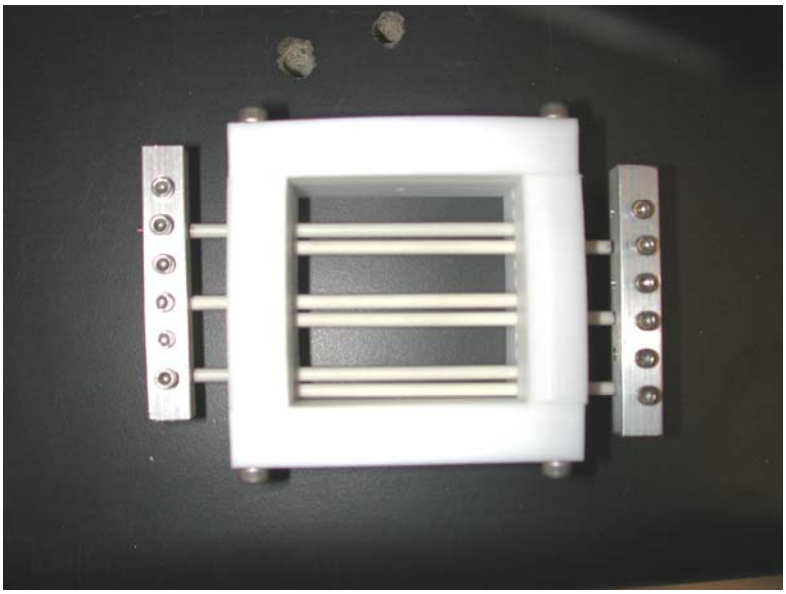

Figure AI.1—Modular Plasma Grid.

media, catalytic media, etc. The appropriate modules are fastened together to provide the appropriate setup which may include, a plasma grid, filter media, ozone catalyst and a test port section. An example built up test section for ozone catalyst testing is shown in **Figure AI.2**.

AI.2 Overall System Design

This section describes the overall concept of the two test stands, giving an overview of design, setup, operation, control and data acquisition. Section 2 gives more thorough explanations of the individual sub-systems and details of operation.

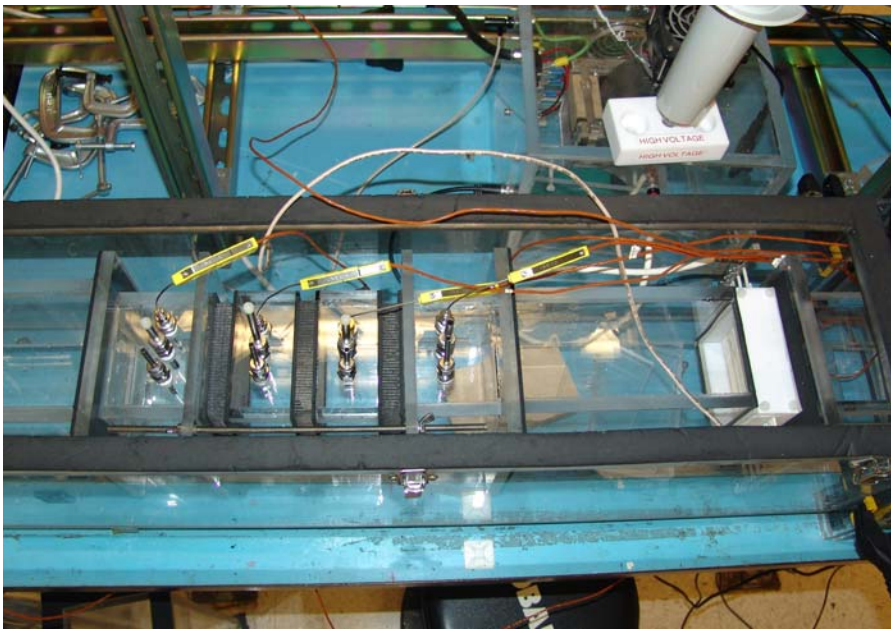

Figure AI.2—Ozone catalyst test setup in PTS-I.

AI.2.1 PTS-I

Figure AI.3 shows a photograph of PTS-I and **Figure AI.4** is a schematic of the test stand. Air is drawn through the system by the combined negative pressure created by the laboratory exhaust system and a dedicated exhaust booster blower. Air enters PTS-I through a PVC pipe located under the test stand table. Air travels through a HEPA filter and enters the outer duct. A 4” x 4” test duct is positioned inside the 8” x 8” outer duct and the outer duct acts simply as a source of filtered air for the inner test duct and as a means of protection for the operator against possible hazards surrounding an operating test—high voltage,

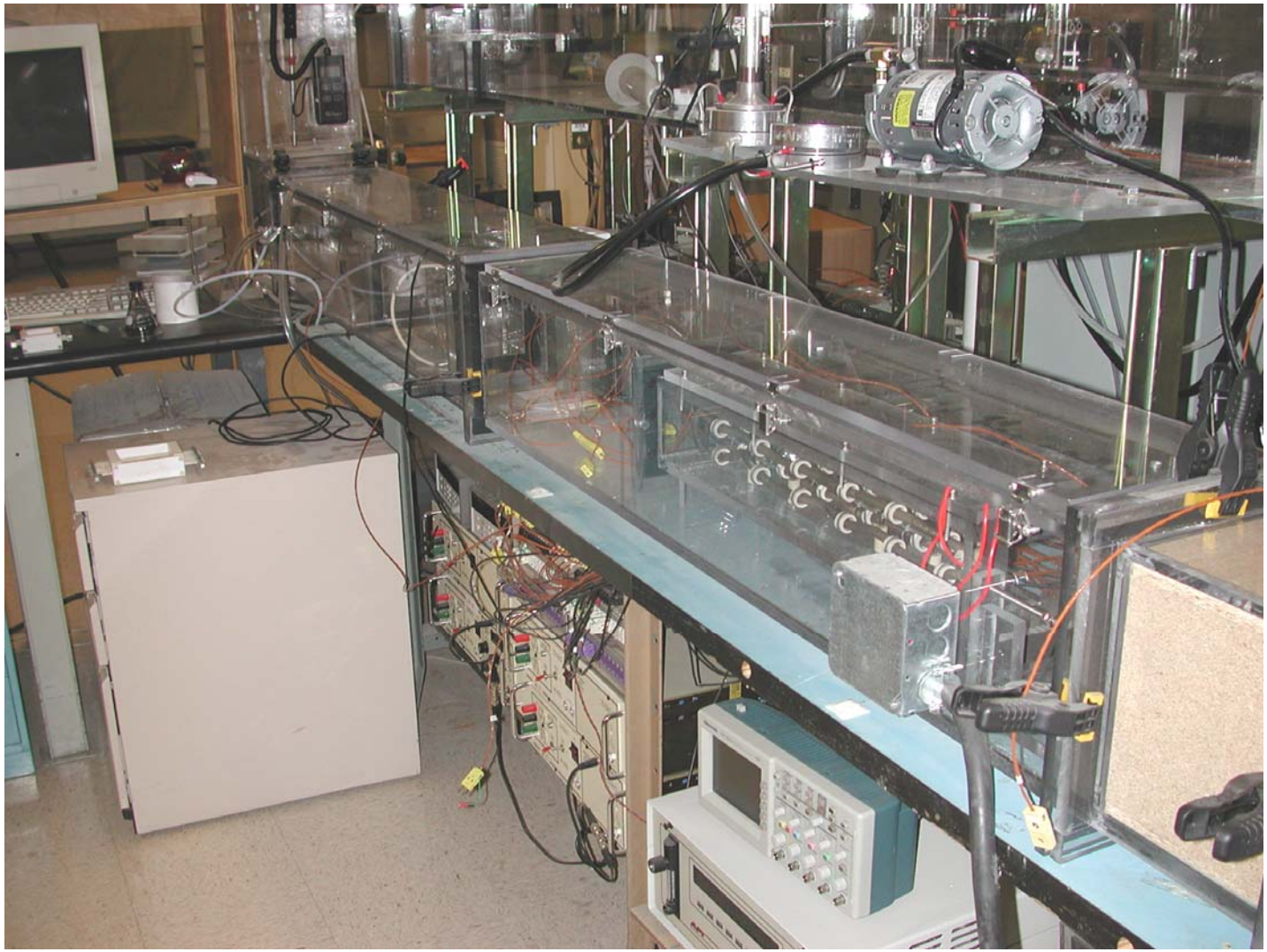

Figure AI.3—PTS I test stand**.**

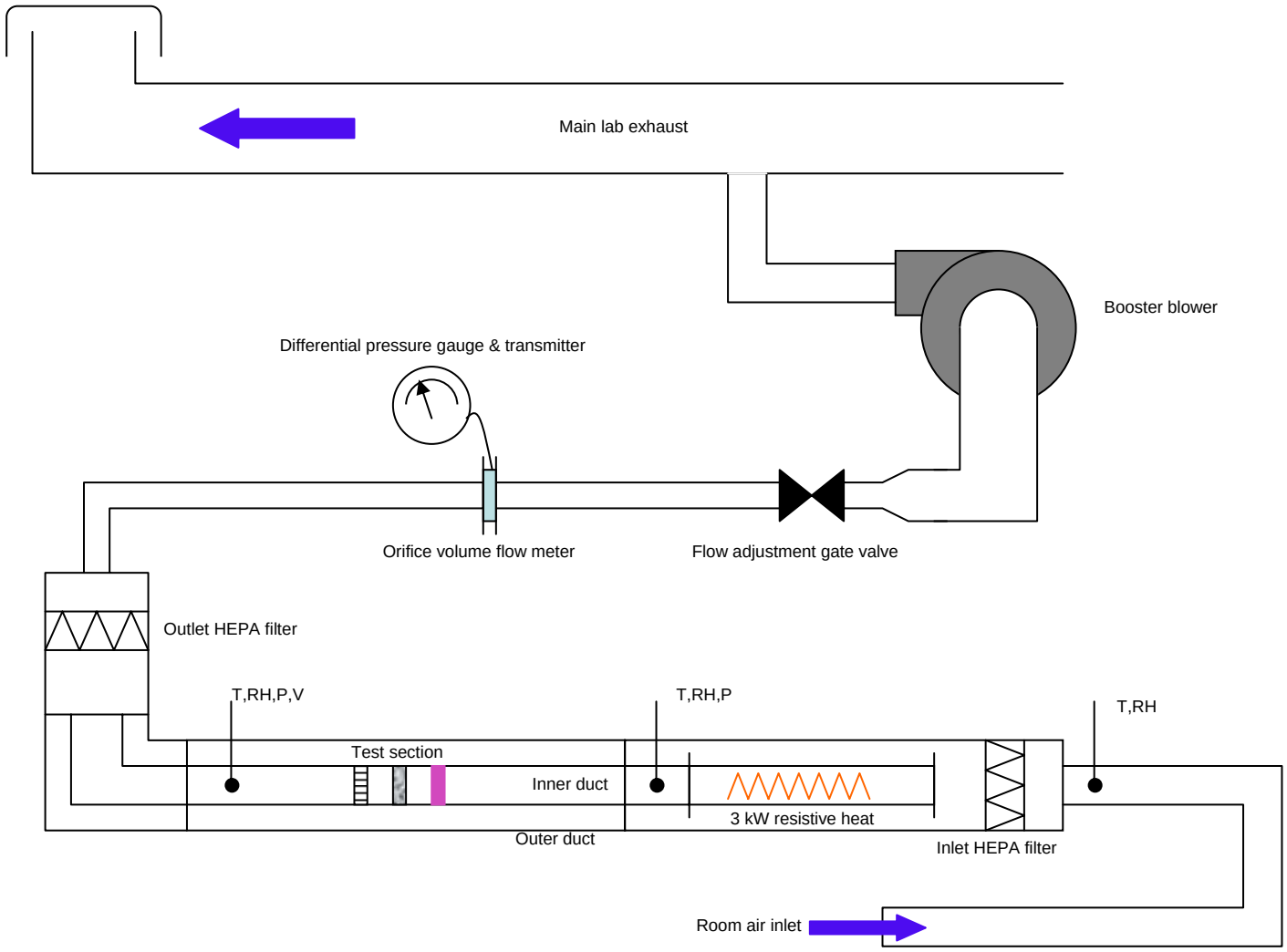

Figure AI.4—PTS I general schematic.

ozone, microorganisms, etc.

The inner duct runs inside the outer duct, the first section of which is a resistive air heating element. Air is drawn into the inner duct, past the heating element and into the test section. The test section can be comprised of any appropriate arrangement of plasma, filter, catalyst and sensing sections according to the needs of the specific test. After leaving the test section, air returns to the outer duct after passing through an exhaust HEPA filter. The exhaust duct makes a 90° turn upwards and transitions to PVC pipe. Above the main test section, the PVC pipe passes though an orifice flow meter and then transitions to a flexible duct connected to an exhaust blower.

The test stand is capable of producing duct Reynolds numbers up to ~$2x10^4$, provided the restrictions to airflow do not exceed limits of static pressure. Total resistance depends on the specifics of an experimental setup, but typically more elements (plasma, filter, catalyst) will cause greater airflow resistance and limit the upper end of testable air velocities. Certain modifications can be made to allow for high velocity testing such as temporary removal of the orifice flow meter, and measuring air velocity with an alternative method—such as with a hot wire anemometer.

PTS-I is equipped with an Agilant data acquisition system connected to a PC providing for 20 input signals, which are pre-wired to accept 10 type-K

thermocouples and 10 analog voltage signals. Additionally, there is a pre-wired set of available 24VDC receptacles to provide instrument power. Data acquisition is via Agilant Benchlink software which provides readily modified data collection setups (sample frequency, display, file writing, etc.). Instruments are connected as needed based on the particulars of an experiment, but there are several permanently connected sensors including ambient (or inlet) air temperature and relative humidity and air volume flow. Semi-permanent thermocouple extension cables are provided for easy connection of ~five or so type-K thermocouples in the general vicinity of the test section. Several Magnahelic differential pressure gauges and transmitters are permanently installed to measure orifice flow meter static pressure drop and pressure drop across the test section. Like most of the instrumentation, these are semi-permanent and can have their configuration changed per the specific needs of a test.

PTS-I is generally used for testing that does not involve introduction of airborne contaminants, microorganism or gaseous. It is typically used for testing plasma versus pre-inoculated microorganism challenges, plasma power consumption profiles, ozone generation and destruction, and fluid flow behavior.

AI.2.2 PTS-II

PTS II is shown schematically in **Figure AI.5** and a photograph is shown in **Figure AI.6**. It is similar in concept to PTS I, in that air is drawn through a similar test duct by vacuum from the combined effects of the plasma exhaust and a dedicated booster blower, however, PTS-II is also outfitted to operate at positive pressure by supplying compressed air at the inlet side. Entering air passes first through a humidifying section which can humidify the incoming air to ~80% RH, however the actual amount that can be added depends on the specifics of the entering air state—dry-bulb and wet-bulb temperature.

After the humidifier section, air passes over a resistive heating element, through a HEPA filter and then converges down to the test duct. The test duct consists of an aerosolization / gas injection section at the beginning followed by a flow development section with upstream sampling ports for microorganisms and gasses and for air state. There is then a section for build up of the specific experimental elements—plasma, filter, catalyst, etc. At the end of the test section there is a downstream sample port for microorganisms and gasses. PTS-II is equipped with two Anderson single-stage impaction samplers for measuring the airborne concentration of microorganisms; they are permanently attached and are positioned upstream and downstream of the test element section.

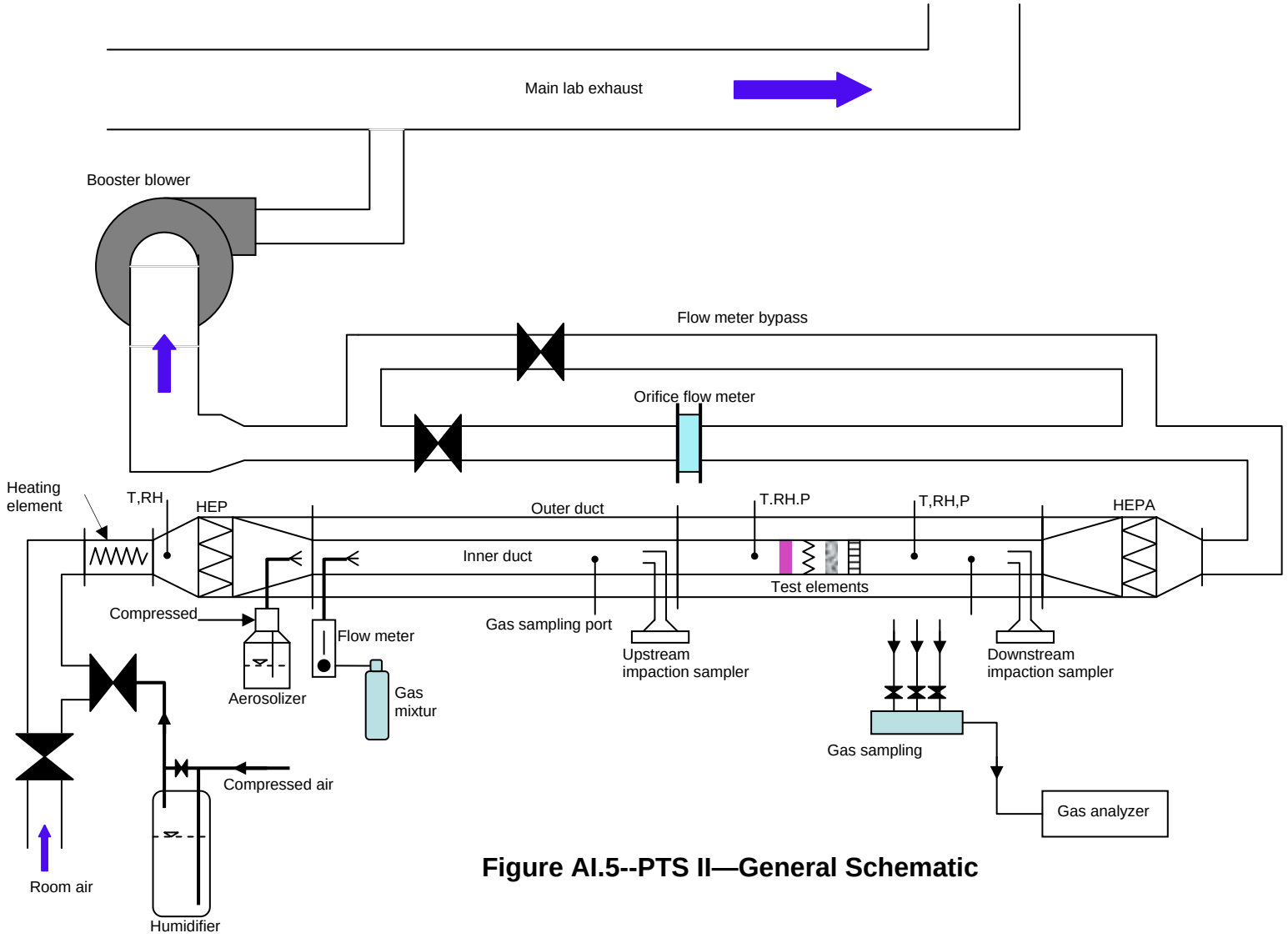

Figure AI.5--PTS II—General Schematic

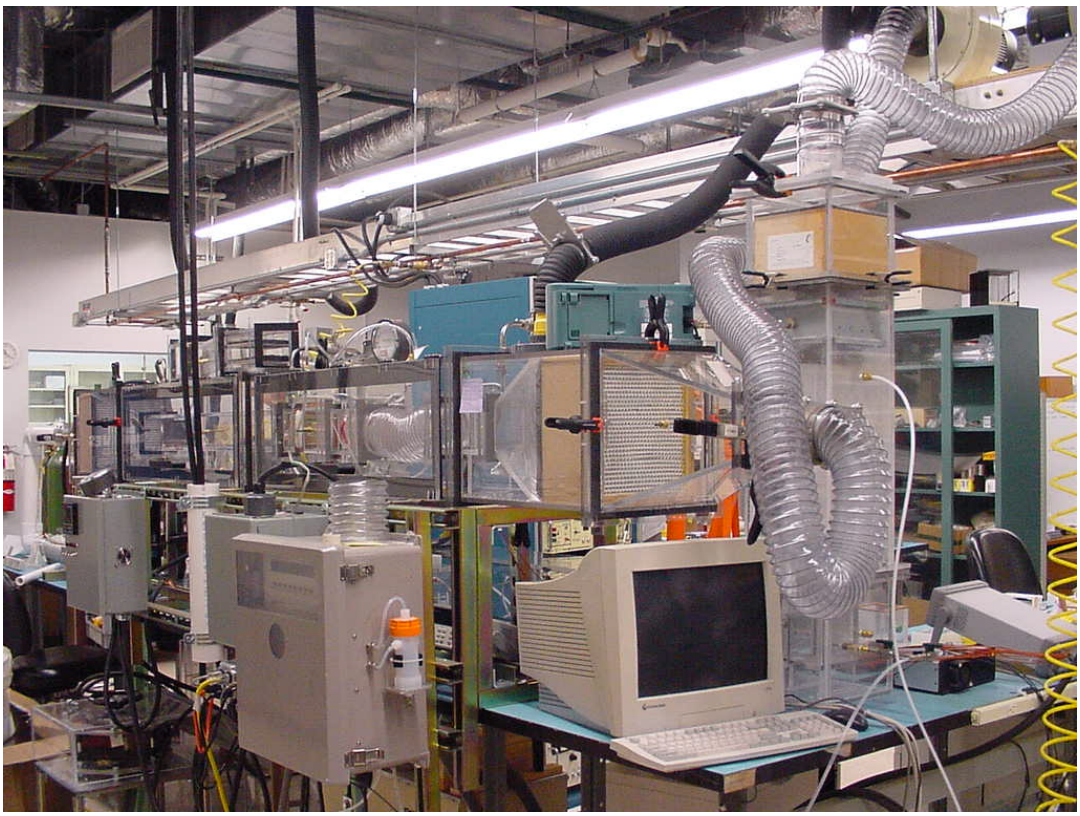

Figure AI.6—PTS II test stand**.**

Exit air is drawn through an exit HEPA filter after leaving the test section where it transitions to a PVC pipe, travels through an orifice flow meter and then exits to the exhaust booster blower. Flow control is via a PVC gate valve in the PVC pipe section downstream of the orifice meter. There is a built in bypass to the orifice meter allowing for higher air velocities in the test section by removing the high static drop orifice meter from the flow path. In such cases, air velocity must be measured by an alternative means. Because flow through PTS-II can be driven both by vacuum on the downstream side and pressure on the upstream

side, the test section can be maintained at zero pressure with respect to ambient; this aids in minimizing possible duct leaks and changes in duct velocity profile.

Like PTS-I, data acquisition is via an Agilant 20 channel mainframe acting as a slave to a PC operating Agilant Benchlink. PTS-II is pre-wired to accept 10 type-K thermocouple inputs and 10 analog voltage signals as well as to provide 12 receptacles for 24 VDC power for instruments. Inlet RH and temperature are permanently connected, also, a thermocouple downstream of the heating element is permanently connected to a PID controller for temperature control. Details of temperature control are covered in Section 2. Magnahelic differential pressure gauges and transmitters are available and semi-permanently connected to the orifice flow meter and to the main duct section referenced to ambient. Again, these systems are designed to be available for easy reconfiguration. PTS-II is equipped with two gas sampling manifolds (generally used for multi-point ozone sampling) which each connect three individually valved input sample tubes to a common output.

AI.3 PTS-II SUB-SYSTEMS

AI.3.1 Air intake & humidity control

PTS-II can operate by drawing in room air under vacuum, with a compressed air feed or with both. The room air draw system operates by drawing air through a PVC pipe at the entrance. Alternatively, the ambient entrance can be valved off and compressed air can be measured into the entrance end of PTS-II. The compressed air system was added to allow for humidification of the inlet air stream by bubbling through a water tower. Beyond the air intake system, air passes through a heating duct and, through a HEPA filter and then on to the test duct.

The humidity control system is pictured in **Figure AI.7** and consists of a vertical section of PVC pipe capped at both ends. Air enters through a dip tube that reaches the bottom of the tank and exits from a second tube at the top of the tank. Water is supplied as needed through a third penetration in the top of the tower and a pressure relief valve is positioned in a fourth penetration. Inlet compressed air passes through an adjustable regulator and then through a sight read flow meter. Through a tee and valve arrangement, the amount of air passing through the humidifier can be adjusted, allowing for infinite control between the inlet air humidity and the maximum humidity attainable.

Figure AI.7—PTS-II humidifier.

The maximum flow rate from the compressed air system is limited, but may be mixed with drawn room air make minor humidity adjustments to tests that require higher volume flows.

AI.3.2 Outer duct

The outer duct section for PTS-II is an acrylic duct with removable side doors for access. It is built in four main modular sections: the first houses the HEPA filter (**Figure AI.8**), the second and third house the inner test ducts and the fourth houses the exit HEPA filter and transitions to the exhaust piping. The sections are flanged at both ends and each flange surface is taped with foam rubber tape to aid in making a reasonably air tight seal between sections. The individual

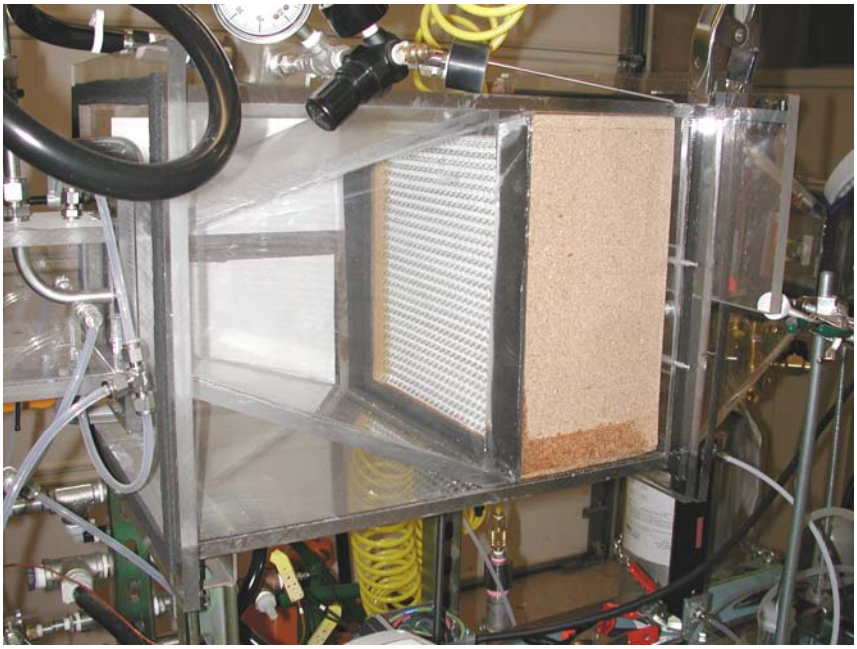

Figure AI.8—PTS II inlet HEPA filter.

sections are clamped together with either spring clamps or small C-clamps, typically with four clamps per junction. The purpose of the outer duct is to house the inlet and exit HEPA filters, to house the inner test duct and to provide a measure of protection to the test operator from dangers present from the operating test elements. There are limited penetrations in the outer duct for sensor wires, plasma power and pressure readings. The PTS-II outer duct is not intended to be air tight, but it is held at a slight negative pressure with a direct connection to the main lab exhaust duct. This makes it act somewhat like a lab hood in that room air is continuously being drawn through the duct and exhausted through the main exhaust system such that any plasma products,

gasses or microorganisms that leak out of the inner test duct will preferentially exit through the exhaust.

AI.3.3 Inner duct

The inner duct is constructed of acrylic with gasketed flanged ends. The first section houses the injection modules for aerosolized microorganisms and VOCs. The last section is permanently attached to the inlet side of the exhaust HEPA filter. In between the first and last sections is approximately a section for positioning test elements. The elements are built up and positioned in the outer duct with appropriate spacers.

AI.3.4 Aerosolization

Microorganism aerosolization into PTS-II is done with a constant flow atomizer whose duct inlet port is just downstream of the inlet HEPA filter (in the same general area as the VOC injector element). An appropriate concentration of microorganisms solution is prepared by the in Wheaton bottles for direct connection to an atomizer. The atomizer is supplied with compressed air. The required microorganism density in solution is dependant on the needs of a particular experiment and can vary significantly. For instance, filter media capture characterization, and any tests employing the

single-stage Anderson samplers requires a lower airborne concentration than testing of high log destruction in an air stream or on a loaded filter.

Prior to and following use with live microorganisms, the atomizer is purged with a 50/50 alcohol/water mixture for 10 minutes followed by an additional 10 minute purge with 100 % distilled water.

AI.3.5 Testing section

The testing section is simply the portion of the inner duct after the injection elements and before the exhaust duct connection. It is a space approximately 8 feet long within the outer duct into which test elements can be placed to build up a particular test apparatus. There are a variety of duct sections, spacers, plasma generators, sampling elements and other components that are used to build up a specific test arrangement. PTS-II uses a short flexible duct section to connect the test section to the exhaust duct.

AI.3.6 Power supply

Plasma power to PTS-II is provided by a Compact Titan power supply connected to a high voltage step up transformer. PTS-II operates with one grounded electrode and one high voltage electrode (**Figure AI.9**). The Compact power supply is wired via the back terminals to a female twist-lock end cap, to which the

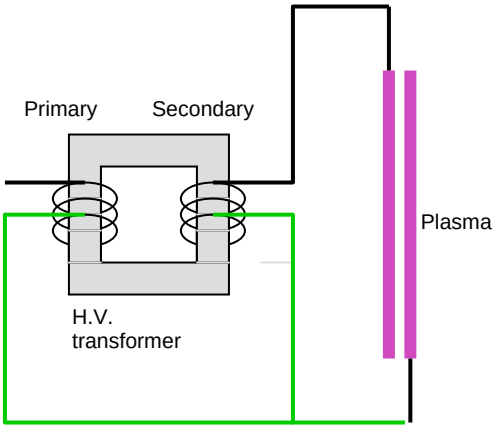

Figure AI.9—Typical PTS high voltage connection.

primary winding of the step-up transformer connects. The transformer is housed in a NEMA 13 enclosure box positioned on top of the outer duct and a short high voltage cable penetrates the duct carrying power for plasma connection. The grounding lead passes through a separate duct penetration. Both the high voltage and grounding leads terminate to alligator clips which are connected to the electrode terminal bars of the plasma generators.

In some circumstances more than one power supply must be connected together to meet voltage or power requirements of particular tests. In these cases, two or more supplies are be wired together on the output side in series or parallel and one of the oscillators is connected to drive all connected supplied in concert.

AI.3.7 Flow Control

After transitioning to PVC pipe, PTS-II process air passes through a straight section of PVC pipe and then through a Lambda Square Inc. orifice flow meter for measuring air volumetric flow.

The orifice flow meters come factory calibrated and the relationship between volume flow and pressure drop is:

$$Q_1 = \left[\frac{Q_2^2 h_1}{h_2} \right]^2 \qquad \text{[AI.1]}$$

or alternatively:

$$h_1 = \frac{Q_1^2 h_2}{Q_2^2} \qquad \text{[AI.2]}$$

where:

Q_1 = measured volume flow rate

h_1 = measured static pressure drop across orifice

Q_2 = factory calibrated maximum flow

h_2 = factory calibrated pressure drop corresponding to maximum flow

Following the orifice flow meter, there is a PVC gate valve for flow adjustment. The orifice flow meter is connected to a magnahelic differential pressure gauge and transmitter which can be visually read for flow adjustment and logged through the DAS system during testing. For an experimental setup, the desired steady-state velocity is converted to a volume flow rate and the corresponding measured static pressure drop through the orifice meter is calculated. The booster fan is turned on if it is needed to meet the flow requirements, and the downstream gate valve is adjusted until the calculated static pressure drop is measured.

In cases where higher volume flow is desired or where air flow resistance from the test setup does not allow adequate flow through the orifice flow meter, there is a bypass pipe that routs air around the orifice meter. If the bypass is used, an alternative means for measuring air velocity or volume flow must be used. PTS-II is equipped with several velocity measuring devices including a hot wire anemometer and a small profile vane anemometer. The orifice flow meters are positioned ~15 duct diameters downstream and ~10 duct diameters upstream of any pipe interruptions (valves, 90°s, tees, etc.) to ensure that air entering the orifice is fully developed and unaffected by flow disturbances near the meter.

AI.3.8 Exhaust

After exiting the flow control gate valve, air travels through a flexible duct and then enters the booster blower. The exhaust of the blower is piped through flexible PVC hose to an inlet port on the main laboratory exhaust.

AI.3.9 Data Acquisition & Control

PTS-II is equipped with automatic data acquisition via an Agilant 34970A portable mainframe and an Agilant 34901A 20 channel multiplexer. The mainframe is connected to a PC through a GPIB to USB interface and the mainframe is slave to the PC running Agilant Benchlink software.

Channels 1-10 are wired for type-K thermocouples and channels 11-20 are wired for uncompensated voltage signals. Wiring connects to a shared connection panel for thermocouples, voltage signals and 24VDC instrument power for both PTS-I and PTS-II. The plugs and receptacles for signal wiring are miniature type and are color coded according to industry standards as described in the Omega Temperature Measurement Handbook: yellow for type-K thermocouples and white for type-U copper/copper or uncompensated signals. Type-E, purple connectors are used for supplying 24 VDC instrument power. This does not follow convention, but purple was chosen for 24 VDC supply.

All signal wiring (thermocouple and voltage) is done with three wire connectors where the third wire is a grounding sleeve. Male and female end connectors are three-wire and require a grounding strap to maintain the grounding leg. At the connection panel, the grounding wire terminates to a strip located directly above the miniature receptacle. Ground wires from the cable lengths leading from the multiplexer to the connection panel also terminate at the connection panel. The connection panel is grounded and serves as the only grounding point for the entire DAS signal wire system. Instrument power is provided via a two wire system and does not carry a ground shield leg; any instrument grounding is done via the instrument signal wire ground leg.

Thermocouples are type-K with an ungrounded junction and a grounded stainless steel sheath. The sheath is connected to the shield grounding leg of the instrument wire. Other analog instruments are wired according to manufacturer specifications.

Benchlink software is used to display readings and log data for experiments. Benchlink is a relatively simple package that allows for easy reconfiguration of the available input channels and their respective displays.

High voltage power measurements are taken with a Tektronix oscilloscope, including voltage, frequency, current and power. A high voltage probe steps down the secondary voltage to a level that can be safely input to the scope.

Likewise, a wide-band Pearson Electronics current transformer provides current input to the scope. Math functions within the scope resolve true power from the measured voltage and current waveforms.

PTS-I and PTS-II share two gas sampling manifolds (typically used for ozone sampling) which allow quick switching between any of three input sources to a common output. The manifold is anodized aluminum with polypropylene (PP) quick-connect connected to PTFE tubing. The individual sample tubes are typically connected to sample ports on the test sections via Swagelock fittings. The output is also PTFE tubing that connects to a Swagelock inlet fitting on the rear of the ozone analyzer.

PTS-II uses a combination of three available ozone analyzers: 0-1 ppmv, 0-1000 ppmv and 0-2000 ppmv. The ozone analyzers can be setup to feed analog signals to the respective DAS systems.

PTS-I and PTS-II share several pieces of hand measuring devices for temperature, relativity, air velocity and carbon monoxide concentration. As well, other equipment can supplement the test stands, such as oscilloscopes and NxOx analyzers.

AI.3.10-Electrode Assemblies

Electrode sets are mounted in machined polymer mounting blocks (traditionally PTFE for its ability to withstand high temperature). The mounting blocks are designed such that all electrodes of one polarity extend out the same side, and all of the other polarity extend out the other side. The terminal ends of the electrodes penetrate partially into the polymer mounting block but do not extend through it. The net effect is a plasma that develops away from the walls of the mounting block and only in the central portion of the cross-section. Electrodes of like polarity are joined electrically with an aluminum bus bar that is machined to fit the electrode spacing. Stainless steel set screws ensure good electrical contact by pressing the copper conductor against the aluminum bus bar. Most mounting blocks are constructed so that all neighboring electrodes are equally spaced, removing the distinction between electrode sets. However, they can also be setup to isolate individual electrodes sets by leaving one or more unfilled slots between sets. This produces what has been termed a tiger-stripe plasma.

The assemblies are inserted in the test stand by sandwiching them between two other appropriate duct elements—usually short ducts with sensor ports. Power is connected by attaching the alligator clip leads of the plasma power supply to the electrode bus bars on either side of the plasma assembly.

APPENDIX II—EXPERIMENTAL DATA (CHEMICAL)

Ozone Generation Data at Red = 1.46×10^{3}

d	0.125	in			
duct diameter	3.5	in	0.0889	m	
duct area	12.25	in^2	0.00790321	m^2	
air density	0.074	lbm/ft^3	1.187	kg/m^3	
M_{air}			29	kg/km	
M_{O3}			48	kg/km	
μ_{air}			1.83E-05	$(N \cdot s)/m^2$	
l/d	28				
g	0.0196	in	0.5	mm	
g/l	0.15748				
C_p, air	0.24	Btu/lb°F	0.001004832	J/(kg K)	
g	0.5	mm	gap distance		
K	9				
ε_0	8.85E-12	$C^2N^{-1}m^{-2}$			
ε	7.97E-11	$C^2N^{-1}m^{-2}$			

Device	# of electrode sets	ave. electrode length cm	total energized length cm
Rigid 10 (1/3)	6	6.46	38.76

Run	Voltage	Frequency	Air Velocity	Air Velocity	Re_d	Power	Power	T_{IN}	T_{OUT}	ΔT	RH_{IN}	Ozone
#	kV	kHz	fpm	m/s	$\rho Ud/\mu$	W	$W \cdot cm^{-1}$	°C	°C	°C	%	PPMv
1	5	5	50	0.254	1.46E+03	17	0.44	23.8	24.9	1.1	50	15
2	6	5	50	0.254	1.46E+03	29.4	0.76	23.8	25.8	2	50	26
3	7	5	50	0.254	1.46E+03	47.5	1.23	23.7	27.5	3.8	50	38
4	8	5	50	0.254	1.46E+03	74.5	1.92	23.8	29.6	5.8	50	50
5	9	5	50	0.254	1.46E+03	114.7	2.96	23.7	33.6	9.9	50	58
6	10	5	50	0.254	1.46E+03	167.7	4.33	23.7	39.7	16	50	51
7	5	6	50	0.254	1.46E+03	19.6	0.51	23.7	25.5	1.8	50	17
8	6	6	50	0.254	1.46E+03	33.4	0.86	23.6	26	2.4	50	28
9	7	6	50	0.254	1.46E+03	54	1.39	23.7	29.4	5.7	50	41
10	8	6	50	0.254	1.46E+03	85.8	2.21	23.6	32.4	8.8	50	51
11	9	6	50	0.254	1.46E+03	135.5	3.50	23.6	37.4	13.8	50	55
12	10	6	50	0.254	1.46E+03	192.8	4.97	23.6	43.5	19.9	50	42
13	5	7	50	0.254	1.46E+03	22.1	0.57	23.5	26.8	3.3	50	19
14	6	7	50	0.254	1.46E+03	38.9	1.00	23.6	28	4.4	50	32
15	7	7	50	0.254	1.46E+03	63.7	1.64	23.6	30.2	6.6	50	46
16	8	7	50	0.254	1.46E+03	102.6	2.65	23.6	34.6	11	50	53
17	9	7	50	0.254	1.46E+03	162	4.18	23.5	41.7	18.2	50	49
18	10	7	50	0.254	1.46E+03	228.2	5.89	23.6	48.4	24.8	50	29
19	5	8	50	0.254	1.46E+03	25.6	0.66	23.5	27.4	3.9	50	23
20	6	8	50	0.254	1.46E+03	44.9	1.16	23.5	28.5	5	50	37
21	7	8	50	0.254	1.46E+03	72.8	1.88	23.4	30.8	7.4	50	48
22	8	8	50	0.254	1.46E+03	118	3.04	23.5	35.3	11.8	50	54
23	9	8	50	0.254	1.46E+03	196.1	5.06	23.6	43.1	19.5	50	41
24	10	8	50	0.254	1.46E+03	262.7	6.78	23.5	50.4	26.9	50	21
25	5	9	50	0.254	1.46E+03	28.6	0.74	23.5	28.2	4.7	50	25
26	6	9	50	0.254	1.46E+03	50.2	1.30	23.5	29.5	6	50	40
27	7	9	50	0.254	1.46E+03	83.7	2.16	23.5	32.4	8.9	50	50
28	8	9	50	0.254	1.46E+03	140.1	3.61	23.4	37.7	14.3	50	52
29	9	9	50	0.254	1.46E+03	223.1	5.76	23.4	46.7	23.3	50	32
30	10	9	50	0.254	1.46E+03	290	7.48	23.4	54.4	31	50	13
31	5	10	50	0.254	1.46E+03	32	0.83	23.3	28.7	5.4	50	28
32	6	10	50	0.254	1.46E+03	56.9	1.47	23.4	30.3	6.9	50	42
33	7	10	50	0.254	1.46E+03	95.5	2.46	23.4	33.5	10.1	50	52
34	8	10	50	0.254	1.46E+03	168.4	4.34	23.4	40.2	16.8	50	46
35	9	10	50	0.254	1.46E+03	248.5	6.41	23.4	49.2	25.8	50	23
36	10	10	50	0.254	1.46E+03	317.5	8.19	23.5	57.8	34.3	50	7

Run	Voltage	Frequency	Air Velocity	Air Velocity	Re_d	Power	Power	T_{IN}	T_{OUT}	ΔT	RH_{IN}	Ozone
#	kV	kHz	fpm	m/s	ρUd/μ	W	$W \cdot cm^{-1}$	°C	°C	°C	%	PPMv
1	5	5	75	0.381	2.20E+03	16.4	0.42	20.6	23.7	3.1	50	17
2	6	5	75	0.381	2.20E+03	26.4	0.68	20.6	24.3	3.7	50	24
3	7	5	75	0.381	2.20E+03	45	1.16	20.6	26	5.4	50	36
4	8	5	75	0.381	2.20E+03	72.4	1.87	20.6	28.3	7.7	50	47
5	9	5	75	0.381	2.20E+03	111.1	2.87	20.5	31.8	11.3	50	53
6	10	5	75	0.381	2.20E+03	161.1	4.16	20.6	36.2	15.6	50	50
7	5	8	75	0.381	2.20E+03	23.1	0.60	20.4	23.6	3.2	50	22
8	6	8	75	0.381	2.20E+03	44.7	1.15	20.4	25.5	5.1	50	35
9	7	8	75	0.381	2.20E+03	70.1	1.81	20.3	27.7	7.4	50	43
10	8	8	75	0.381	2.20E+03	117.7	3.04	20.4	31.8	11.4	50	48
11	9	8	75	0.381	2.20E+03	199.5	5.15	20.3	38.6	18.3	50	38
12	10	8	75	0.381	2.20E+03	271.6	7.01	20.4	45.6	25.2	50	22
13	5	10	75	0.381	2.20E+03	29.7	0.77	20.2	25.2	5	50	26
14	6	10	75	0.381	2.20E+03	54.7	1.41	20.3	27.4	7.1	50	38
15	7	10	75	0.381	2.20E+03	89.8	2.32	20.4	29.9	9.5	50	45
16	8	10	75	0.381	2.20E+03	173.3	4.47	20.4	37.5	17.1	50	38
17	9	10	75	0.381	2.20E+03	245.9	6.34	20.4	44.6	24.2	50	23
18	10	10	75	0.381	2.20E+03	318.8	8.22	20.4	51.4	31	50	12

Run	Voltage	Frequency	Air Velocity	Air Velocity	Re_d	Power	Power	T_{IN}	T_{OUT}	RH_{IN}	Ozone	Ozone
#	kV	kHz	fpm	m/s	ρUd/μ	W	$W•cm^{-1}$	°C	°C	%	PPMv	$mole•s^{-1}$
1	5	5	100	0.508	2.93E+03	16.1	0.42	23.1	23.2	50	17	2.79E-06
2	6	5	100	0.508	2.93E+03	28.3	0.73	21.9	23.9	50	24	3.94E-06
3	7	5	100	0.508	2.93E+03	45.9	1.18	21.8	24.9	50	32	5.26E-06
4	8	5	100	0.508	2.93E+03	71	1.83	21.7	26.9	50	40	6.57E-06
5	9	5	100	0.508	2.93E+03	114.6	2.96	21.6	30.2	50	46	7.56E-06
6	10	5	100	0.508	2.93E+03	156.1	4.03	21.5	33.8	50	44	7.23E-06
7	5	8	100	0.508	2.93E+03	24.3	0.63	21.8	23.6	50	21	3.45E-06
8	6	8	100	0.508	2.93E+03	44.2	1.14	21.6	24.7	50	30	4.93E-06
9	7	8	100	0.508	2.93E+03	73.4	1.89	21.5	27	50	39	6.41E-06
10	8	8	100	0.508	2.93E+03	117.6	3.03	21.3	30.7	50	41	6.74E-06
11	9	8	100	0.508	2.93E+03	195.3	5.04	21.1	37.2	50	33	5.42E-06
12	10	8	100	0.508	2.93E+03	263.4	6.80	21	43.3	50	20	3.29E-06
13	5	10	100	0.508	2.93E+03	29.6	0.76	20.6	24.6	50	23	3.78E-06
14	6	10	100	0.508	2.93E+03	53.8	1.39	20.4	26.1	50	32	5.26E-06
15	7	10	100	0.508	2.93E+03	93	2.40	20.5	28.6	50	39	6.41E-06
16	8	10	100	0.508	2.93E+03	167.4	4.32	20.4	34.4	50	36	5.92E-06
17	9	10	100	0.508	2.93E+03	241.7	6.24	20.3	41.2	50	23	3.78E-06
18	10	10	100	0.508	2.93E+03	316.2	8.16	20.2	48.1	50	10	1.64E-06

Run	Voltage	Frequency	Air Velocity	Air Velocity	Re_d	Power	Power	T_{IN}	T_{OUT}	RH_{IN}	Ozone
#	kV	kHz	fpm	m/s	ρUd/μ	W	$W \cdot cm^{-1}$	°C	°C	%	PPMv
1	5	5	200	1.016	5.86E+03	17.5	0.42	17.7	20.9	51.5	9.9
2	6	5	200	1.016	5.86E+03	29.5	0.71	17.7	20.9	51.5	16.3
3	7	5	200	1.016	5.86E+03	46	1.11	17.8	21.6	51.5	25.9
4	8	5	200	1.016	5.86E+03	67.5	1.63	17.8	23	51.5	35.8
5	9	5	200	1.016	5.86E+03	100	2.42	17.9	25.1	51.5	48.4
6	10	5	200	1.016	5.86E+03	128	3.10	17.9	27.2	51.5	58.9
7	5	6	200	1.016	5.86E+03	20	0.48	18	19.8	51.5	11
8	6	6	200	1.016	5.86E+03	33.5	0.81	18	20.7	51.5	18.7
9	7	6	200	1.016	5.86E+03	51	1.23	18	21.7	51.5	27.8
10	8	6	200	1.016	5.86E+03	80	1.94	18	23.7	51.5	39.4
11	9	6	200	1.016	5.86E+03	110	2.66	18	26	51.5	51.6
12	10	6	200	1.016	5.86E+03	148	3.58	18	28.2	51.5	63.5
13	5	7	200	1.016	5.86E+03	22	0.53	18.1	20	50	12.3
14	6	7	200	1.016	5.86E+03	37	0.90	18.1	21	50	20.3
15	7	7	200	1.016	5.86E+03	60	1.45	18.1	22.5	50	31.3
16	8	7	200	1.016	5.86E+03	91	2.20	18.1	24.7	50	42.9
17	9	7	200	1.016	5.86E+03	126	3.05	18.1	26.6	50	55
18	10	7	200	1.016	5.86E+03	170	4.11	18.1	29.7	50	66.7
19	5	8	200	1.016	5.86E+03	25	0.60	18.4	21	50	14
20	6	8	200	1.016	5.86E+03	45	1.09	18.4	21.9	50	23.3
21	7	8	200	1.016	5.86E+03	70	1.69	18.4	23.5	50	34.9
22	8	8	200	1.016	5.86E+03	103	2.49	18.4	25.7	50	48.1
23	9	8	200	1.016	5.86E+03	145	3.51	18.4	28.7	50	61.4
24	10	8	200	1.016	5.86E+03	195	4.72	18.4	32	50	71
25	5	9	200	1.016	5.86E+03	27	0.65	18.5	21.1	50	15
26	6	9	200	1.016	5.86E+03	47	1.14	18.5	22.3	50	25
27	7	9	200	1.016	5.86E+03	79	1.91	18.5	24.3	50	38.5
28	8	9	200	1.016	5.86E+03	112	2.71	18.5	26.6	50	51.1
29	9	9	200	1.016	5.86E+03	162	3.92	18.5	30	50	65.2
30	10	9	200	1.016	5.86E+03	220	5.32	18.5	33.7	50	74.2
31	5	10	200	1.016	5.86E+03	30	0.73	18.5	21.7	50	16.5
32	6	10	200	1.016	5.86E+03	51	1.23	18.5	22.7	50	26.8
33	7	10	200	1.016	5.86E+03	85	2.06	18.5	25.1	50	41.2
34	8	10	200	1.016	5.86E+03	130	3.14	18.5	28.1	50	55.6
35	9	10	200	1.016	5.86E+03	182	4.40	18.5	32.3	50	69.4
36	10	10	200	1.016	5.86E+03	250	6.05	18.5	36.6	50	78.4

APPENDIX III—EXPERIMENTAL DATA (BIOLOGICAL)

duct diameter 0.0889 m
air velocity 50 fpm 0.254 m/s

1 hour

sample	η	x_j-x_m	$(x_j-x_m)^2$	z_0	$P(z_0)$	$[0.5-P(z_0)]$
1	0.270	-0.14	0.02	1.10	0.3643	0.14
2	0.436	0.03	0.00	0.23	0.0910	0.41
3	0.515	0.11	0.01	0.86	0.3051	0.19
mean (x_m)	0.41	σ^2 =	0.01			
standard deviation	0.12	σ =	0.12			

2 hours

sample	η	x_j-x_m	$(x_j-x_m)^2$	z_0	$P(z_0)$	$[0.5-P(z_0)]$
4	0.542	0.01	0.00	0.83	0.2967	0.20
5	0.533	0.00	0.00	0.28	0.1103	0.39
6	0.510	-0.02	0.00	1.11	0.3665	0.13
mean (x_m)	0.53	σ^2 =	0.00			
standard deviation	0.02	σ =	0.02			

3 hours

sample	η	x_j-x_m	$(x_j-x_m)^2$	z_0	$P(z_0)$	$[0.5-P(z_0)]$
7	1.749	0.52	0.27	1.01	0.3438	0.16
8	1.224	-0.01	0.00	0.01	0.0040	0.50
9	0.720	-0.51	0.26	0.99	0.3389	0.16
mean (x_m)	1.23	σ^2 =	0.18			
standard deviation	0.51	σ =	0.51			

4 hours

sample	η	x_j-x_m	$(x_j-x_m)^2$	z_0	$P(z_0)$	$[0.5-P(z_0)]$
10	1.527	0.19	0.04	0.34	0.1331	0.37
11	1.783	0.45	0.20	0.79	0.2852	0.21
12	0.688	-0.64	0.42	1.13	0.3708	0.13
mean (x_m)	1.33	σ^2 =	0.22			
standard deviation	0.57	σ =	0.57			

5 hours

sample	η	x_j-x_m	$(x_j-x_m)^2$	z_0	$P(z_0)$	$[0.5-P(z_0)]$
13	5.610	1.13	1.28	0.58	0.2190	0.28
14	5.610	1.13	1.28	0.58	0.2190	0.28
15	2.210	-2.27	5.14	1.15	0.3749	0.13
mean (x_m)	4.48	σ^2 =	2.57			
standard deviation	1.96	σ =	1.96			

6 hours

sample	η	x_j-x_m	$(x_j-x_m)^2$	z_0	$P(z_0)$	$[0.5-P(z_0)]$
16	4.010	0.70	0.49	0.53	0.2019	0.30
17	4.135	0.82	0.68	0.62	0.2324	0.27
18	1.789	-1.52	2.32	1.15	0.3749	0.13
mean (x_m)	3.31	σ^2 =	1.16			
standard deviation	1.32	σ =	1.32			

7 hours

sample	η	x_j-x_m	$(x_j-x_m)^2$	z_0	$P(z_0)$	$[0.5-P(z_0)]$
19	4.913	0.57	0.32	0.92	0.3212	0.18
20	4.436	0.09	0.01	0.15	0.0596	0.44
21	3.682	-0.66	0.44	1.07	0.1700	0.33
mean (x_m)	4.34	σ^2 =	0.26			
standard deviation	0.62	σ =	0.62			

8 hours

sample	η	x_j-x_m	$(x_j-x_m)^2$	z_0	$P(z_0)$	$[0.5-P(z_0)]$
22	5.610	1.00	1.00	1.15	0.3749	0.13
23	4.010	-0.60	0.36	0.69	0.2549	0.25
24	4.214	-0.40	0.16	0.46	0.1700	0.33
mean (x_m)	4.61	σ^2 =	0.25			
standard deviation	0.87	σ =	0.87			

9 hours

sample	η	x_j-x_m	$(x_j-x_m)^2$	z_0	$P(z_0)$	$[0.5-P(z_0)]$
25	4.436	0.71	0.51	0.43	0.1664	0.33
26	4.913	1.19	1.42	0.71	0.2611	0.24
27	1.816	-1.91	3.63	1.14	0.3729	0.13
mean (x_m)	3.72	σ^2 =	0.93			
standard deviation	1.67	σ =	1.67			

duct diameter 0.0889 m
air velocity 100 fpm 0.508 m/s

	sample	η	x_j-x_m	$(x_j-x_m)^2$	z_0	$P(z_0)$	$[0.5-P(z_0)]$
1 hour	1	0.145	-0.35	0.12	0.62		0.50
	2	0.197	-0.29	0.09	0.53		0.50
	3	1.131	0.64	0.41	1.15		0.50
	mean (x_m)	0.49	σ^2 =	0.21			
	standard deviation	0.55	σ =	0.55			
2 hours	sample	η	x_j-x_m	$(x_j-x_m)^2$	z_0	$P(z_0)$	$[0.5-P(z_0)]$
	4	0.670	-0.10	0.01	0.29		0.50
	5	0.496	-0.27	0.07	0.82		0.50
	6	1.131	0.37	0.13	1.11		0.50
	mean (x_m)	0.77	σ^2 =	0.07			
	standard deviation	0.33	σ =	0.33			
3 hours	sample	η	x_j-x_m	$(x_j-x_m)^2$	z_0	$P(z_0)$	$[0.5-P(z_0)]$
	7	0.473	0.19	0.04	1.10		0.50
	8	0.238	-0.04	0.00	0.26		0.50
	9	0.138	-0.15	0.02	0.84		0.50
	mean (x_m)	0.28	σ^2 =	0.02			
	standard deviation	0.17	σ =	0.17			
4 hours	sample	η	x_j-x_m	$(x_j-x_m)^2$	z_0	$P(z_0)$	$[0.5-P(z_0)]$
	10	1.377	-0.38	0.15	1.15		0.50
	11	1.992	0.23	0.05	0.69		0.50
	12	1.916	0.15	0.02	0.46		0.50
	mean (x_m)	1.76	σ^2 =	0.07			
	standard deviation	0.34	σ =	0.34			
5 hours	sample	η	x_j-x_m	$(x_j-x_m)^2$	z_0	$P(z_0)$	$[0.5-P(z_0)]$
	13	2.181	-0.10	0.01	0.71		0.50
	14	2.446	0.16	0.03	1.14		0.50
	15	2.221	-0.06	0.00	0.43		0.50
	mean (x_m)	2.28	σ^2 =	0.01			
	standard deviation	0.14	σ =	0.14			
6 hours	sample	η	x_j-x_m	$(x_j-x_m)^2$	z_0	$P(z_0)$	$[0.5-P(z_0)]$
	16	2.314	-0.31	0.10	0.32		0.50
	17	1.851	-0.77	0.60	0.80		0.50
	18	3.707	1.08	1.17	1.12		0.50
	mean (x_m)	2.62	σ^2 =	0.62			
	standard deviation	0.97	σ =	0.97			

7 hours

sample	η	x_j-x_m	$(x_j-x_m)^2$	z_0	$P(z_0)$	$[0.5-P(z_0)]$
19	2.888	0.12	0.01	0.21		0.50
20	2.157	-0.61	0.38	1.09		0.50
21	3.265	0.49	0.24	0.88		0.50
mean (x_m)	2.77	σ^2 =	0.21			
standard deviation	0.56	σ =	0.56			

8 hours

sample	η	x_j-x_m	$(x_j-x_m)^2$	z_0	$P(z_0)$	$[0.5-P(z_0)]$
22	5.640	0.00	0.00	#DIV/0!		0.50
23	5.640	0.00	0.00	#DIV/0!		0.50
24	5.640	0.00	0.00	#DIV/0!		0.50
mean (x_m)	5.64	σ^2 =	0.00			
standard deviation	0.00	σ =	0.00			

9 hours

sample	η	x_j-x_m	$(x_j-x_m)^2$	z_0	$P(z_0)$	$[0.5-P(z_0)]$
25	5.640	0.00	0.00	#DIV/0!		0.50
26	5.640	0.00	0.00	#DIV/0!		0.50
27	5.640	0.00	0.00	#DIV/0!		0.50
mean (x_m)	5.64	σ^2 =	0.00			
standard deviation	0.00	σ =	0.00			

10 hou

sample	η	x_j-x_m	$(x_j-x_m)^2$	z_0	$P(z_0)$	$[0.5-P(z_0)]$
25	5.640	0.00	0.00	#DIV/0!		0.50
26	5.640	0.00	0.00	#DIV/0!		0.50
27	5.640	0.00	0.00	#DIV/0!		0.50
mean (x_m)	5.64	σ^2 =	0.00			
standard deviation	0.00	σ =	0.00			

duct diameter 0.0889 m
air velocity 200 fpm 1.016 m/s

1 hour

sample	η	x_i-x_m	$(x_i-x_m)^2$	z_0	$P(z_0)$	$[0.5-P(z_0)]$
1	-0.275	-0.28	0.08	1.15	0.3749	0.13
2	0.125	0.12	0.01	0.48	0.1844	0.32
3	0.173	0.17	0.03	0.67	0.2486	0.25
mean (x_m)	0.01	σ^2 =	0.04			
standard deviation	0.25	σ =	0.25			

2 hours

sample	η	x_i-x_m	$(x_i-x_m)^2$	z_0	$P(z_0)$	$[0.5-P(z_0)]$
4	0.067	-0.12	0.01	0.58	0.2190	0.28
5	0.067	-0.12	0.01	0.58	0.2190	0.28
6	0.415	0.23	0.05	1.15	0.3749	0.13
mean (x_m)	0.18	σ^2 =	0.03			
standard deviation	0.20	σ =	0.20			

3 hours

sample	η	x_i-x_m	$(x_i-x_m)^2$	z_0	$P(z_0)$	$[0.5-P(z_0)]$
7	-0.262	-0.19	0.04	0.57	0.2157	0.28
8	-0.266	-0.20	0.04	0.58	0.2190	0.28
9	0.324	0.39	0.15	1.15	0.3749	0.13
mean (x_m)	-0.07	σ^2 =	0.08			
standard deviation	0.34	σ =	0.34			

4 hours

sample	η	x_i-x_m	$(x_i-x_m)^2$	z_0	$P(z_0)$	$[0.5-P(z_0)]$
10	-0.275	-0.33	0.11	0.78	0.2823	0.22
11	-0.097	-0.15	0.02	0.35	0.1368	0.36
12	0.522	0.47	0.22	1.13	0.3708	0.13
mean (x_m)	0.05	σ^2 =	0.12			
standard deviation	0.42	σ =	0.42			

5 hours

sample	η	x_i-x_m	$(x_i-x_m)^2$	z_0	$P(z_0)$	$[0.5-P(z_0)]$
13	-0.195	-0.26	0.07	0.57	0.2157	0.28
14	-0.205	-0.27	0.07	0.59	0.2224	0.28
15	0.586	0.52	0.27	1.15	0.3749	0.13
mean (x_m)	0.06	σ^2 =	0.14			
standard deviation	0.45	σ =	0.45			

6 hours

sample	η	x_i-x_m	$(x_i-x_m)^2$	z_0	$P(z_0)$	$[0.5-P(z_0)]$
16	0.221	-0.33	0.11	0.74	0.2704	0.23
17	0.323	-0.23	0.05	0.51	0.1950	0.31
18	0.280	-0.27	0.07	0.61	0.2291	0.27
19	1.321	0.77	0.60	1.76	0.4608	0.04
20	0.832	0.28	0.08	0.65	0.2422	0.26
21	0.309	-0.24	0.06	0.54	0.2054	0.29
mean (x_m)	0.55	σ^2 =	0.16			
standard deviation	0.44	σ =	0.44			

7 hours

sample	η	x_i-x_m	$(x_i-x_m)^2$	z_0	$P(z_0)$	$[0.5-P(z_0)]$
22	0.060	-0.49	0.24	1.00	0.3413	0.16
23	-0.084	-0.64	0.40	1.29	0.1554	0.34
24	0.661	0.11	0.01	0.22	0.0871	0.41
25	0.525	-0.03	0.00	0.06	0.0239	0.48
26	1.066	0.51	0.26	1.05	0.3531	0.15
27	1.086	0.53	0.28	1.08	0.3599	0.14
mean (x_m)	0.55	σ^2 =	0.20			
standard deviation	0.49	σ =	0.49			

8 hours

sample	η	x_i-x_m	$(x_i-x_m)^2$	z_0	$P(z_0)$	$[0.5-P(z_0)]$
28	0.636	-0.24	0.06	0.68	0.2517	0.25
29	1.209	0.33	0.11	0.95	0.0438	0.46
30	1.101	0.22	0.05	0.64	0.2389	0.26
31	0.356	-0.52	0.27	1.48	0.4306	0.07
32	0.742	-0.13	0.02	0.38	0.1480	0.35
33	1.211	0.33	0.11	0.95	0.3289	0.17
mean (x_m)	0.88	σ^2 =	0.10			
standard deviation	0.35	σ =	0.35			

9 hours

sample	η	x_j-x_m	$(x_j-x_m)^2$	z_0	$P(z_0)$	$[0.5-P(z_0)]$
34	0.619	-0.40	0.16	1.26	0.3962	0.10
35	1.211	0.20	0.04	0.63	0.2357	0.26
36	1.389	0.37	0.14	1.19	0.3830	0.12
37	1.258	0.24	0.06	0.78	0.2823	0.22
38	0.878	-0.14	0.02	0.43	0.1664	0.33
39	0.729	-0.28	0.08	0.91	0.3186	0.18
mean (x_m)	1.01	σ^2 =	0.08			
standard deviation	0.31	σ =	0.31			

10 hou

sample	η	x_j-x_m	$(x_j-x_m)^2$	z_0	$P(z_0)$	$[0.5-P(z_0)]$
40	1.213	-0.38	0.14	0.69	0.2549	0.25
41	2.224	0.63	0.40	1.15	0.3749	0.13
42	1.338	-0.25	0.06	0.46	0.1772	0.32
mean (x_m)	1.59	σ^2 =	0.20			
standard deviation	0.55	σ =	0.55			

11 hou

sample	η	x_j-x_m	$(x_j-x_m)^2$	z_0	$P(z_0)$	$[0.5-P(z_0)]$
43	3.428	0.79	0.63	1.15	0.3749	0.13
44	2.149	-0.49	0.24	0.70	0.2580	0.24
45	2.328	-0.31	0.09	0.44	0.1700	0.33
mean (x_m)	2.64	σ^2 =	0.32			
standard deviation	0.69	σ =	0.69			

12 hou

sample	η	x_j-x_m	$(x_j-x_m)^2$	z_0	$P(z_0)$	$[0.5-P(z_0)]$
46	2.048	0.14	0.02	0.36	0.1406	0.36
47	2.216	0.31	0.10	0.77	0.2794	0.22
48	1.446	-0.46	0.21	1.13	0.3708	0.13
mean (x_m)	1.90	σ^2 =	0.11			
standard deviation	0.40	σ =	0.40			

13 hou

sample	η	x_j-x_m	$(x_j-x_m)^2$	z_0	$P(z_0)$	$[0.5-P(z_0)]$
49	5.43	1.83	3.34	1.00		0.50
50	1.780	-1.82	3.33	1.00		0.50
51	3.600	0.00	0.00	0.00		0.50
mean (x_m)	3.60	σ^2 =	2.22			
standard deviation	1.83	σ =	1.83			

VITAE

Mr. Domitrovic earned a Bachelor of Science degree in Civil Engineering in 1992 from Carnegie Mellon University, Pittsburgh, PA, followed by a Master of Science degree in Construction Management in 1995 from the University of Florida, Gainesville, FL. He worked from 1995 through 2002 as a research engineer at the Buildings Technology Center of the Oak Ridge National Laboratory on building systems research, primarily on efficiency of HVAC systems. From 2002 through 2006 he worked as a project manager for Atmospheric Glow Technologies, Knoxville, TN for development of plasma based air purification technologies. Mr. Domitrovic is currently president of Redwood Electric Inc., a Knoxville based electrical contractor.